ATOMIC MOBILITY IN THIN SOLID Pd_2Si FILMS

by

EDMUND CHARLES ZINGU

Dissertation presented to the
University of Cape Town
in fulfilment of the requirements
for the degree of

DOCTOR OF PHILOSOPHY

Department of Physics

January 1985

ABSTRACT

A theory for the growth kinetics of planar silicide formation in single- and bi-layer metal silicon systems has been developed on the basis that the chemical potential gradient in the growing layer is the driving force for diffusion. The predictions of the theory, when applied to single layer metal-silicon systems, is in agreement with other theories and with experimental results. Planar growth of the outer silicide layer in bilayer metal-silicon systems is predicted to proceed linearly with time, both when controlled by an interfacial reaction and when limited by diffusion through the interposed silicide layer (when this layer is sufficiently thick). In the latter case it is predicted that the growth rate of the outer silicide layer is inversely proportional to the thickness of the interposed layer.

These predictions of the theory have been tested with reference to the Si/Pd/Cr thin film system and have been found to be veritable. A detailed investigation of the thermal behaviour of the Si/Pd/Cr system which is transformed to $Si/Pd_2Si/CrSi_2$, has been carried out and various techniques, including Rutherford backscattering spectrometry, glancing angle X-ray diffraction, and scanning and transmission electron microscopy, were used to characterize the specimens. Linear growth of $CrSi_2$ on Pd_2Si is observed irrespective of the Si substrate orientation or Pd_2Si layer thickness. The activation energy associated with $CrSi_2$ growth on thin and thick polycrystalline Pd_2Si is 1.7 ± 0.2eV, while values of 1.6 ± 0.2eV and 2.1 ± 0.2eV are found respectively for thin and thick epitaxial Pd_2Si layers formed on Si <III> substrates. The growth of $CrSi_2$ on thick Pd_2Si layers has been shown to be diffusion limited. Using a thin tungsten layer as an inert marker, silicon and palladium are found to diffuse with comparable fluxes during Pd_2Si growth. Silicon proves to be the only diffusing species in Pd_2Si during $CrSi_2$ growth on both epitaxial and polycrystalline Pd_2Si.

By sandwiching the Pd_2Si layer between Si and Cr, Pd and Ge, Ni and Si respectively, the flux of Si, Pd and Ni through Pd_2Si could be monitored. This provided a means of determining the atomic mobility of Si and Pd, and the grain boundary diffusivity of Ni in Pd_2Si. The mobility of Si is found to be orders of magnitude lower than that of Pd when extrapolated to around 200°C. The mobility of Si in polycrystalline Pd_2Si (activation energy 1.7 ± 0.2eV) is higher than in epitaxial Pd_2Si (activation energy 2.1 ± 0.2eV). These activation energy values suggest that Si is transported through Pd_2Si during $CrSi_2$ growth by vacancy diffusion. The activation energy of Ni grain boundary diffusion in polycrystalline Pd_2Si is 1.2 ± 0.2eV, which is also believed to be that of Pd grain boundary diffusion through Pd_2Si.

In using lateral diffusion couples, the atomic mobility of Pd (activation energy 1.1 ± 0.2eV) is also found to be much larger than that of Si. Very large distribution of grain size (up to 1μm) suggests that Pd diffusion is via vacancies in the Pd_2Si lattice. Although both Pd and Si diffuse through Pd_2Si during its conventional growth, the various experimental results suggest that the atomic mobility of Pd is much larger than that of Si in Pd_2Si when Pd and Si transport through Pd_2Si is isolated. The dominant transport mechanism for both Pd and Si proves to be vacancy diffusion.

to my parents

to my family

ACKNOWLEDGEMENTS

I am indebted to a number of people without whose assistance this work would not have been possible:

Dr R Pretorius, Ion-solid Interaction Division, Van de Graaff Group, National Accelerator Centre, for his guidance, participation and supervision of this investigation, and for his constructive criticism of this manuscript;

Dr C Comrie, Physics department, University of Cape Town, for his interest, support and supervision, and for labouring through this manuscript;

Prof J W Mayer, Materials Science and Engineering Department, Cornell University, USA, for granting me the opportunity to carry out research in his department. His stimulating discussion, encouragement and supervision, and the efforts to make my family's stay in Ithaca pleasant, are greatly appreciated;

the Director and staff of the Van de Graaff Group at the National Accelerator Centre (previously known as SUNI), for the use of the facilities;

the Director, Materials Science and Engineering Department, Cornell University, USA, for the use of the facilities and for financial support;

Ms J Jörgensen, Messrs S Hendricks and P Groenewald for figure preparation and photography;

Ms S Dayce for undertaking the arduous task of typing the manuscript;

the Council for Scientific and Industrial Research for financial assistance;

the Council of the University of the Western Cape for granting me leave;

members of the Mayer research group at Cornell University for assistance and stimulating discussions;

members of the Solid State Research Division at SUNI: Drs M O Simpson, A Botha and W Strydom, for their kind assistance;

my parents for their moral support and encouragement;

Julia, my wife, for her kind understanding and patience,

and finally to my son Edmund for his "understanding". He never hesitated to show his disapproval in my going to the laboratory. A typical conversation at the time of my departure was: "Where are you going Dad?" "To work." "Don't go, stay by me." Now that this is done, maybe we can make up for lost time.

INDEX

CHAPTER 1

INTRODUCTION

Extensive research into electronic materials has paved the way for the rapid evolution of electronic devices from the single planar silicon transistor in 1958 [1] to modern integrated circuits. Semiconductor-metal contacts are critical parts of integrated circuits. Most of the individual electronic devices (transistors and diodes) which make up an integrated circuit are connected by means of low resistance semiconductor-metal contacts (ohmic contacts). When the semiconductor is lightly doped, the contact can be rectifying (Schottky barrier contact). This particular property is exploited in the fabrication of Schottky barrier diodes which are used mainly as clamping diodes in integrated circuits. Various considerations such as controlled barrier height, good adhesion to silicon and low resistance ohmic contact have contributed to silicide-forming metals such as Pt, Pd, Ti or W being favoured for contacts in silicon-based integrated circuits. The excellent properties of these contacts are ascribed to the fact that during process temperature excursions, the metals react with the Si substrate to form metal silicides. The critical metal-silicon interface is thereby displaced to within the silicon substrate (silicon-silicide interface) where it is relatively free of contamination.

Although the physical and metallurgical aspects of these contacts have enjoyed tremendous attention, recent trends in device fabrication have aroused new interest in silicon/metal contacts. An example of a new development is the use of salicides

(self aligned metal silicide layers) in MOS devices [2]. A comprehensive understanding of silicon/metal interactions (metal silicide formation) is therefore essential to support the advancing silicon technology.

As the integrated circuit technology has developed, the metallization schemes used for contacts and interconnects have become more complex. A typical scheme is shown in Figure 1 - 1 which is a partial cross-section through an integrated circuit, showing an ohmic contact between the silicon and the silicide layer.

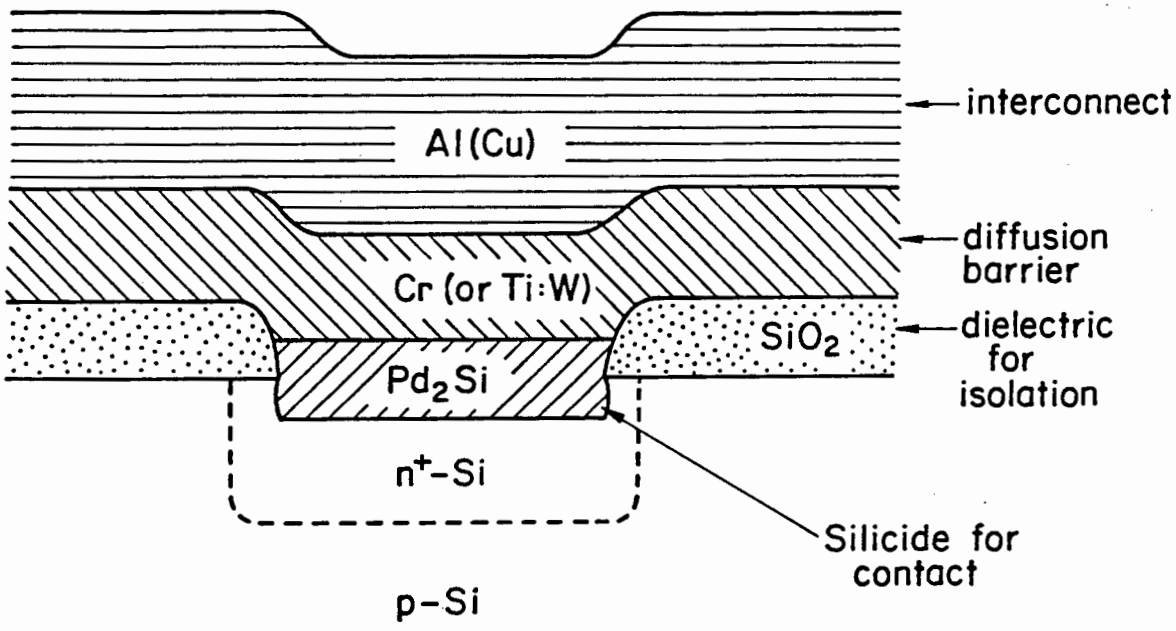

FIG 1-1 Partial cross-section through an integrated circuit showing a complex metallization scheme.

The feature to be observed is the metallization scheme at the contact window: $Si/Pd_2Si/Cr/Al$. The stability of such a multilayer scheme will contribute to the production yield and reliability of the device. Upon heat treatment during device

fabrication, interdiffusion in these multilayer structures is inevitable. A thorough knowledge and understanding of the thermal behaviour of such multilayer metal/silicon systems is therefore important for designing devices (selecting metallization schemes) and planning their processing (heat treatment).

Theoretical treatments of metal silicide formation upon thermal interdiffusion of metal/silicon binary couples have been documented by several authors [3-5]. The experimental research pertaining to metal silicide formation is extensive and is reviewed in several books and articles [3,6,7]. In contrast to this well covered area of metal silicide formation, multilayer metal silicide formation has not attracted as much attention. A theory for characterizing its complex growth kinetics is non-existant and experimental studies are limited.

The purpose of this investigation was to develope an approach for modelling silicide formation in bilayer metal silicon systems. Having tested the validity of the model with respect to a particular system, it was applied in developing a diffusion membrane technique for measuring the atomic mobility in compound thin films.

The experimental techniques used in this investigation are discussed in Chapter 2. The procedure for preparing thin film samples used for multilayer interdiffusion and lateral diffusion studies is followed by a brief description of the analytical techniques used to characterize the samples.

A model which characterizes silicide formation in bilayer metal/silicon sytems, is developed in Chapter 3. Various concepts used in this model are also relevant to binary metal/silicon systems. The theory of silicide formation in binary systems is therefore reformulated in order to establish these concepts. Subsequently, this theory is extended to the complex silicide formation in bilayer metal/silicon systems.

Experimental results of the thermal behaviour of the $Si/Pd_2Si/Cr$ systems are presented in Chapter 4. A comprehensive study of the growth kinetics of the outer silicide layer is reported. Various effects such as the microstructure and the thickness of the interposed silicide layer are investigated. The validity of the model developed in the previous chapter is checked by comparing its predictions with experimental results.

The flux ratio of the diffusing atom species during silicide growth, as determined with the aid of tungsten marker atoms, is discussed in Chapter 5. These results are evaluated in relation to previously published results of experiments in which different techniques were used.

The diffusion membrane technique which was used to determine the Si and Pd mobilities in Pd_2Si is fully described in Chapter 6. In addition, a study of Ni grain boundary diffusion in Pd_2Si is also reported. All these results are used to postulate a diffusion mechanism in Pd_2Si during its growth.

Lateral diffusion, which provides an elegant technique for determining the mobility of the individual components during compound growth, is treated in Chapter 7. The experimental results for the mobility of Pd in Pd_2Si are reported here.

Finally, the investigation as presented here is summarized and concluded in Chapter 8.

CHAPTER 2

EXPERIMENTAL

2.1 SPECIMEN PREPARATION

2.1.1 Preparation of thin film structures

Substrates of single crystal <100> and <111> oriented silicon and oxidized silicon (SiO_2) were used in these studies. The substrates approximately 1 cm^2, were degreased ultrasonically in ethanol, acetone, and trichloroethylene, and rinsed in deionized water. Prior to loading these samples into the high vacuum chamber for thin film deposition, the substrates were etched in a 20% HF solution to remove the native oxide layer. This step was omitted in the case of SiO_2 substrates.

After loading, the deposition chamber was evacuated to a background pressure better than 10^{-7} Torr. The pressure while depositing the various thin films by means of electron beam evaporation, was between 3 and 8 x 10^{-7} Torr. Multilayer thin film structures were obtained by depositing the various layers sequentially without breaking vacuum.

The thin film samples were then annealed in a quartz tube vacuum furnace. A vacuum better than 10^{-6} Torr was maintained during the anneal. When different samples required identical heat treatments, such samples were annealed simultaneously.

2.1.2 Preparation of lateral diffusion couples

Two different sample configurations were used for lateral diffusion studies namely device structures and island structures (see Chapter 7). The island structures were prepared as follows: A thin layer of silicon (or metal) approximately 500 Å thick was deposited onto SiO_2 or Al_2O_3 substrates. This was followed by the positioning of a Si mask over the substrate (in contact). The Si mask contained 400 x 400 μm^2 square openings etched into it. A relatively thick metal (or silicon) layer was deposited through the mask. After removal of the mask, the deposition was rounded off with a thin layer of SiO_2 (200 Å). This SiO_2 layer serves to limit contamination and to exclude surface diffusion during high temperature (400-700°C) anneals. The entire deposition was performed without breaking vacuum so as to reduce interfacial contamination. The above procedure resulted in a thin silicon (or metal) layer on an inert substrate with well defined islands of metal (or silicon) on it. Prior to annealing, the samples were cleaved into smaller pieces containing one or more islands.

The device structure samples were prepared similar to the procedures which are usually followed in the fabrication of electronic devices (see Fig. 2-1). A thin layer of oxide (500 Å) was grown on a Si <100> wafer in dry oxygen. Standard photolithographic procedure was followed to obtain a patterned layer of photoresist on the oxide layer. The pattern consisted of lines of widths varying between 5 and 40 μm. The

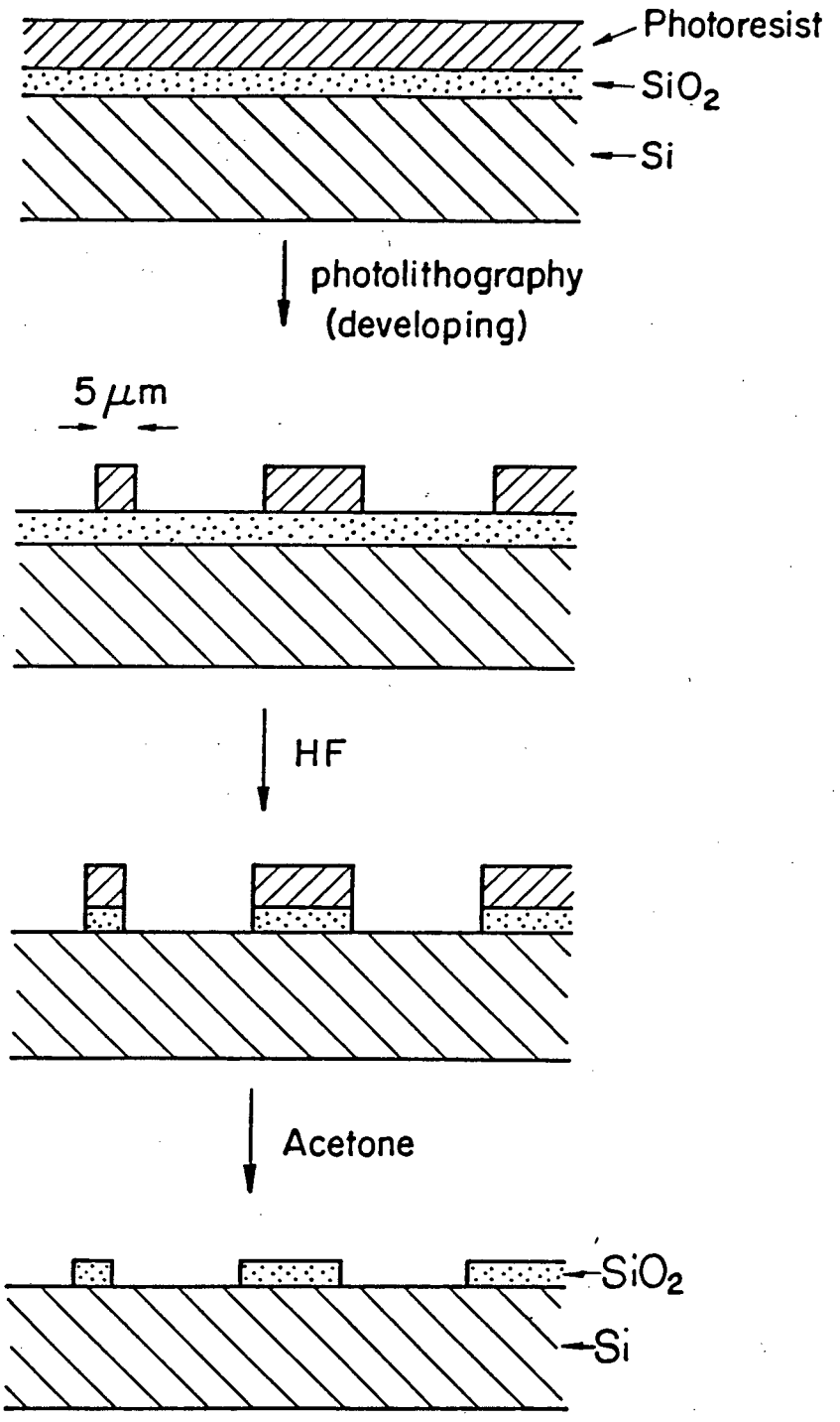

FIG 2-1 Sample preparation procedure for device structures for lateral diffusion studies.

samples were etched in 4% HF to expose the Si substrate through windows in the SiO_2 (lines patterned on it). Subsequently the patterned photoresist was removed by etching the samples in acetone. Finally, a thick metal layer (3000 Å) was deposited on these samples followed by a thin layer of SiO_2 (200 Å). The various stages of the sample preparation prior to metallization are schematically shown in Figure 2-1.

The samples used for lateral diffusion studies were etched in dilute HF after annealing, prior to characterization by S E M. This was done to remove the thin SiO_2 covering layer on the samples so that the silicon signal during Energy Dispersive Spectroscopy (E D S) is attributed to the initially deposited silicon only.

2.2 ANALYTICAL TECHNIQUES

2.2.1 Backscattering analysis

The use of ion backscattering for analysis of solids was first reported in 1913 by Geiger and Marsden [8]. The scattering effects were subsequently explained in terms of the Rutherford atomic model. The technique has developed in a well established tool for near-surface micro-analysis of materials. An excellent treatment of backscattering analysis is found in reference [9]. In brief, the technique consists of placing the sample to be analyzed in a beam of monoenergetic ions (H^+, He^+, or He^{++}) and analyzing the ions which are scattered from the sample with respect to their energy. A schematic representation of the geometry of sample and ion beam is shown in Fig. 2-2.

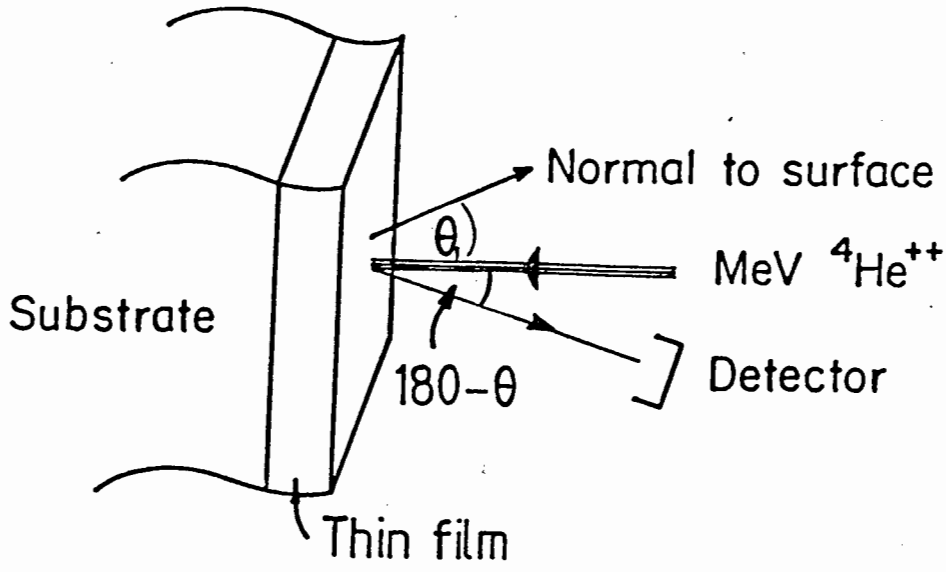

FIG 2-2 Sample and ion beam geometry for back-scattering analysis

The energy of the incident ions provided by an accelerator is typically between 1 and 3 MeV. Since the beam spot is about 1 mm², the samples to be analyzed should have uniform lateral composition over at least such a dimension. This technique was therefore not suitable for analyzing the structures used in the lateral diffusion studies (5-400 μm).

Since the scattering angle is very large (170°) and the energy of the projectile is a few MeV, screening by electrons can be ignored and the scattering is therefore fully described by the Rutherford scattering law. The maximum energy of the back-scattered particle is fixed by the mass of the projectile m, the mass of the target M, the energy of the projectile E_o and the scattering angle θ according to the formula:

$$E = E_o\left\{\frac{m\cos\theta + \sqrt{M^2 - (m^2\sin^2\theta)}}{m + M}\right\}^2 \qquad (2\text{-}1)$$

$$= E_o\, K$$

The energy of particles scattered back from heavy mass elements is therefore higher than that of particles which had interactions with light elements. A qualitative analysis of the sample is therefore possible. The differential scattering cross-section based on Coulomb interaction is given by:

$$\frac{d\sigma}{d\Omega} = \left(\frac{zZe^2}{2E_o\sin^2\theta}\right)^2 \frac{\{\cos\theta + [1 - \frac{m}{M}\sin\theta)^2]^{\frac{1}{2}}\}^2}{[1 - (\frac{m}{M}\sin\theta)^2]^{\frac{1}{2}}} \qquad (2\text{-}2)$$

where Ω is the finite solid angle spanned by the detector and Z and z are the atomic numbers of the target and projectile respectively. A consequence of the Z-dependence of the cross-section is that high Z-number (large mass) atoms will result in large signals which further enhances the spectroscopic ability of the technique.

Only a fraction of the incident ions interact with the surface atoms. Most projectiles penetrate the target sample and loose energy by electronic stopping. The energy loss is given by:

$$\Delta E = \int_0^{t/\cos\theta_1} dE/dx\; dx \qquad (2\text{-}3)$$

where t is the penetration depth and θ_1 the angle between the incident ion beam and the sample surface normal. The inte-

grand $^{dE}/_{dx}$ is a slowly varying function of energy. The ions which are backscattered from target atoms below the surface, leave the sample with an energy:

$$E = \left[E_o - \int_0^{t/\cos\theta_1} {}^{dE}/_{dx}\, dx\right] K - \int_{t/\cos\theta_2}^{o} {}^{dE}/_{dx}\, dx \qquad (2\text{-}4)$$

where θ_2 is the angle between a backscattered ion and the sample surface normal. A sample of infinite thickness will therefore give rise to a continuous energy spectrum whereas a thin film will correspond to an energy peak of which the width is a measure for the thickness of the film. This technique therefore yields depth information as well as qualitative information about the target.

The number of counts at a particular energy in the spectrum is determined by the atomic density of the target material at the corresponding depth. The height of the energy spectrum can therefore be used to determine the composition of the film at any depth. Two different elements at the same depth will have separate corresponding signals in the backscattering energy spectrum (provided the atomic numbers are sufficiently different). By comparing the heights of the two signals, the composition at that particular depth can be determined according to the approximate expression:

$$\frac{n_A}{n_B} = \frac{H_A/\sigma_A}{H_B/\sigma_B} \qquad (2\text{-}5)$$

where σ is the average differential scattering cross-section,

n_A/n_B is the composition ratio and, H_A and H_B are the heights of A and B signals respectively. By extending this principle to the entire compound layer, a composition profile can be established from the corresponding signals in the backscattering spectrum.

A typical but fictitious backscattering spectrum is shown in Figure 2-3. The arrows on the spectrum indicate the calculated energies of the ions scattered back from an atom of A,B or C if located on the surface on the sample. Note the relative

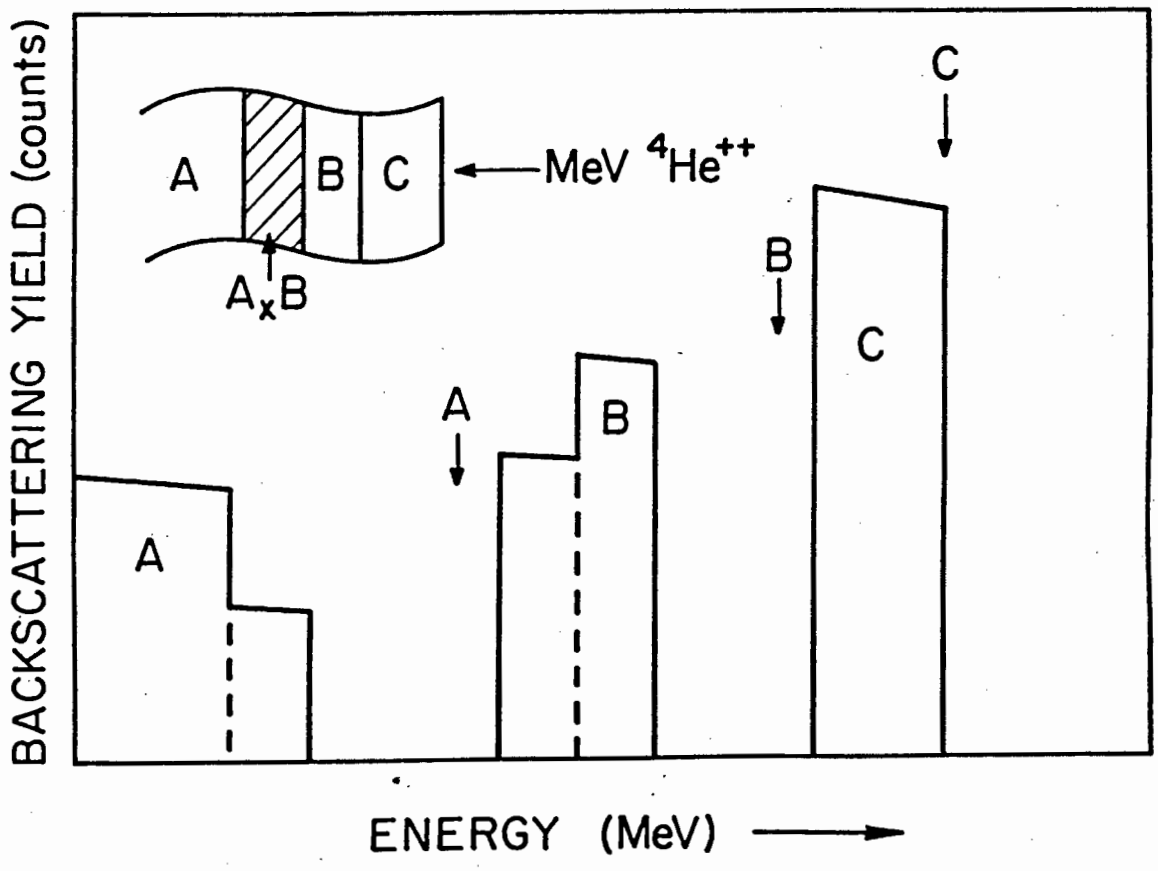

FIG 2-3 Fictitious backscattering spectrum of a multi-layer specimen

surface positions of the three elements and corresponding heights of each signal. It is seen that signals A and B are shifted to lower energies indicating that neither elements are at the surface. The high energy step in signal A and the low energy step in signal B correspond to the layer with composition A_xB, interposed between pure A and B. The composition ratio x is obtained from the heights of these steps.

In Fig. 2-3, the heights of the various signals are shown to increase slightly with decrease in energy. This is a consequence of (2-2) and (2-3). Equation (2-2) implies that the differential scattering cross-section is inversely proportional to the square of the energy of the colliding projectile. From (2-3) it follows that the energy of the colliding projectile deeper into the target is lower than that near the surface due to the energy loss. The differential scattering cross-section therefore increases with depth below the target surface (decrease in energy). If the atomic density of the film is uniform, the corresponding signal height in the backscattering spectrum will increase with decrease in energy $\left(\text{height} \propto \frac{1}{(\text{energy})^2}\right)$.

The ordered array of atoms in a crystal will influence the interaction between the mega-electron volt projectile ions and the atoms in the crystal. The collective nature of the interaction comes about because of the correlation of the scattering events from the ordered atoms. When the energetic ion approaches the atomic row at a glancing angle, the small deflection due to scattering from the first atom determines the

impact parameter (also scattering angle) of the collision with the second atom, and this in turn determines the impact with the third atom etc.. The net effect is the steering of the trajectories of the incident projectile ions. The steered or channelled ions are confined to the spaces or channels between the atomic rows. This channeling condition thus exists when the ion beam is almost parallel to the crystallographic axes and leads to a many-fold decrease in the number of close encounter collisions such as Rutherford backscattering [10]. The reduction in the yield of backscattered particles is therefore observed when a single crystal specimen is positioned in such a manner that a crystallographic axis is aligned with the projectile beam. Imagine a specimen consisting of a single crystal substrate covered with a thin film. Channeling of ion beams in the case of an aligned specimen, will then be evident in both the substrate and the thin film on its surface if the thin film is epitaxial. Channeling is therefore an elegant technique to establish the epitaxy of a grown or deposited thin film. Polycrystalline or amorphous materials do not show overall channeling effects.

The essential features of backscattering analysis have been described in order to illustrate its use for determining qualitative atomic depth profiles. The limitations of the technique are:

(1) The atomic mass resolution decreases with mass number. (It can however be compensated for by increasing the projectile energy).

(2) Small concentrations of low mass atoms in heavier mass matrices are difficult to detect because of the unfavourable ratio of scattering cross-sections.

(3) The depth resolution is typically 150-200 Å. This can be improved by increasing θ_1 and/or θ_2, although overlapping of signals will limit the maximum values of θ_1 and θ_2 which are useful.

2.2.2 X-ray diffraction

The phase indentification of the various compounds were made using Read and Guinier glancing angle X-ray diffraction cameras. In the case of the Read camera, the structure of the thin film sample is identified in a manner similar to that employed in the Debye Scherrer camera. The Guinier camera which is usually used for more accurate determination of lattice spacings operates on the principle of focusing cameras, in particular the Seemann Böhlin camera. The general principles of both these cameras are described in references [11,12]. Given the camera constant and diffraction line spacings, the phases were identified with the aid of ASTM (American Society for Testing Materials) powder compilations.

2.2.3 Electron microscopy

Two characteristic properties of the lateral diffusion zone need to be monitored when studying lateral phase growth - the lateral extent of the diffusion zone and the phase of the compounds formed. To this end, the scanning electron microscope

was used to obtain images of the surface morphology of the lateral diffusion structures. The phases of the compounds in the various diffusion regions were identified using energy dispersive spectroscopy while operating the microscope at 4-5 kV. Specially prepared samples which were sufficiently thin were analyzed by means of transmission electron diffraction for compound phase identification and by transmission electron microscopy for grain size measurements.

CHAPTER 3

THEORY OF SILICIDE GROWTH KINETICS

3.1 INTRODUCTION

A limited number of experimental studies on the planar growth of silicide layers in bilayer metal-silicon systems have been reported. A theory of the growth kinetics of such silicide layers has not been documented. Upon interdiffusion in binary couples (not necessarily metal-silicon) several intermediate compound phases can be formed. Multiphase growth in binary couples has been treated by several authors [5,13-15]. These theories are however not directly applicable to tertiary systems (e.g. bilayer metal-silicon systems) in spite of the analogy between the two systems(multiphase layers in binary couples and single phase layers in multilayer metal-silicon systems). It is therefore necessary to develope a theory specifically for silicide growth in bilayer metal-silicon systems in order to interpret experimental data. In this chapter the theory of the growth kinetics of a single phase in binary couples is reformulated. In the customary approach, a concentration gradient is considered to be the driving force for diffusion through the growing layer. The diffusion process is therefore characterized by the diffusion coefficient (section 3.2.3). A different approach will be followed in this work. Here the chemical potential gradient across the growing compound layer is considered to be the driving force for diffusion. The mobility now becomes the important parameter which characterizes the migration of the atoms during phase growth (section 3.2.5).

Various concepts will be developed in this section and will subsequently be applied when formulating a theory for the kinetics of layer growth in bilayer metal-silicon systems (section 3.3.3). This theory is in essence just an extension of the theory applicable to binary couples.

3.2 PHASE GROWTH IN METAL-SILICON BINARY COUPLES

3.2.1 Growth kinetics

Consider a binary couple consisting of metal (symbol M) and silicon (Si) which upon interdiffusion forms a compound M_ySi. The stoichiometric ratio of M to Si in M_ySi is represented by y. Planar growth of M_ySi is usually characterized by two parameters, the linear rate constant R_{M_ySi}, and the parabolic rate constant $\tilde{B}_{M_ySi}$. The linear rate constant describes the planar growth of the compound during the initial stage of M-Si interdiffusion. The thickness of the M_ySi layer L, grown in time t is then given by:

$$L = R_{M_ySi} \cdot t \qquad (3\text{-}1)$$

This stage of layer growth is commonly known as the linear kinetics stage since the grown layer thickness is linearly proportional to the time. The magnitude of the linear rate constant is usually determined by the rate of reaction at one of the two intefaces, Si/M_ySi or M_ySi/M.

Following the linear regime, the kinetics generally go over into the parabolic regime where:

$$L^2 = 2\tilde{B}_{M_ySi} \cdot t \qquad (3\text{-}2)$$

The phase growth process which was initially determined by an interfacial reaction, is slowed down and controlled by diffusion of M and/or Si through the growing M_ySi layer. In this regime, $L^2 \propto t$. The magnitude of the parabolic rate constant is determined by the mobility of the diffusing atoms. Every compound-forming interaction in binary couples is initially interfacial reaction controlled (linear) and ultimately becomes diffusion limited (parabolic). The stage at which the kinetics change over from linear to parabolic depends on the relative magnitudes of R_{M_ySi} and $\tilde{B}_{M_ySi}$. Both of these parameters are expected to be temperature dependent and can in principle be related to more fundamental properties of the interacting system. In this work the symbol $\tilde{B}$ rather than the commonly used $\tilde{D}$ is used for the parabolic rate constant since it will be shown further on that the parabolic rate constant is more closely related to the mobility B rather than to the diffusivity D.

In the following section, possible interfacial reactions will be proposed. These reactions form the basis for the model for compound growth which is to be developed in this chapter. The common approach for establishing relations between the growth rate constants and other fundamental properties of the interdiffusing couple, is the solving of the appropriate diffusion equation (section 3.2.3). A different approach will be followed in sections 3.2.4 and 3.2.5 where it will be shown how the chemical potential concept can be applied in establishing these relations. Particular attention will be given to the idea of

local thermodynamic equilibrium at the interfaces.

3.2.2 Interfacial reactions

During compound formation in binary couples, there is transport of atoms through the compound layer. Since atomic transport in solids is esentially due to the mobility of point defects, it is necessary to consider the reactions and equilibrium of the point defects in the compound phase. In non-ionic solid state reactions, for example metal/metal or metal/semiconductor reactions, electrical potential gradients do not occur so that point defects are not formed in pairs (Fenkel or Schottky pairs). Instead point defects are present as one type of defect only, which are vacancies in close-packed structures (e.g. Pd_2Si) [16]. Hence it will be assumed that the transport mechanism during M_ySi formation is vacancy duffusion. For the sake of simplicity, silicon will be considered to be the only diffusing species. In the event that M or both M and Si diffuse, the treatment which is to follow can easily be adapted.

Proceeding, specific atom/vacancy reactions are postulated at the two interfaces, following an approach commonly used in metal oxidation studies [17].

M_ySi/M interface

A metal atom from the M phase attaches itself to the M_ySi phase in a regular M sublattice position, thereby creating a Si vacancy in the Si sublattice.

$$M \rightarrow M^{x} + V_{Si} \qquad \Delta g^{M} \qquad (3\text{-}3)$$

where M represents a metal atom from metal lattice

M^{x} represents a metal atom in the M_y Si lattice on a M sublattice site.

V_{Si} represents a Si vacancy in the M_ySi lattice (Si sublattice)

Δg^{M} is the partial molar free energy change associated with the reaction at the metal/silicide interface.

Since new M atoms join the existing M_ySi phase, this interface is referred to as the advancing interface. The free energy change is defined in terms of the standard (equilibrium) free energy change $\Delta g^{M,e}$ (see reference 18):

$$\Delta g^{M} = \Delta g^{M,e} + RT \ln \left\{ \frac{\left[M^{x}\right]\left[V_{Si}\right]_{M}}{[M]} \right\} \qquad (3\text{-}4)$$

where R is the universal gas constant and;

T is the temperature

Here the brackets [] represent the concentration e.g. $\left[M^{x}\right]$, the concentration of M^{x}. The subscript in $\left[V_{Si}\right]_{M}$ indicates that it is a concentration measured at the interface near the M layer (M_ySi/M interface). The standard free energy change (partial molar) is, in turn, defined in terms of the equilibrium concentrations:

$$\Delta g^{M,e} = -RT \ln \frac{[M^x]^e \, [V_{Si}]^e_M}{[M]^e} \qquad (3\text{-}5)$$

where $[M^x]^e$ is the concentration of M^x when local equilibrium prevails at the interface. The superscript e in $\Delta g^{M,e}$ or $[M]^e$ indicates that these are the magnitudes of the parameters measured when equilibrium prevails. The vacancy concentration in metals and metallic compounds is typically 10^5 cm^{-3} compared to the atomic concentration of metals around 10^{23} cm^3 [16]. Even if the vacancy concentration would increase many-fold, the atomic concentration can be considered to remain approximately constant. The difference between the concentrations $[V_{Si}]$ and $[V_{Si}]^e$ can therefore be significant, while $[M^x]$ or $[M]$ can be considered not to deviate from their equilibrium values. Therefore:

$$[M] = [M]^e$$

and

$$[M^x] = [M^x]^e \qquad (3\text{-}6)$$

The equalities (3-6) hold even when thermodynamic equilibrium does not prevail at the interface. From (3-4), (3-5) and (3-6):

$$\Delta g^M = - RT \ln \frac{[V_{Si}]^e_M}{[V_{Si}]_M} \qquad (3\text{-}7)$$

It follows from (3-7) that Δg^M is zero when local equilibrium prevails at this interface ($[V_{Si}]_M = [V_{Si}]^e_M$).

The Si vacancy concentration is initially different from $\left[V_{Si}\right]_M^e$ and approaches its equilibrium value as described by a first order differential equation, assuming first order kinetics in equation (3-3):

$$\frac{d}{dt}\left[V_{Si}\right]_M = k_M\left\{\left[V_{Si}\right]_M^e - \left[V_{Si}\right]_M\right\} \qquad (3\text{-}8)$$

where k_M is the reaction rate constant.

Si/M_ySi interface

The Si vacancies which were created at the M_ySi/M interface during M_ySi phase growth do not accumulate there but migrate to the Si/M_ySi interface where they are annihilated. The Si layer provides Si atoms which fill the Si vacancies in the silicide layer near the Si/M_ySi interface as the vacancies arrive. The postulated interfacial reaction is:

$$Si + V_{Si} \rightarrow Si^x \qquad \Delta g^{Si} \qquad (3\text{-}9)$$

Following the approach used at the M_ySi/M interface, the time variation of the vacancy concentration is given by:

$$\frac{d}{dt}\left[V_{Si}\right]_{Si} = k_{Si}\left\{\left[V_{Si}\right]_{Si}^e - \left[V_{Si}\right]_{Si}\right\} \qquad (3\text{-}10)$$

An expression analogous to (3-7) can be found for the free energy change associated with the interfacial reaction (3-9):

$$\Delta g^{Si} = -RT \ln \frac{\left[V_{Si}\right]_{Si}}{\left[V_{Si}\right]^{e}_{Si}} \qquad (3\text{-}11)$$

The equilibrium (standard) free energy change associated with reaction (3-9) is given by:

$$\Delta g^{Si,e} = -RT \ln \frac{\left[Si^{x}\right]^{e}}{\left[Si\right]^{e}\left[V_{Si}\right]^{e}_{Si}} \qquad (3\text{-}12)$$

which is analogous to (3-5).

The combination of the reactions at the two interfaces (3-7) and (3-10) represents the formation reaction of the M_ySi phase.

$$M + Si \rightarrow M^{x} + Si^{x}$$

The sum of the standard molar free energy changes in (3-5) and (3-12) (i.e. $\Delta g^{M,e}$ and $\Delta g^{Si,e}$) is therefore related to the standard free energy change of formation ΔG^{o}_{f} of the M_ySi phase. The vacancy concentration $\left[V_{Si}\right]_{M}$ and $\left[V_{Si}\right]_{Si}$ at the two interfaces are not equal. When combining (3-7) and (3-10) to obtain the overall formation reactions as above, this fact was ignored. It will therefore be found that

$$\Delta g^{M,e} + \Delta g^{Si,e} > \Delta G^{o}_{f}$$

It can be shown that:

$$\Delta g^{M,e} + \Delta g^{Si,e} = \Delta G^{o}_{f} + \Delta G^{o}_{f} / q^{s}_{Si}$$

where q^{s}_{Si} is the stoichiometric atomic fraction of Si in M_ySi.

3.2.3 Diffusion through the compound

The magnitude of $[V_{Si}]$ at the two interfaces viz. $[V_{Si}]_{Si}$ and $[V_{Si}]_{M}$ are not equal nor do they vary independently of each other. The two equations (3-7) and (3-10) are incorporated into the boundary conditions (source and sink equations) of the diffusion equation (Fick's second law) in the growing compound layer, where D_V is the vacancy diffusion coefficient [19]:

$$\frac{\partial}{\partial t}[V_{Si}] = D_V \frac{\partial^2}{\partial x^2}[V_{Si}] \qquad (3\text{-}14)$$

The boundary conditions are essentially the expanded continuity equations at the interfaces. At the Si/M_ySi interface:

$$\frac{\partial}{\partial t}[V_{Si}]_{Si} = D_V \frac{\partial^2}{\partial x^2}[V_{Si}]_{Si} - k_{Si}[V_{Si}]_{Si}$$

The last term on the right hand side represents the rate of annihilation of the vacancies. At the M_ySi/M interface:

$$\frac{\partial}{\partial t}[V_{Si}]_{M} = D_V \frac{\partial^2}{\partial x^2}[V_{Si}]_{M} + k_M [V_{Si}]_{M} - \frac{\partial}{\partial x}[V_{Si}]_{M} \frac{dL}{dt}$$

The second term on the r.h.s. represents the rate of vacancy production whereas the third term represents the vacancies incorporated in the newly grown layer of thickness dL formed in the time interval dt. The mathematical problem in (3-14) is commonly referred to as a moving boundary problem. The solution of (3-14) with the accompanying boundary conditions is complex and no exact (analytical) solution has been reported. The linear and parabolic growth rates would follow from its solution. A solution to equation (3-14) will not be attempted here.

Deal et al. and Gösele et al. have treated the problem of planar phase growth in binary couples. Having made gross approximations, the authors arrived at similar solutions to the moving boundary problem [5,20]. The essential feature of their solutions is that in the initial stage of phase formation, the growth is nearly linear and it eventually becomes parabolic. There are however important differences in the approach followed here and that taken in references [5,20]. In this work the vacancies (Si) have been considered as the migrating species as well as the reaction rate determining species. The atoms are considered as the migrating species in references [5,20] and the authors do not propose specific interfacial reactions. The rate constants in (3-8) and (3-10) and the diffusion coefficient in (3-14) will therefore have different meanings as compared to similar parameters in references [5,20].

If vacancy diffusion is the transport mechanism then the atomic diffusion coefficient will be proportional to the vacancy concentration. In applying Fick's first law in [5,20], the authors assume an atomic concentration gradient which implies a significant vacancy concentration gradient. This makes the diffusion coefficient to be used in the diffusion equation strongly variable. Fick's second law in the form of (3-14) is no longer applicable so that the solution in [5] and [20] could be erroneous. In this work the diffusion coefficient of vacancies is assumed to be independent of the vacancy concentration, so that (3-14) remains valid when the migrating vacancies are considered.

From the solution of the diffusion equation (3-14) relations between R_{M_ySi}, $\tilde{B}_{M_ySi}$, k_{Si}, k_M, and D_V are established. Assuming that D_V, k_{Si}, and k_M are known in the M_ySi phase, it is still not possible to determine $\tilde{B}_{M_ySi}$ since the concentration gradient needs to be known too. This makes the theories in [5] and [20] inadequate for any quantitative determinations although the qualitative predictions of the theories are in agreement with experimental results.

A different approach will be taken in the following sections where the driving force for diffusion will be considered. Instead of solving the diffusion equation, the chemical potential difference (driving force for diffusion) across the growing compound phase is computed and from it, the linear and parabolic rate constants determined respectively.

3.2.4 Chemical potential difference

Consider a binary couple M (for metal) and Si, which has partially interdiffused with the formation of M_ySi. A schematic of this couple is shown in Figure 3-1. The free energy of this system is illustrated in Figure 3-2. Each phase in the system is represented by a free energy vs. composition curve. The minimum free energy of M_ySi corresponds to the free energy of formation ΔG_f^o. The shapes of all three curves are not known but they are in principle determined by the defect formation energy in M_ySi, Si, and M respectively [21]. Although ΔG_f^o is relatively insensitive to temperature variations, the width and curvature of the curves are strongly influenced by the temperature.

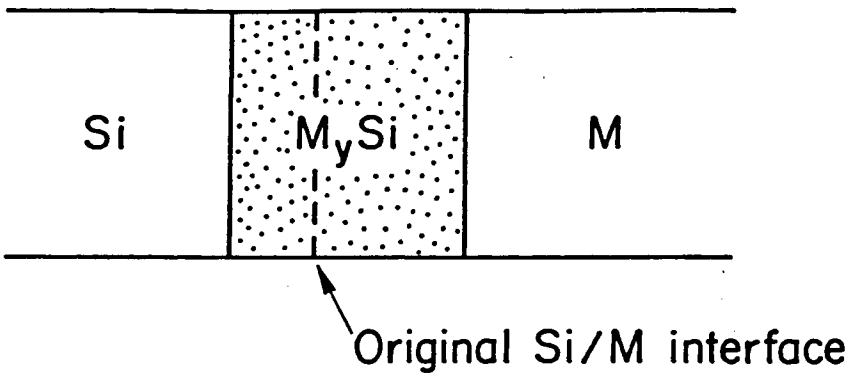

FIG 3-1 Schematic of a partially reacted Si/M binary couple.

When the M_ySi phase is isolated (complete consumption of both Si and M during M_ySi growth), the M/Si atomic ratio is determined by the original quantities of M and Si and can be anywhere in the phase field (between B and C in Figure (3-2)). However, when M_ySi is bounded by M and Si as in Figure 3-1, the situation is very different. A necessary condition for local equilibrium at the two interfaces is that the chemical potential of M and Si at the two phase boundaries must be unique. The values of the chemical potentials are obtained by constructing common tangents to the free energy curves of the two phases which co-exist in equilibrium. The common tangent construction technique is based on the relation between chemical potential and free energy:

$$\mu_M = \frac{\partial G}{\partial q_M}$$

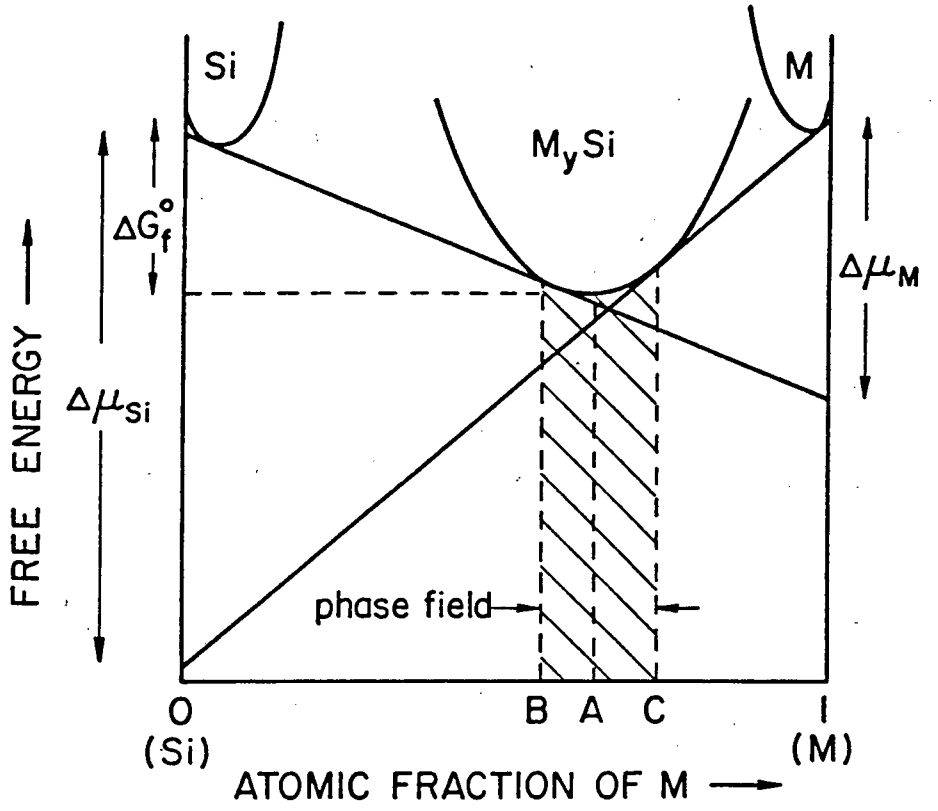

FIG 3-2 Free energy versus composition diagram showing the pure and intermediate phases.

where μ_M is the chemical potential of M, G is the free energy per gram atom and q_M is the atomic fraction of M [21]. The contact points of the common tangents determine the M/Si atomic ratios at the two interfaces. The M_ySi will therefore have an atomic ratio B near the Si/M_ySi interface and a ratio C near the M_ySi/M interface (see Figure 3-2). The M_ySi phase region is thus said to be Si-rich near the Si/M_ySi phase boundary and M-rich near the M_ySi/M phase boundary. The atomic ratio in the M_ySi phase region will vary between these two extremes, B and C. This variation in M/Si atomic ratio can be accommodated in various ways, in particular through point defects (vacancies

and interstitials) in the M and Si sub-lattice respectively. In a compound with a close-packed structure, these defects are expected to be vacancies. The bulk of the M_ySi layer will therefore deviate slightly from stoichiometry with an atomic ratio, different (less than and greater than) from the value indicated by A in Figure 3-2.

The chemical potentials of M and Si at the phase boundaries are represented by the intercepts of the common tangents at the M and Si free energy axes respectively. The driving forces for diffusion of M and Si through M_ySi are the respective equilibrium chemical potential differences across the M_ySi region which can be expressed as follows:

$$\Delta\mu_M^e \cong \Delta G_f^o/q_M^s \qquad (3\text{-}15(a))$$

$$\Delta\mu_{Si}^e \cong \Delta G_f^o/q_{Si}^s \qquad (3\text{-}15(b))$$

where ΔG_f^o is the standard free energy of formation of M_ySi and q_M^s and q_{Si}^s are the stoichiometric atomic fractions of M and Si in the M_ySi compound, with

$$q_M^s/q_{Si}^s = y$$

and

$$q_M^s + q_{Si}^s = 1$$

The equilibrium chemical potential differences $\Delta\mu_M^e$ and $\Delta\mu_{Si}^e$ are illustrated in Figure 3-2.

The construction of the common tangent to the free energy curves is justified, assuming that local thermodynamic equilibrium exists at the interface. This implies that the two different phases co-exist in equilibrium at the interface. The chemical potential of say Si in Si is therefore equal to the chemical potential of Si in M_ySi near the Si/M_ySi interface. The equilibrium chemical potential difference of Si across the M_ySi layer is therefore equal to the difference between the chemical potential of Si in the Si layer and Si in the M layer.

It was pointed out in section 3.2.1 that during the initial stage of interdiffusion (linear regime) the concentrations of Si vacancies at the interfaces are in the process of approaching their equilibrium values so that local equilibrium does not prevail. The equilibrium chemical potential differences $\Delta\mu^e_{Si}$ and $\Delta\mu^e_M$ as given by (3-15) are then no longer the driving forces for diffusion through the growing compound layer M_ySi. The difference between the chemical potential of M in the M and Si phases respectively is approximately given by (3-15(a)), irrespective of whether equilibrium prevails at the phase boundaries. Similarly the difference between the chemical potential of Si in the Si and M phases is given by (3-15(b)).

It is necessary to consider the free energy balance for the enitre M_ySi growth process in order to compute the driving force for diffusion under non-equilibrium conditions. Three sub-processes which together, constitute the growth process,

can be characterized. These are the reaction at the Si/M_ySi interface, the migration of Si atoms (migration of Si vacancies in the opposite direction) and the reaction at the M_ySi/M interface. The partial molar free energy change of Si for the growth process ($\Delta\mu^e_{Si}$) is the sum of the free energy changes associated with each sub-process:

$$\therefore \Delta\mu^e_{Si} = \Delta g^{Si} + \Delta\mu_{Si} + \Delta g^{M} \qquad (3\text{-}16(a))$$

The free energies Δg^{Si} and Δg^{M} are associated with the interfacial reactions in (3-9) and (3-3) respectively and expressions for these free energy changes, previously derived, are given once more (see (3-11) and (3-7)):

$$\Delta g_{Si} = -RT \ \ell n \frac{\left[V_{Si}\right]_{Si}}{\left[V_{Si}\right]^e_{Si}}$$

$$\Delta g_{M} = -RT \ \ell n \frac{\left[V_{Si}\right]^e_{M}}{\left[V_{Si}\right]_{M}}$$

The chemical potential difference of Si across the M_ySi layer $\Delta\mu_{Si}$ (also referred to as the partial molar free energy change) is seen to be less than or equal to the equilibrium chemical potential difference $\Delta\mu^e_{Si}$ when (3-16(a)) is rewritten as:

$$\Delta\mu_{Si} = \Delta\mu^e_{Si} - \Delta g_{Si} - \Delta g_{M} \qquad (3\text{-}16(b))$$

During the initial stage of phase growth (linear regime), equilibrium does not prevail at one of the two interfaces. (It is unlikely that both interfacial reactions will have the same

reaction rate constant and subsequently approach equilibrium at the same rate). The growth process is therefore entirely controlled by a single interfacial reaction (say (3-9) at the Si/M_ySi interface). The associated free energy change will be Δg_{Si} as given in (3-11). Since local equilibrium prevails at the M_ySi/M interface, the associated free energy change Δg_M is zero. In the extreme case where diffusion through the M_ySi layer is very rapid the change in vacancy concentration at the interface is independent of the flux through the growing layer.

In order to determine the time dependence of the driving force for diffusion $\Delta\mu_{Si}$, it is necessary to determine the time dependence of Δg_{Si} from the differential equation:

$$\frac{d}{dt}\left[V_{Si}\right]_{Si} = k_{Si}\left\{\left[V_{Si}\right]^{e}_{Si} - \left[V_{Si}\right]_{Si}\right\} \quad (3\text{-}10)$$

Solution to this equation is:

$$\left[V_{Si}\right]_{Si} - \left[V_{Si}\right]^{e}_{Si} = \left\{\left[V_{Si}\right]^{o}_{Si} - \left[V_{Si}\right]^{e}_{Si}\right\}e^{-k_{Si}t}$$

Here $\left[V_{Si}\right]^{o}_{Si}$ is the initial value of $\left[V_{Si}\right]_{Si}$, i.e. its value in the very early stage of phase growth. Since local equilibrium is assumed at the other interface (as a result of a fast interfacial reaction), the entire layer will initially have a vacancy concentration $\left[V_{Si}\right]^{e}_{M}$, being the equilibrium concentration at the M_ySi/M interface. Therefore:

$$\left[V_{Si}\right]^{o}_{Si} = \left[V_{Si}\right]^{e}_{M}$$

so that

$$\left[V_{Si}\right]_{Si} - \left[V_{Si}\right]_{Si}^{e} = \left\{\left[V_{Si}\right]_{M}^{e} - \left[V_{Si}\right]_{Si}^{e}\right\} e^{-k_{Si}t}$$

Furthermore the M_ySi layer is relatively silicon-rich (low Si vacancy concentration) near the Si/M_ySi interface and metal-rich (high Si-vacancy concentration) near the M_ySi/M interface so that

$$\left[V_{Si}\right]_{M}^{e} >> \left[V_{Si}\right]_{Si}^{e}$$

In the initial stage of layer growth, the non-equilibrium Si vacancy concentration is close to its initial value $\left[V_{Si}\right]_{M}^{e}$ and therefore also much greater than $\left[V_{Si}\right]_{Si}$ so that

$$\left[V_{Si}\right]_{Si} \simeq \left[V_{Si}\right]_{M}^{e} \; e^{-k_{Si}t}$$

which can be rewritten as

$$\ell n\left[V_{Si}\right]_{Si} = \ell n\left[V_{Si}\right]_{M}^{e} - k_{Si}t$$

and hence:

$$\ell n\frac{\left[V_{Si}\right]_{Si}}{\left[V_{Si}\right]_{Si}^{e}} = \ell n\left[V_{Si}\right]_{M}^{e} - \ell n\left[V_{Si}\right]_{Si}^{e} - k_{Si}t$$

Substituting in (3-11):

$$\Delta g_{Si} = -RT\,\ell n\left[V_{Si}\right]_{M}^{e} + RT\,\ell n\left[V_{Si}\right]_{Si}^{e} + RTk_{Si}t \qquad (3\text{-}17)$$

It can be shown that the first two terms on the rhs in (3-17) reduce to $\Delta\mu_{Si}^{e}$ (see appendix B). Equation (3-17) then becomes:

$$\Delta g_{Si} = \Delta\mu_{Si}^{e} + RT\,k_{Si}t.$$

Substituting in (3-16(b)) with $\Delta g^M = 0$:

$$\Delta\mu_{Si} = -RTk_{Si}t \qquad (3\text{-}18)$$

The magnitude of $\Delta\mu_{Si}$ is seen to increase linearly with time ($\Delta\mu_{Si}$ is negative and decreases) and has an initial value of zero. The free energy balance as suggested by (3-16) is graphically illustrated in Figure 3-3. The various positions (direction) of the tangents to the M_ySi free energy curve, as the layer growth progresses, is now described, starting from the very early stage of layer growth. If the two interfacial

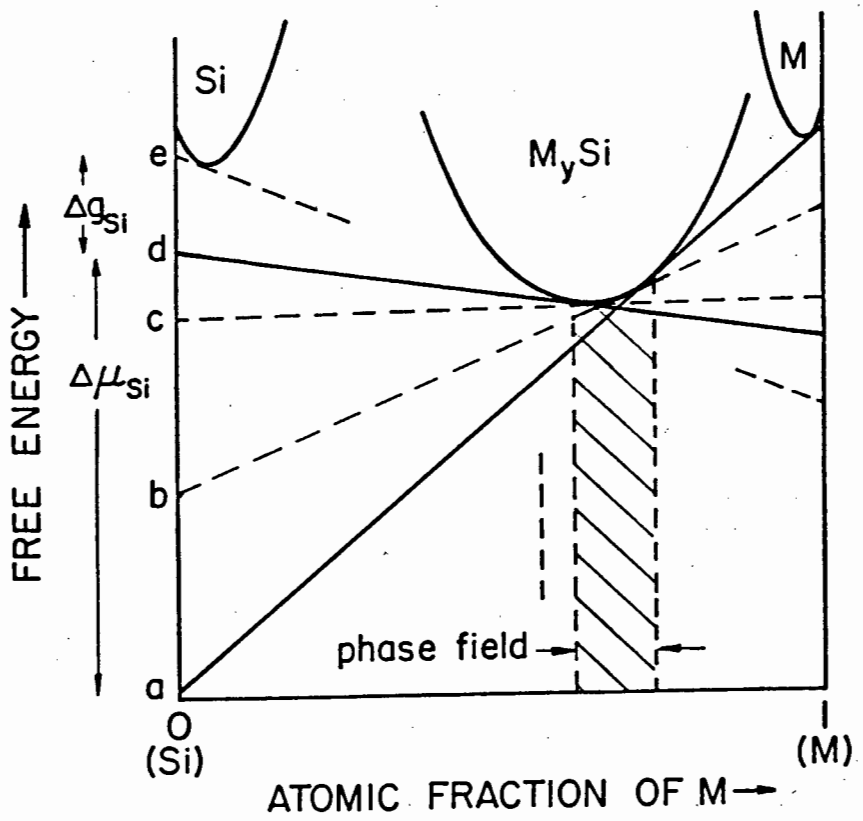

FIG 3-3 Tangents drawn for the case of non-equilibrium at one of the interfaces. Local equilibrium is assumed at the M_ySi/M interface so that one of the tangents is common to the free energy curves of the two phases in equilibrium.

reactions were equally slow (an unusual case), the tangents to the M_ySi free energy curve would initially be horizontal, intercepting the Si free energy axis in c (minimum free energy of M_ySi). However, with a fast reaction at the M_ySi/M interface the two tangents to the M_ySi free energy curve will immediately move to position indicated by a (local equilibrium at the M_ySi/M interface). The one common tangent will remain in this position implying local equilibrium at the M_ySi/M interface. The other tangent will move through positions b,c,d and finally e when equilibrium at the Si/M_ySi interface is also achieved. During this process the magnitude of Δg_{Si} decreases while the magnitude of $\Delta\mu_{Si}$ increases (linearly with time during the initial stage). Once equilibrium is reached at both interfaces ($\Delta g_{Si} = 0$ and $\Delta g_M = 0$) the chemical potential difference of Si across the M_ySi layer is equal to the equilibrium value $\Delta\mu^e_{Si}$.

In the following section it will be shown how the growth kinetics are controlled by the chemical potential difference. The two extreme cases will be considered namely the initial non-equilibrium stage when one interfacial reaction completely controls the growth, and the equilibrium stage where diffusion limits the growth.

3.2.5 Mobility and the growth rate constants

The flux of diffusing atoms J as a result of a concentration gradient ∇C is given by Fick's first law [19]:

$$J = -D\nabla C \qquad (3\text{-}19(a))$$

where D is the diffusion coefficient of the diffusing atoms.

A more general expression for the flux is the phenomenological equation attributed to Onsager [19]:

$$J = -BC\nabla\mu \qquad (3\text{-}19(b))$$

where C is the concentration, B the mobility and $\nabla\mu$ the gradient of the chemical potential of the diffusant.

It was pointed out in 3.2.2 that relations such as (3-19(a)) which involve concentration gradients are inadequate for quantitative determinations since the concentration gradients across the compound layers are usually unknown. The alternative expression (3-19(b)) is more attractive since the chemical potential is a more accessible parameter as was shown in section 3.2.3. The chemical potential gradient $\nabla\mu$ is effectively the driving force for diffusion, also in cases where the concentration gradient is negligible. A consequence of using (3-19(b)) rather than (3-19(a)) is that the mobility B rather than the diffusivity D, co-determines the flux. These two parameters have different meanings and should not be confused. They are inter-related:

$$D = RTB \left\{1 + \frac{\partial(\ell n\ \gamma)}{\partial(\ell n\ C)}\right\} \qquad (3\text{-}20)$$

where γ is the activity coefficient [19]. The symbols R and T have their usual meanings. The activity coefficient is not a well known function and is very often and incorrectly, (e.g. in [20]) assumed to be constant (indepedent of concentration) so that D = RTB. This could introduce serious errors into calculations based on (3-19(a)).

The mobility B is fundamentally defined as the proportionality constant between the driving force for diffusion ($\Delta\mu$ in equation (3-19(b))) and the drift velocity of the diffusing atoms (flux in equation (3-19(b))). The physical significance of the mobility is realized by considering the diffusion process on an atomic scale and consequently deriving an expression for B from first principles. This is done in Appendix C. The mobility B is shown to have an Arrhenius-type of temperature dependence, similar to that of the diffusion coefficient D. The activation energy associated with the mobility is however shown to be different to that associated with the diffusion coefficient.

During the growth of M_ySi, a layer of thickness L is formed in time t. The diffusing species are still considered to be silicon only. There is no significant built-up of Si concentration in the M_ySi layer since it is stoichiometric or near-stoichiometric. The Si flux J_{Si} should therefore be uniform. If the growth direction is indicated by x, then we may integrate (3-19(b)) with respect to x:

$$\int_0^L J_{Si}\,dx = -\int_0^L B_{Si}[Si^x]\frac{\partial \mu_{Si}}{\partial x}dx$$

where $[Si^x]$ is the Si concentration in the M_ySi layer.

$$J_{Si}\int_0^L dx = -B_{Si}[Si^x]\int_0^L \frac{\partial \mu_{Si}}{\partial x}dx$$

$$J_{Si}L = -B_{Si}[Si^x]\Delta\mu_{Si} \qquad (3\text{-}21)$$

The parameter $\Delta\mu_{Si}$ represents the chemical potential difference of the diffusant (Si) across the M_ySi layer of thickness L. It is not necessarily equal to its equilibrium value $\Delta\mu^e_{Si}$ (see 3.2.4). The flux is in turn related to the growth rate

$\frac{dL}{dt}$ of the M_ySi layer:

$$J_{Si} = [Si^x] \frac{dL}{dt} \qquad (3\text{-}22)$$

Combining (3-21) and (3-22):

$$LdL = -B_{Si} \Delta\mu_{Si} dt \qquad (3\text{-}23)$$

The growth kinetics (time dependence of L) are now determined in the two limiting cases:

Linear regime

On substituting (3-18) for $\Delta\mu_{Si}$ in (3-23) and integrating with respect to t:

$$LdL = RT\, k_{Si} B_{Si}\, t\, dt$$

$$\therefore \quad L = \sqrt{RT\, k_{Si} B_{Si}}\, t \qquad (3\text{-}24)$$

The thickness of the M_ySi layer therefore increases linearly with time and the linear rate constant is given by:

$$R_{M_ySi} = \sqrt{RT\, B_{Si} k_{Si}} \qquad (3\text{-}25)$$

Parabolic regime

The equilibrium value of $\Delta\mu_{Si}$, i.e. $\Delta\mu^e_{Si}$ is substituted in (3-23). Upon integration:

$$\frac{L^2}{2} = -B_{Si} \Delta\mu^e_{Si}\, t \qquad (3\text{-}26)$$

This is the equation of a parabola. The thickness L increases linearly with the square root of time and the parabolic rate constant is given by:

$$\tilde{B}_{M_ySi} = \frac{L^2}{2t}$$

$$\tilde{B}_{M_ySi} = -B_{Si} \cdot \Delta\mu^e_{Si} \qquad (3\text{-}27)$$

It is seen that the parabolic rate constant is a direct measure for the atomic mobility of the diffusant (when one of the two components is the dominant diffusing species). Although it appears in (3-27) that the parabolic rate constant is negative, it should be borne in mind that the chemical potential difference $\Delta\mu^e_{Si}$ is negative (diffusion from a high to a low potential). The negative sign of $\Delta\mu^e_{Si}$ is also evident from (3-15) since the free energy change associated with exothermic compound formation is negative.

On comparing (3-25) to the expressions obtained in [5,20], it is seen that they are different even if the incorrect substitution D = RTB is made (see 3-20)). The expression for the parabolic rate constant in (3-27) also differs from those derived by the authors in [5,20]. In (3-27) it is seen that the parabolic rate constant is proportional to the atomic mobility ($\Delta\mu^e_{Si}$ is almost independent of temperature) whereas the authors in [5,20] found the rate constant to depend on the diffusion coefficient. The mobility of an atom is a measure of the ease with which the atom can migrate when the oppor-

tunity arises (vacancy is available). The activation energy determined from the parabolic growth rate thus reflects the migration energy of the vacancies when vacancy diffusion is the transport mechanism. The activation energy of atomic diffusion on the other hand is the resultant of the migration and formation energies of the vacancy [19]. This explains why the activation energy obtained from parabolic rate measurements is much lower than the values usually associated with self diffusion processes. The suprisingly low activation energy has up to now been explained in terms of grain boundary diffusion rather, than vacancy diffusion, being the dominant transport mechanism.

The approach followed above, where the mobility rather than the diffusivity is considered as the controlling parameter, is seen to result in relatively simple and usefull expressions for the rate constants. The concepts developed will subsequently be used in extending the approach to silicide formation during bilayer metal-silicon interdiffusion.

3.3 BILAYER METAL/SILICON INTERDIFFUSION

3.3.1 Sequence of silicide formation

Silicide formation in bilayer metal-silicon systems is complex because of the various competing reactions (metal-silicon and metal-metal interdiffusion). The complete reaction can usually be divided into a number of pseudo-binary interdiffusion reactions. Consider the system Si/M1/M2 where M1 and M2 are two different metal layers on a silicon substrate. The

first stage of the silicide formation reaction will be determined by the relative reactivities of Si/M1 and M1/M2 couples. The metal-metal interdiffusion case will not be considered here since it leads to the silicide formation in tertiary systems, which is outside the scope of this work. During the Si/M1 interdiffusion, the multilayer system is transformed to Si/$M1_y$Si/M2 (see Figure 3-4). The M2 layer is inactive during this process so that the growth kinetics of $M1_y$Si are similar to the binary couple case as described in section 3.2.1.

Upon subsequent interdiffusion, three of the possible interactions can be distinguished and these are illustrated in Figure 3-4.

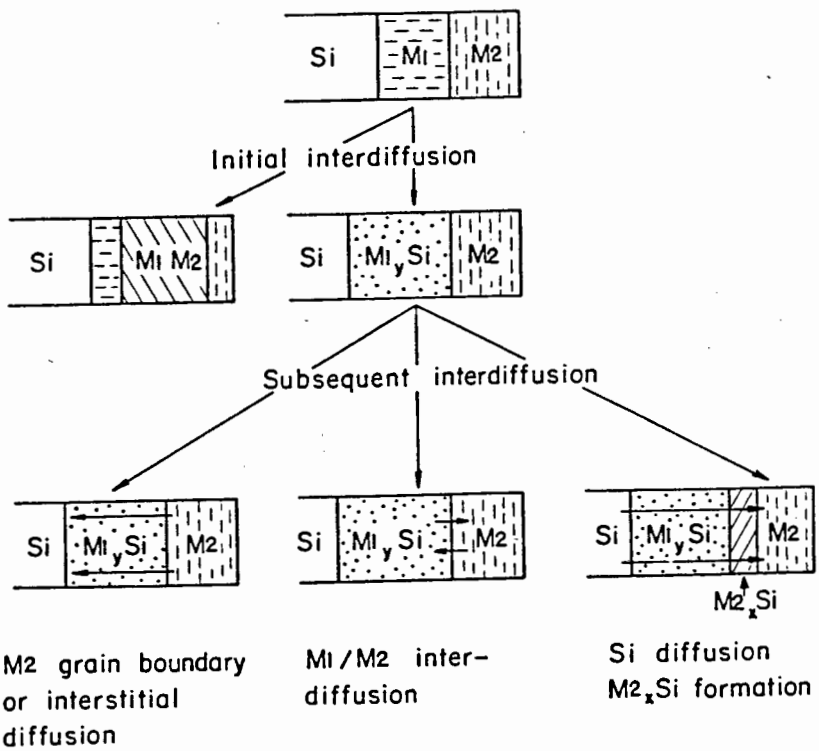

FIG 3-4 Possible interdiffusion schemes in the Si/M1/M2 system. Si diffusion with $M2_x$Si formation is of particular importance.

The interactions are:

1) grain boundary or interstitial diffusion of M2 into and through $M1_ySi$;

2) substitutional interdiffusion of M1 and M2 and;

3) Si diffusion into M2 with phase formation.

Although variations and combinations of these interactions are possible, only the interactions in 3) will be considered. This will result in planar silicide formation yielding a $Si/M1_ySi/M2_xSi$ structure, assuming that the $M1_ySi$ phase does not change due to the Si transport process.

The growth kinetics of the $M2_xSi$ layer will be determined by the slowest interfacial reaction and the mobility of the diffusant in both $M1_ySi$ and the growing $M2_xSi$ layers. In order to determine the diffusant flux from which the growth rate is determined, it is necessary to consider the interfacial reactions and subsequently the driving force for diffusion.

3.3.2 Interfacial reactions

The mechanism whereby equilibrium is established during $M2_xSi$ growth on $M1_ySi$ is similar to that during $M1_ySi$ growth as explained in section 3.2.2. Silicon vacancies are created or annihilated at the various interfaces and migrate through the

silicide layers. These interfacial reactions together with the vacancy fluxes will establish the various equilibrium vacancy concentrations at the interfaces.

Consider the case where M2 has partially reacted to form $M2_xSi$. It is assumed that neither M1 nor M2 diffuse during this formation process. The reactions and vacancy concentration variation at the various interfaces are now given:

<u>$M2_xSi$/M2 interface</u>

$$M2 \rightarrow M2^x + V_{Si} \qquad \Delta g^{M2} \qquad (3\text{-}27)$$

The corresponding vacancy concentration variation is given by:

$$\frac{d}{dt}\left[V_{Si}^{M2_xSi}\right]_{M2} = k_1\left\{\left[V_{Si}^{M2_xSi}\right]_{M2}^{e} - \left[V_{Si}^{M2_xSi}\right]_{M2}\right\} \qquad (3\text{-}28)$$

The symbols in the above equations have their usual meaning. The notation for concentration has been adapted in order to indicate the specific silicide layer e.g. $\left[V_{Si}^{M2_xSi}\right]_{M2}$ indicates the Si vacancy concentration in the $M2_xSi$ layer near the M2 layer, i.e. at the $M2_xSi$/M2 interface.

<u>$M1_ySi/M2_xSi$ interface</u>

The reaction at this interface is considered to be a combination of two reactions on either side of the interface. Silicon atoms are effectively transported across the interface.

Ml_ySi side:

$$Si^{xl} \rightarrow Si + V_{Si}^{Ml_ySi} \qquad (3\text{-}29)$$

$M2_xSi$ side:

$$Si + V_{Si}^{M2_xSi} \rightarrow Si^{x2} \qquad (3\text{-}30)$$

On combining these two equations:

$$Si^{xl} + V_{Si}^{M2_xSi} \rightarrow Si^{x2} + V_{Si}^{Ml_ySi} \qquad \Delta g^{M} \qquad (3\text{-}31)$$

where Δg_{Si}^{M} has been used for $\Delta g_{Si}^{Ml/M2}$, the partial molar free energy change associated with the complete interfacial reaction. Si^{xl} and Si^{x2} indicate Si atoms on lattice sites in the Ml_ySi and $M2_xSi$ layers respectively.

The vacancy concentration variation due to the individual reactions are given by:

$$\frac{d}{dt}\left[V_{Si}^{Ml_ySi}\right]_M = k_2 \left\{\left[V_{Si}^{Ml_ySi}\right]_M^e - \left[V_{Si}^{Ml_ySi}\right]_M\right\}$$

and

$$\frac{d}{dt}\left[V_{Si}^{M2_xSi}\right]_M = k_3 \left\{\left[V_{Si}^{M2_xSi}\right]_M^e - \left[V_{Si}^{M2_xSi}\right]_M\right\}$$

<u>Si/Ml_ySi interface</u>

$$Si + V_{Si}^{Ml_ySi} \rightarrow Si^{x} \qquad \Delta g^{Si} \qquad (3\text{-}32)$$

The corresponding equations for the vacancy variation with time is:

$$\frac{d}{dt}\left[V_{Si}^{Ml_ySi}\right] = k_4 \left\{\left[V_{Si}^{Ml_ySi}\right]_{Si}^{e} - \left[V_{Si}^{Ml_ySi}\right]_{Si}\right\}$$

The growth kinetics of the $M2_xSi$ layer will be dependent on the relative magnitudes of the reaction rate constants k_1, k_2, k_3 and k_4, and the mobility of Si in the Ml_ySi and $M2_xSi$ layers respectively. A solution of the diffusion equation in both silicide layers, subject to the numerous boundary conditions will not be attempted. The same approach as in section 3.2.5 will however be followed. The driving force for diffusion in the various limiting cases will be considered. Of the four interfacial reactions, it is only the slowest reaction that may possibly control the growth kinetics. The particular choice will not affect the final results of the model, so that we may assume that $M2_xSi/M$ interfacial reaction is the slowest without any loss of generality.

3.3.3 Growth kinetics of $M2_xSi$

The $Ml_ySi/M2_xSi$ interface constitutes a three component system so that a ternary free energy diagram should in principle be used to determine the chemical potential of Si, analogous to the procedure followed in section 3.2.4. If no metal-metal interdiffusion takes place then the Ml_ySi layer merely serves as a membrane through which Si is transported. No ternary compounds are formed and therefore the ternary free energy dia-

gram is unnecessary.

Since it is assumed that Si is the only diffusing species during $M2_xSi$ growth, the chemical potential of Si at the various interfaces needs to be considered. Using (3-15), the chemical potential of Si at the $M2_xSi/M2$ interface on the M2 side, is seen to be related to the free energy of formation of $M2_xSi$:

$$(\mu_{Si})^{M2} = \Delta G_g^{o(M2_xSi)}/n$$

where $n = q_{Si}^s$ the stoichiometric atomic fraction of Si in $M2_xSi$. The chemical potential of Si in the silicon layer near the Si/Ml_ySi interface is by definition zero (or near zero).

The free energy balance is now considered in order to obtain an expression analogous to (3-16(b))

$$\Delta G_f^{o(M2_xSi)}/n = \Delta g^{Si} + \Delta\mu_{Si}^{Ml_ySi} + \Delta g^{M} + \Delta\mu_{Si}^{M2_xSi} + \Delta g^{M2} \qquad (3\text{-}33)$$

which is the difference between the chemical potential of Si in Si and Si in M2. The various terms in (3-33) are explained in the schematic in Figure 3-5(a). In section 3.3.2 it was argued that only one (the slowest) interfacial reaction needs to be considered. The reactions at the other two interfaces are assumed to be relatively fast so that local equilibrium prevails at those interfaces (see section 3.2.2). The reaction energies Δg^{Si} and Δg^{M} associated with the reactions at

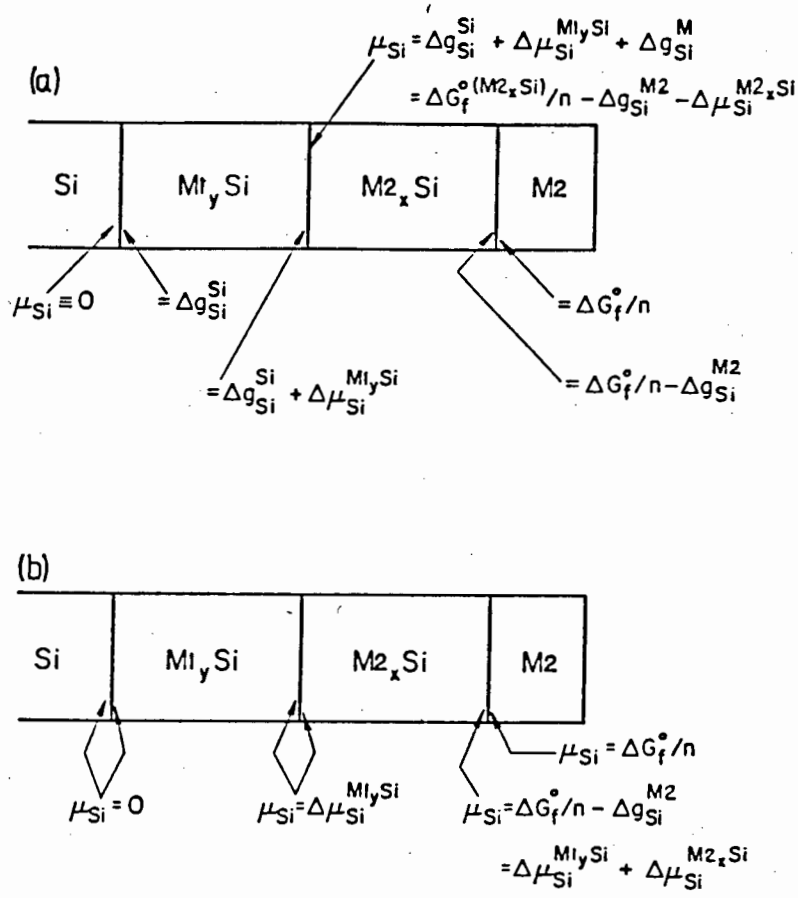

FIG 3-5 The chemical potential of Si, μ_{Si}, in a bi-layer metal silicon system,
(a) general case and
(b) local equilibrium at the Si/Ml_ySi and Ml_ySi/$M2_xSi$ interfaces.

the Si/Ml_ySi and Ml_ySi/$M2_xSi$ interfaces respectively are assumed zero. Therefore the chemical potential at the various interfaces have the values as indicated in Figure 3-5(b), so that:

$$\Delta G_f^{o(M2_xSi)}/n = \Delta\mu_{Si}^{Ml_ySi} + \Delta\mu_{Si}^{M2_xSi} + \Delta g^{M2} \qquad (3\text{-}34)$$

The growth kinetics of the $M2_xSi$ layer will be determined by the dominant term in (3-34). Three limiting cases can be characterized and in each case the flux through the $M2_xSi$ layer

(which is identical to the Si flux through the Ml_ySi layer since there is no Si-concentration build-up and since silicon is assumed to be the only diffusing species in both silicide layers) can be expressed uniquely.

a) $\Delta\mu_{Si}^{Ml_ySi}$ is dominant in (3-34) so that:

$$\Delta\mu_{Si}^{Ml_ySi} \simeq \Delta G_f^{o(M2_xSi)}/n$$

The silicon flux as was given by (3-21) now becomes:

$$J_{Si} = - \frac{B_1 \Delta G_f^{o(M2_xSi)} \left[Si^{x1}\right]}{nY_1}$$

where Y_1 is the thickness of the Ml_ySi layer and B_1 is the Si mobility in Ml_ySi. The effective mobility is now defined as:

$$\bar{B} = -B\Delta\mu^{max}$$

where $\Delta\mu^{max}$ is the maximum chemical potential difference of the diffusing atom with mobility B. The flux equation above becomes:

$$J_{Si} = \left[Si^{x1}\right] \bar{B}_1/Y_1$$

The controlling parameter is therefore $\bar{B}_1/Y_1$ which is associated with diffusion through the Ml_ySi layer.

b) $\Delta\mu_{Si}^{M2_xSi}$ is dominant in (3-34) so that:

$$\Delta\mu_{Si}^{M2_xSi} \simeq \Delta G_f^{o(M2_xSi)}/n$$

As shown in (a), the silicon flux is given by:

$$J_{Si} = \left[Si^{x2}\right] \bar{B}_2/Y_2$$

The controlling parameter is therefore $\bar{B}_2/Y_2$ associated with diffusion through the $M2_xSi$ layer.

c) Δg^{M2} is dominant. This is similar to the linear kinetics regime discussed in section 3.2.5. Differentiating (3-24) and substituting in (3-22):

$$J_{Si} = \left[Si^{x2}\right]\sqrt{RTB_2k_1}$$
$$= \left[Si^{x2}\right] K_1$$

where $K_1 = \sqrt{RTB_2k_1}$ is called the effective reaction rate, associated with the reaction rate k_1. (The effective reaction rate is in fact the linear growth rate constant of $M2_xSi$, grown from a M2-Si couple in the case where the reaction at the $M2_xSi/M2$ interface limits the linear growth). In this particular case where Δg^{M2} is dominant, the flux controlling parameter is the effective reaction rate constant K_1.

The particular process (diffusion or interfacial reaction) which controls the growth is determined by the relative magnitudes of the three parameters ($\bar{B}_1/Y_1$, $\bar{B}_2/Y_2$ and K_1) which are all measures for the Si flux through the silicide bilayer. In Figure 3-6, the growth kinetics is illustrated for a number of limiting cases. In Figure 3-6(a), $\bar{B}_1/Y_1 >> K_1$ and $\bar{B}_1/Y_1 >> \bar{B}_2/Y_2$. The growth of $M2_xSi$ is therefore unaffected by the $M1_ySi$ layer. Initially, the growth is linear with time (interfacial reaction limited) and finally it becomes diffusion limited when the thickness of the $M2_xSi$ layer Y_2 has

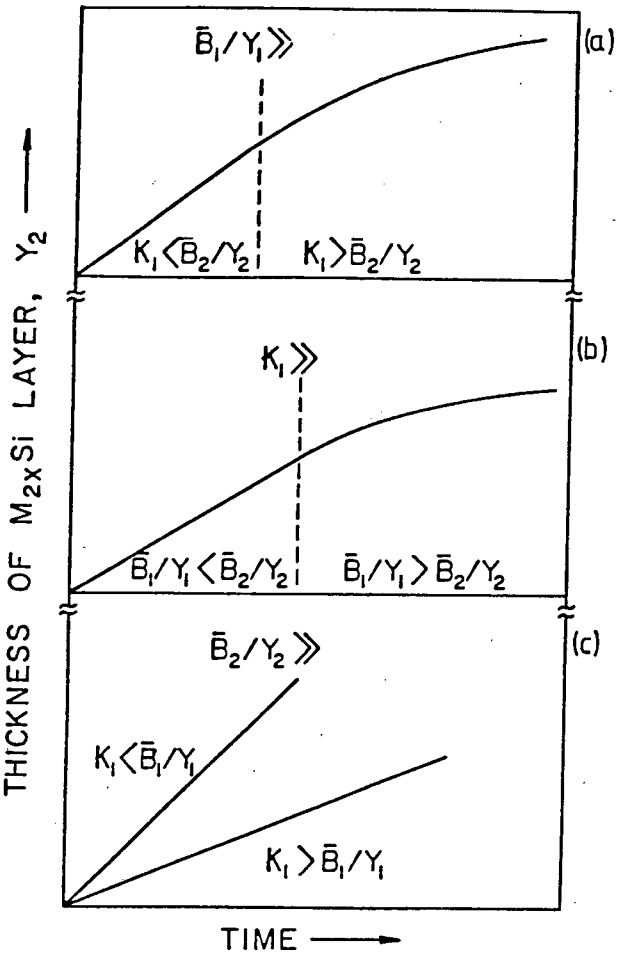

FIG 3-6 Growth kinetics of the $M2_xSi$ layer growth for various cases:

(a) High mobility B_1 : $\bar{B}_1/Y_1 >> K_1$ and $\bar{B}_1/Y_1 >> \bar{B}_2/Y_2$

(b) Fast reaction : $K_1 >> \bar{B}_1/Y_1$ and $K_1 >> \bar{B}_2/Y_2$

(c) High mobility B_2 : $\bar{B}_2/Y_2 >> K_1$ and $\bar{B}_2/Y_2 >> \bar{B}_1/Y_1$.

become sufficiently large so that $K_1 > \bar{B}_2/Y_2$.

Figure 3-6(b) illustrates the case of fast interfacial reaction kinetics: $K_1 >> \bar{B}_1/Y_2$, and $K_1 >> \bar{B}_2/Y_2$. The growth rate of the $M2_xSi$ layer initially remains constant (linear growth) while $\bar{B}_1/Y_1 < \bar{B}_2/Y_2$. Since Y_2 increases with time, the situation will eventually be reached where $\bar{B}_1/Y_1 > \bar{B}_2/Y_2$. The growth becomes parabolic since it is now limited by diffusion through $M2_xSi$, the thickness of which increases with time.

The case illustrated in Figure 3-6(c) ($\bar{B}_2/Y_2 >> K_1$ and $\bar{B}_2/Y_2 >> \bar{B}_1/Y_1$) is of interest in this work. Because of the high Si mobility in $M2_xSi$, the growth kinetics of $M2_xSi$ is controlled either by the interfacial reaction when $K_1 < \bar{B}_1/Y_1$ or by diffusion through $M1_ySi$ when $K_1 > \bar{B}_1/Y_1$. These two types of kinetics are both characterized by linear growth but the one type does not change into the other during $M2_xSi$ growth. In both cases however, the kinetics eventually become parabolic as shown in the two figures above (a) and (b)), when Y_2 has increased sufficiently so that $\bar{B}_2/Y_2 < K_1$ or $\bar{B}_2/Y_2 < B_1/Y_1$. The linear kinetics regime will be further analyzed in the following section.

3.3.4 Linear kinetics of bilayer metal silicide growth

When the interfacial reaction controls the growth of the $M2_xSi$ layer, the growth rate is given by an expression similar to (3-25):

$$\frac{dY_2}{dt} = K_1 = \sqrt{RTB_2 \cdot k_1} = R_o \qquad (3\text{-}35)$$

This represents the maximum growth rate of $M2_xSi$ on the interposed $M1_ySi$ layer and this rate is henceforth denoted by R_o. Since R_o (B_2 and k_1) is constant at constant temperature, it is obvious that (3-35) implies linear growth at constant temperature. The growth rate R_o (K_1) is not necessarily the

same as the linear growth rate measured in the case of $M2_xSi$ growth directly on Si (i.e. without the interposed $M1_ySi$ layer) since in that case it might be a different interfacial reaction controlling the growth (e.g. $Si/M2_xSi$ interface).

Linear growth is also evident when $\bar{B}_1/Y_1 < K_1$. This can be seen from the following. Local equilibrium prevails at the interface so that Δg^{M2} in (3-34) is zero. Since $\bar{B}_1/Y_1 << \bar{B}_2/Y_2$, therefore, $\Delta\mu_{Si}^{M2_xSi}$ is near zero (condition for unique flux), so that

$$\Delta\mu_{Si}^{M1_ySi} \simeq \Delta G_f^{o(M2_xSi)}/n \qquad (3\text{-}36)$$

The Si flux through the $M1_ySi$ layer is given by:

$$J_{Si} = B_1\left[Si^{x1}\right]\frac{\Delta\mu_{Si}^{M1_ySi}}{Y_1} \qquad (3\text{-}37)$$

and the growth of the $M2_xSi$ layer is given by:

$$\frac{dY_2}{dt} = J_{Si}/\left[Si^{x2}\right] \qquad (3\text{-}38)$$

From (3-38), (3-37), and (3-36):

$$\frac{dY_2}{dt} = B_1\frac{\left[Si^{x1}\right]}{\left[Si^{x2}\right]}\frac{\Delta G_f^{o(M2_xSi)}}{n\,Y_1} \qquad (3\text{-}39)$$

$$= R_2$$

$$< R_O$$

The growth rate R_2 is now less than the maximum rate R_O in (3-35) as can be shown by substituting $\bar{B}_1/Y_1 < K_1$ into (3-39).

The mobility B_1 and the reaction rate constant K_1 (also R_o) are characteristic parameters of a particular system and therefore constant at constant temperature. The thickness of the Ml_ySi layer Y_1, will therefore determine whether the linear kinetics are controlled by an interfacial reaction or by diffusion through the Ml_ySi layer. A critical thickness Y_o is defined and is to be used as a criterium for determining which factor controls the linear growth. When $Y_1 < Y_o$, it is implied that $Y_1 < \bar{B}_1/K_1$ (since $K_1 < \bar{B}_1/Y_1$) so that the $M2_xSi$ layer growth is limited by the interfacial reaction. When $Y_1 > Y_o$, ($Y_1 > \bar{B}_1/K_1$) the $M2_xSi$ layer growth is limited by Si diffusion through the Ml_ySi layer. The two regimes of Y_1 will be referred to as the "thin" and "thick" regimes. This model for linear growth in bilayer metal silicon interaction therefore predicts that:

$$\frac{dY_2}{dt} = R_o \text{ for } Y_1 < Y_o$$
$$\frac{dY_2}{dt} = R_2 < R_o \text{ for } Y_1 > Y_o \qquad (3\text{-}40)$$

It is seen in (3-39) that $\frac{dY_2}{dt}$ is influenced by Y_1. The Y_1 dependence of $\frac{dY_2}{dt}$ can therefore be expressed as:

$$\frac{dY_2}{dt} = R_o = \text{constant, for } Y_1 < Y_o$$

and (3-41)

$$\frac{dY_2}{dt} \alpha\ 1/Y_1 \quad \text{for} \quad Y_1 > Y_o$$

The variation of dY_2/dt with $1/Y_1$ as implied by (3-41) is graphically illustrated in Figure 3-7. This particular plot

is not universal but is influenced by the temperature (which affects both R_o and Y_o).

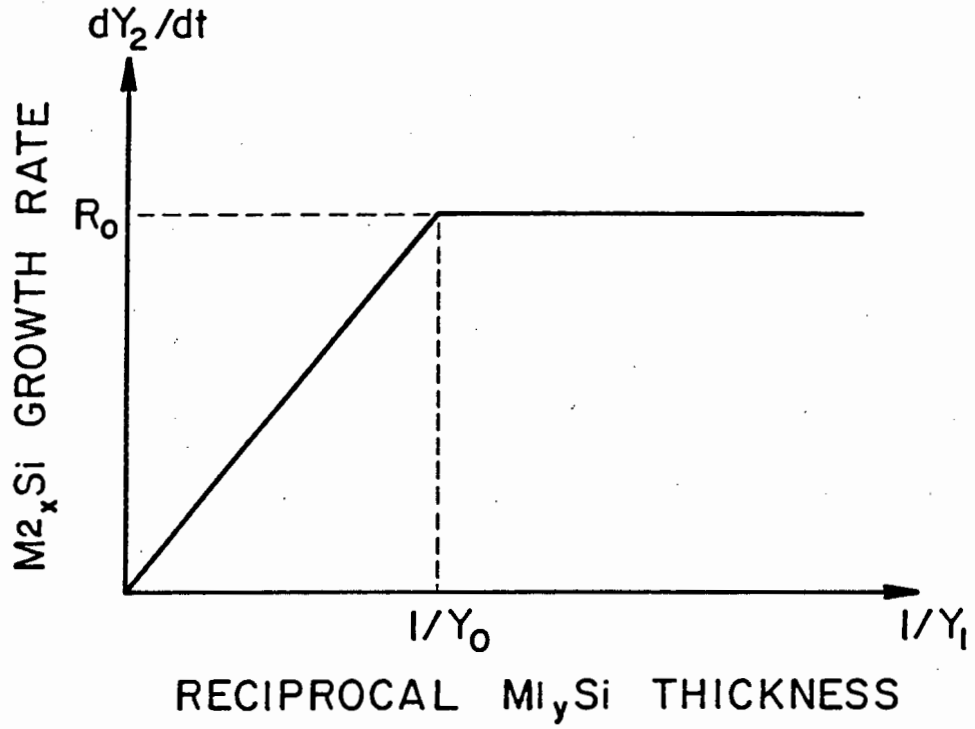

FIG 3-7 Variation of $M2_xSi$ growth rate with reciprocal $M1_ySi$ thickness as predicted by the model.

The significance of the linear kinetics discussed in this section should be viewed in comparison to the kinetics of phase growth in binary couples as discussed in 3.2.1. Linear growth in binary couples is without exception due to a controlling interfacial reaction. In the case of bimetal silicide growth, linear kinetics is no longer a sufficient condition for interfacial reaction controlled growth. It is necessary to investigate the thickness effect of the interposed layer in order to establish the growth controlling factor.

The predictions of this model for bilayer metal silicide growth have been tested in the Si/Pd/Cr system and the experimental results are presented in Chapter 4. It was argued in 3.3.3 that the interposed metal silicide layer serves as a membrane through which Si is transported. A diffusion membrane technique was there developed to determine the mobility of components in a compound based on (3-39). The results of this technique used to determine the mobility of Pd and Si in Pd_2Si are discussed in Chapter 6.

CHAPTER 4

Si/Pd/Cr THIN FILM SYSTEM

4.1 INTRODUCTION

The bilayer metal-silicon system which is to be used for testing the validity of the model developed in Chapter 3, should exhibit specific features such as limited metal-metal interdiffusion and distinctly different silicide formation temperatures of the two metals. It will be shown further on that the Si/Pd/Cr system is an excellent choice, displaying most of the required features. The Si-Pd and Si-Cr binary systems have been studied extensively. In the following sections a brief summary of the reported investigations will be given, in particular those features which pertain to this research. This will be followed by a presentation of experimental results of the thermal behaviour of the Si/Pd/Cr structure, in which specific attention will be given to the effect of interposed Pd_2Si thickness on the growth rate of $CrSi_2$.

4.1.1 Cr/Si interaction

Metallic chromium or its silicide is not generally favoured for wide use in integrated circuits as Schottky barrier contacts because of the low barrier height of chromium silicide [6]. An interposed layer of Cr is occasionally used say between Pt and Si to improve the adhesion of the contact metallization [22]. Another application of Cr stems from its ability to serve as a diffusion barrier to Al (see 4.1.3). The above-mentioned applications and other characteristic features of chromium silicide have stimulated studies regarding

the Cr/Si interaction [23-27].

The first phase to form around 400°C during Cr/Si interaction is $CrSi_2$ [23-25]. This is the most Si-rich phase indicated on the equilibrium phase diagram shown in Figure 4-1. Chromium

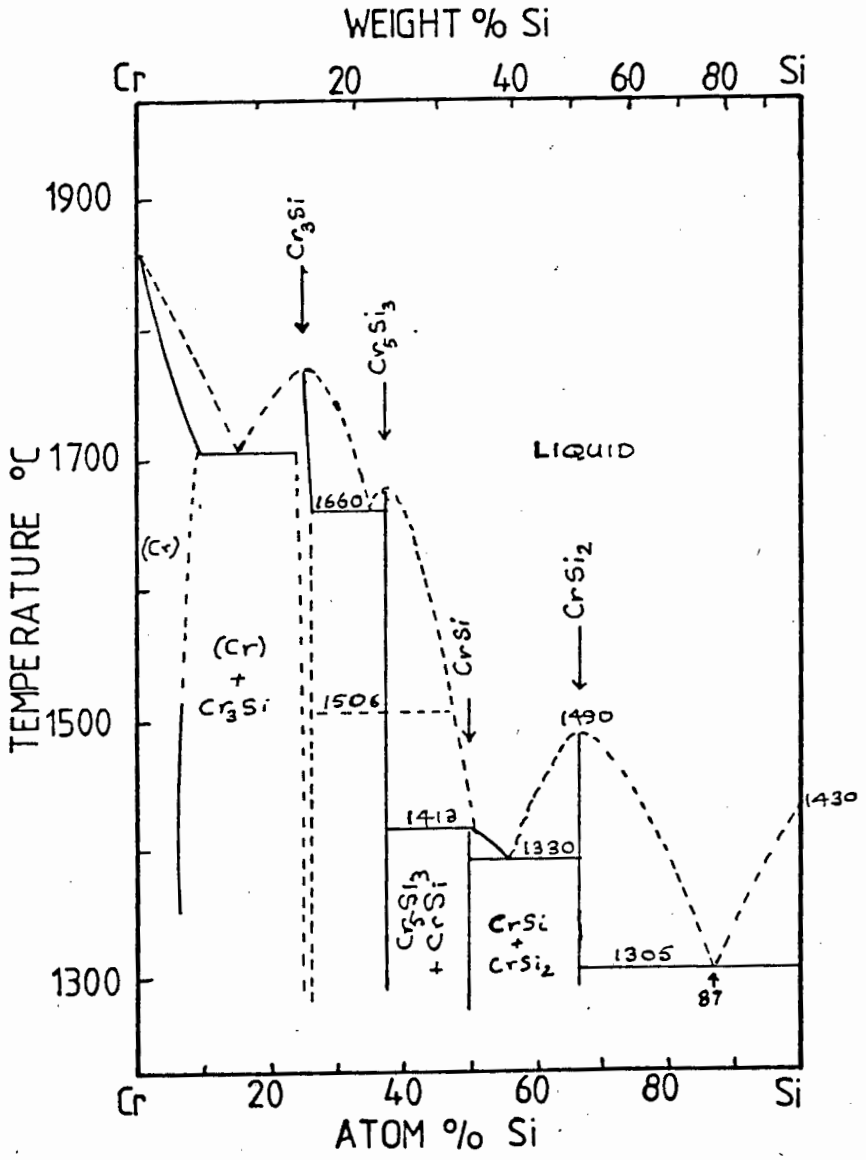

FIG 4-1 Equilibrium phase diagram of Cr-Si (from reference 27).

silicide formation on silicon substrates (unlimited Si-supply) therefore yields one phase only, namely $CrSi_2$. The growth of $CrSi_2$ is found to be limited by an interfacial reaction with an activation energy ranging between 1.5 and 1.7 eV [23,24]. It is believed that the reaction at the $CrSi_2$/Cr interface controls the $CrSi_2$ growth. By implanting Xe marker atoms into either the Si or the Cr layer, Martinez et al. showed that Si is the dominant diffusing species during $CrSi_2$ growth [24]. These results are supported by Botha et al. who found that Si is extremely mobile in $CrSi_2$ [26].

4.1.2 Pd/Si interaction

The wide use of palladium silicide for Schottky barriers and ohmic contacts in microelectronic devices has stimulated extensive research into its growth kinetics, micro-structrue and electrical properties [28-36]. During Si/Pd interdiffusion, Pd_2Si is the first phase to form. It has been found to form at extremely low temperatures (room temperature) and remains stable up to 750°C above which it transforms to PdSi, in the case of unlimited Si supply [28,29]. This particular phase sequence is anticipated since PdSi is the adjacent phase, richer in silicon, as can be seen in the phase diagram shown in Figure 4-2. When grown on Si<100> or amorphous Si substrates, Pd_2Si is polycrystalline with the hexagonal C-axis preferentially aligned normal to the surface [30]. Because of only a small mismatch (2%) between the Si<111> and Pd_2Si lattice constants (basal plane), Pd_2Si grows epitaxial on Si<111> substrates [30,31]. The degree of epitaxy

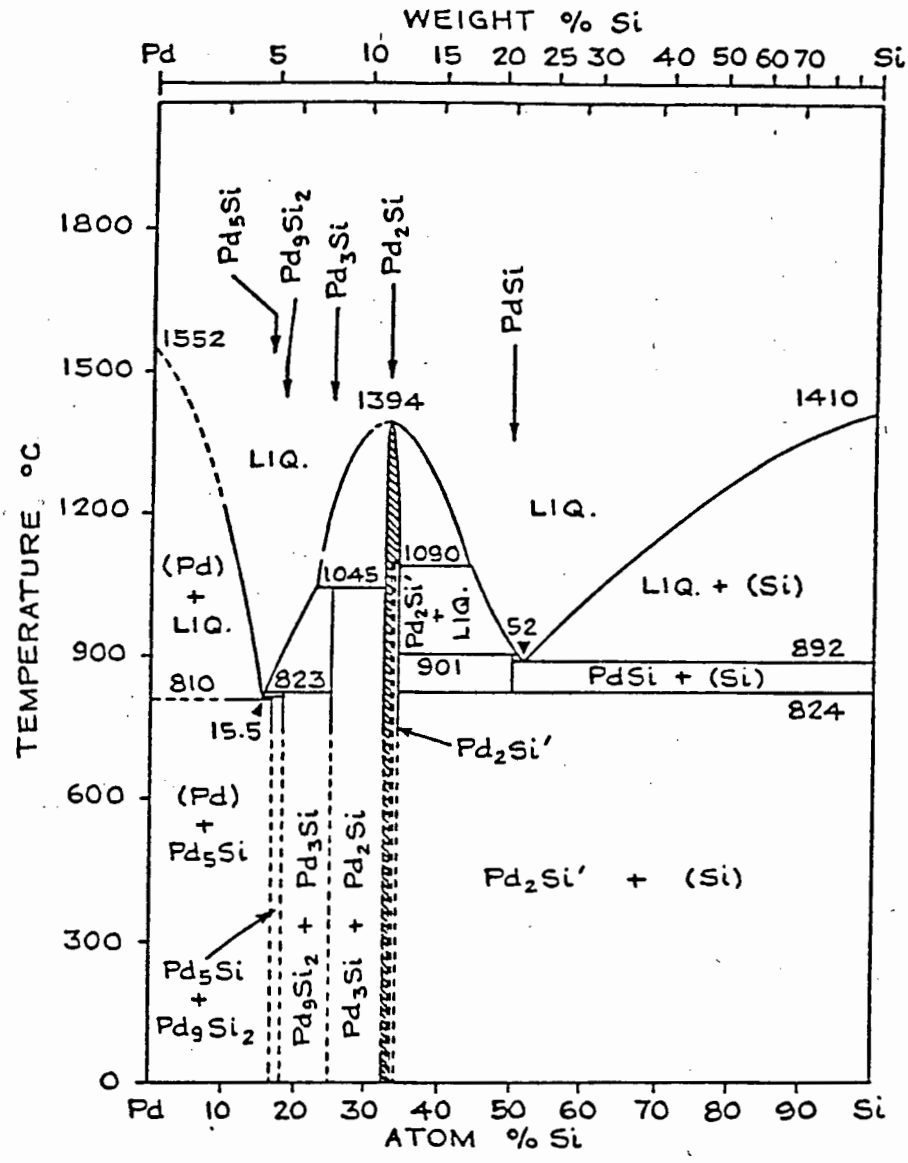

FIG. 4-2 Equilibrium phase diagram of Pd-Si (from reference 27).

is found to increase dramatically with increase in formation temperature. A limited degree of improvement is obtained upon post annealing at elevated temperatures [31].

The growth kinetics are diffusion controlled with reported activation energy values between 0.9 and 1.5 eV [29-32]. Contrary to earlier reported results, Cheung et al. recently reported the parabolic rate constant to be sensitive to the microstructure and orientation of the Si substrate [31].

Marker experiments tend to indicate that both Si and Pd diffuse through Pd_2Si during its growth [33-36]. This makes Pd_2Si unique since in all the other metal silicides it has been found that either the metal or the Si is the dominant moving species during first-phase growth in binary metal-silicon couples.

4.1.3 Chromium as a diffusion barrier to Al

A typical contact metallization scheme such as Si/Pd_2Si is usually followed by a layer of Al for interconnection. Since the final heat treatment following the Al layer deposition is around 400°C, the stability of Al on the underlying silicide layer is important. Penetration of Al through the silicide and into the Si substrate at these temperatures is however observed [37].

It has been demonstrated that an interposed refractory metal layer of Cr, Ti, or V between the Al and silicide layers can serve as a diffusion barrier to Al [38-40]. The barrier mechanism is based on the compound formation between the refractory metal and Al [41]. A typical diffusion barrier such as an Cr layer will also form a silicide during heat treatment at temperatures exceeding 400°C. The effectiveness of the diffusion barrier is thus diminished through the consumption of Cr during silicide growth. A thorough knowledge of the silicide formation of Cr on underlying metal silicide layers is therefore imperative in order to utilize the diffusion barrier potential of Cr.

4.1.4 Bilayer silicides

The growth of $CrSi_2$ on polycrystalline Pd_2Si on Si has been investigated by Olowolafe et al. [23]. Analogous studies of $TiSi_2$ and VSi_2 on both epitaxial and polycrystalline Pd_2Si on Si were also reported by Finstad et al. [42] and Mayer et al. [43]. The growth rates of $CrSi_2$, $TiSi_2$ and VSi_2 were found to be unaffected by the thickness of the interposed Pd_2Si layer. This is not necessarily contrary to the predictions of the model developed in Chapter 3. (See 3.3.4) It is plausible that in these reported studies the Pd_2Si layer did not exceed the critical thickness which is necessary for observing the thickness effect. In a similar study of $CrSi_2$ growth on PtSi and NiSi respectively, Naude et al. did not report any interposed layer thickness dependence of the $CrSi_2$ growth rate [44].

The above-mentioned results tend to suggest that the thickness of an interposed silicide layer does not affect the growth rate of the outer silicide layer. The Si/Pd/Cr thin film combination was nevertheless chosen to test the validity of the model developed in Chapter 3, because it displays the following attractive features:

1. Upon heat treatment Pd_2Si forms at relatively low temperatures (100 to 400°C) and remains stable up to 750°C (see 4.1.2).

2. Chromium silicide usually forms only at temperatures above 400°C (see 4.1.1). It is therefore relatively

easy to effect silicide formation in the Si/Pd/Cr system in two separate stages.

3. No Pd-Cr interdiffusion has been observed prior to or during Pd_2Si formation [23], in spite of the relatively high solubility of Cr in Pd [45].

4. The Pd_2Si and $CrSi_2$ layers have not been found to intermix at temperatures up to 600°C [23].

5. Since Pd_2Si grows epitaxially on Si<111> and non-epitaxially on Si<100> (see 4.1.2), the effect of the microstructure of the interposed silicide on the growth rate of the outer silicide layer can be investigated.

A report of an extensive study of the thermal behaviour of the Si<111>/Pd/Cr thin film combination is represented here. This is followed by an account of a comparitive study of the Si<111>/Pd/Cr and Si<100>/Pd/Cr systems with reference to $CrSi_2$ formation on Pd_2Si.

4.2 EXPERIMENTAL PROCEDURE

Substrates consisting of 1 cm^2 pieces of Si <100> and Si <111> were chemically cleaned prior to metal deposition. Thin films of Pd and Cr were sequentially deposited onto the substrates. The thickness of the Pd layer varied between 200 and 1 500 Å on Si<111> substrates whereas the maximum Pd thickness on Si<100> substrates was 1 µm. The Cr layer thickness was approximately 750 Å for most of the samples.

The samples with relatively thin layers of Pd were pre-annealed at 380°C for ten minutes. The pre-annealing time was increased to fifty minutes for thicker Pd samples. No $CrSi_2$ was found to form during the pre-annealing stage whereas Pd_2Si formation was complete after such heat treatments. Further annealing was performed at temperatures between 400 and 500°C for various periods of time up to three hours. Where samples of different Pd thicknesses required identical heat treatment, these samples were annealed simultaneously. The silicide formation upon the various heat treatment stages is schematically shown in Figure 4-3 .

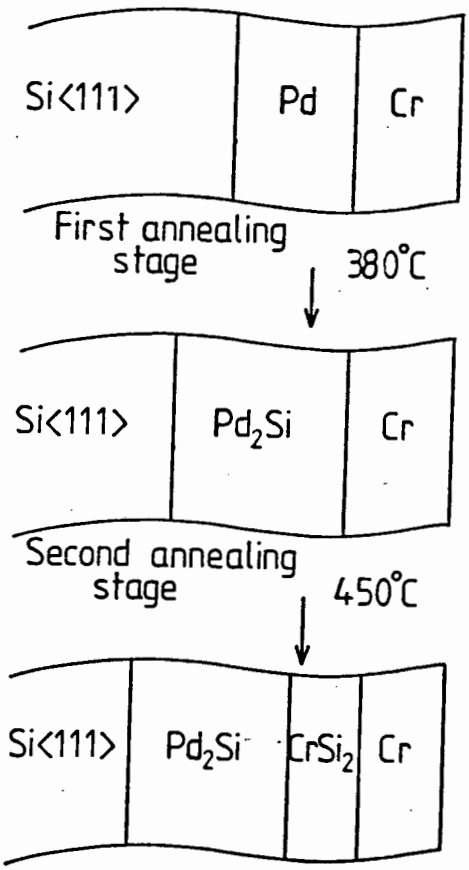

FIG 4-3 Schematic showing the sample composition before and after the various annealing stages

Rutherford backscattering spectrometry employing 2-3 MeV alphas was used to characterize the samples with respect to composition and thickness of the metal and silicide layers. The phase of the various compounds formed was identified by means of glancing angle X-ray diffraction. For Pd_2Si grown on Si <111>, the epitaxy of the silicide layer was confirmed by channeling and X-ray diffraction.

The interfaces between the Si/Pd_2Si and $Pd_2Si/CrSi_2$ layers were studied by means of scanning electron microscopy. Selective etching was used to expose the various interfaces.

4.3 RESULTS

4.3.1 $CrSi_2$ growth kinetics in the Si<111>/Pd_2Si/Cr system

Figure 4-4 shows typical Rutherford backscattering spectra of Si <111>/Pd/Cr samples with identically deposited metal layers. The two spectra in Fig. 4-4(a) are of a sample prior to annealing and of one after being pre-annealed at 380°C for ten minutes. When comparing these two spectra, it can be seen that the Cr signal has remained unchanged which implies that the Cr has not reacted or interdiffused during the first annealing stage. The broadening of the Pd signal and the appearance of the Si step indicate that palladium silicide has formed. The composition Pd_2Si is established by comparing the heights of the Pd signal to the step-height of the Si signal. The phase of this silicide was not identified by means of glancing angle X-ray diffraction since the characteristic Pd_2Si lines on the powder photograph were absent due to the epitaxy of Pd_2Si grown on Si <111>.

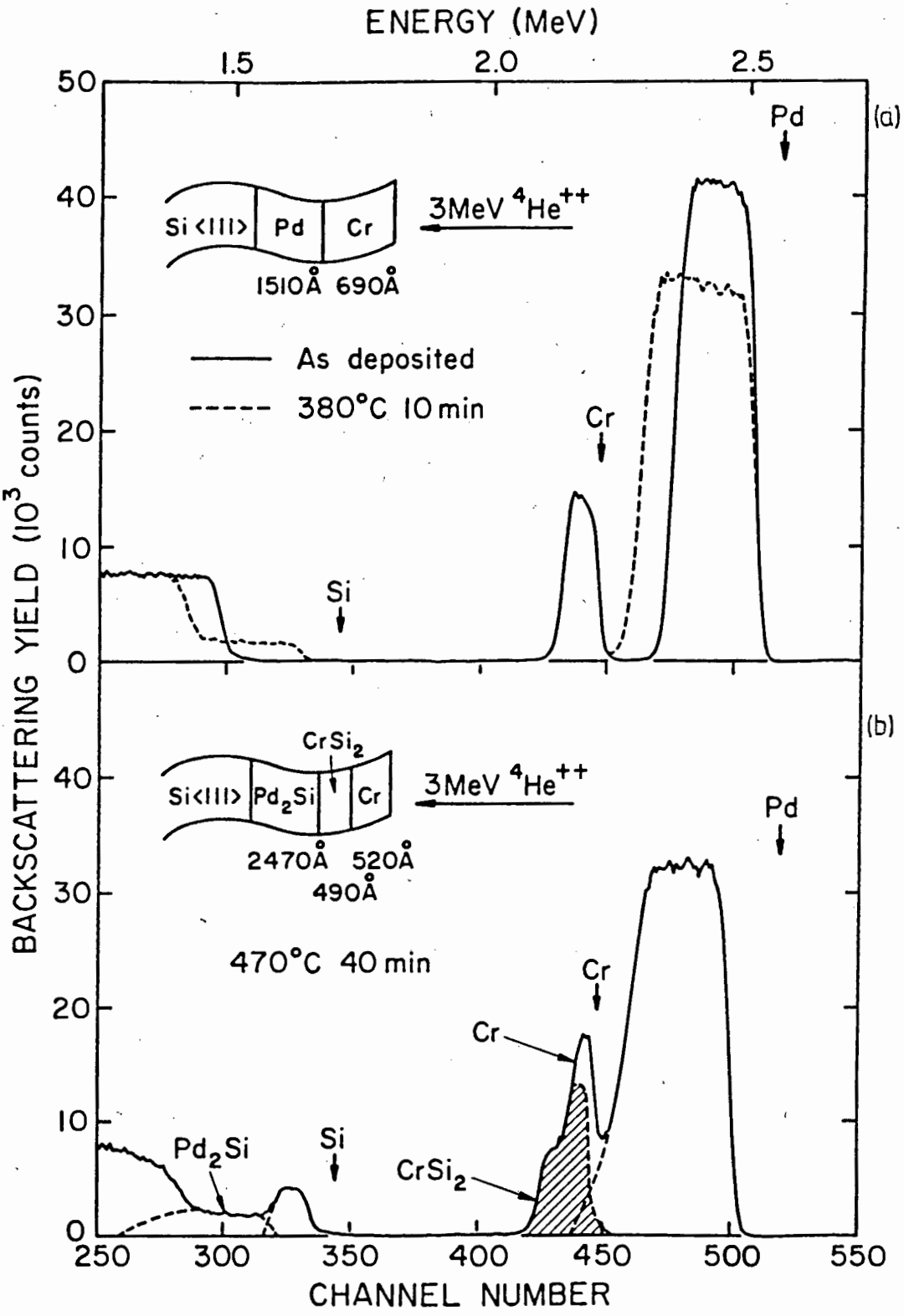

FIG 4-4 Backscattering spectra showing silicide formation in the Si<111>/Pd/Cr thin film system at various annealing stages. The bold arrows indicate the energy of alphas scattered from elements when located on the surface of the sample.

The change in the Cr signal and the second step in the Si signal (high energy side) in the third spectrum (Figure 4-4(b)) indicate that $CrSi_2$ has formed after further annealing. The widths of the Cr signal and the corresponding Si-step are both measures of the thickness of $CrSi_2$. The heights of these two signals were used to establish the composition of the chromium silicide layer and the phase was identified by means of glancing angle X-ray diffraction.

By measuring the thickness of the $CrSi_2$ formed after isothermal anneals of increasing duration, the rate of $CrSi_2$ formation was determined. The thickness of $CrSi_2$ formed on approximately 1400 Å of epitaxial Pd_2Si on Si <111>, plotted

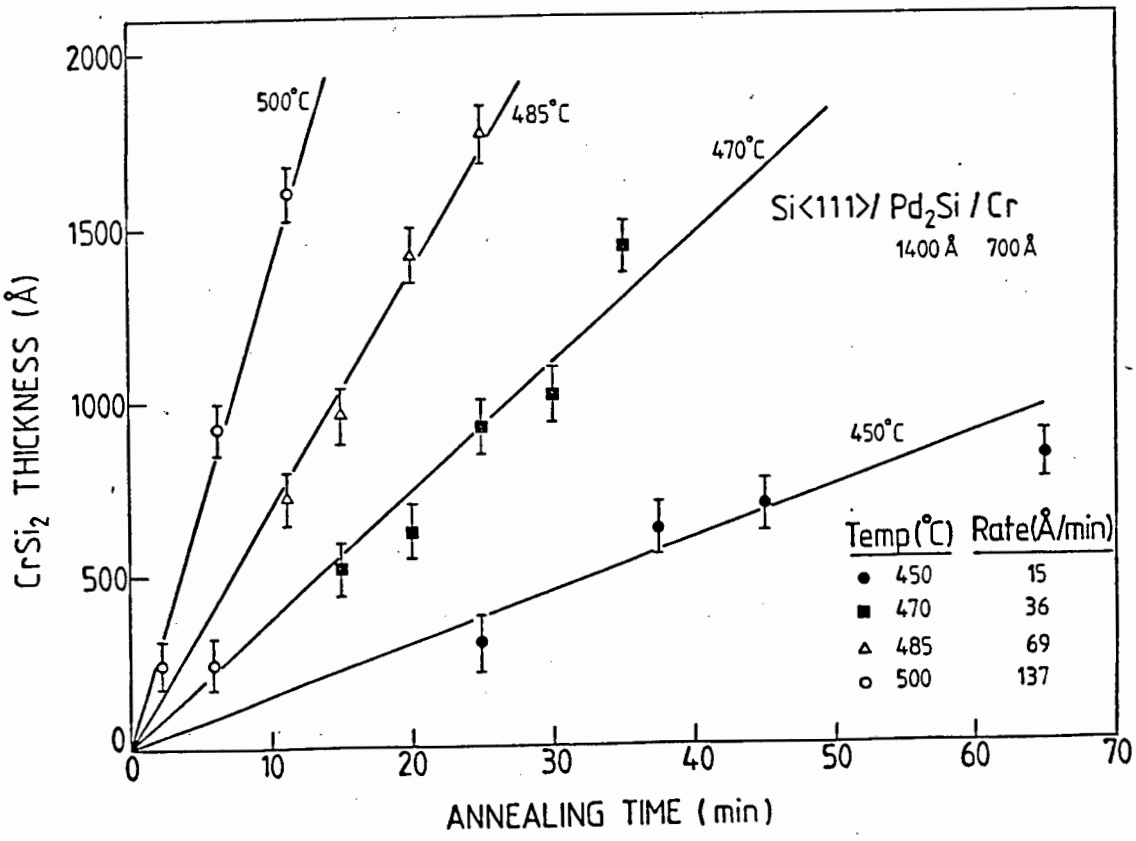

FIG 4-5 The thickness of $CrSi_2$ formed on 1400 Å Pd_2Si measured at various temperatures

against the annealing time is shown in Figure 4-5. The linearity of these curves indicate that the silicide formation process is limited by an interfacial reaction or by diffusion through a layer of constant thickness. It was found that the thickness of the epitaxial Pd_2Si layer (therefore also the deposited Pd layer) has a dramatic effect on the rate of $CrSi_2$ growth. Figure 4-6 shows a plot of $CrSi_2$ thickness formed,

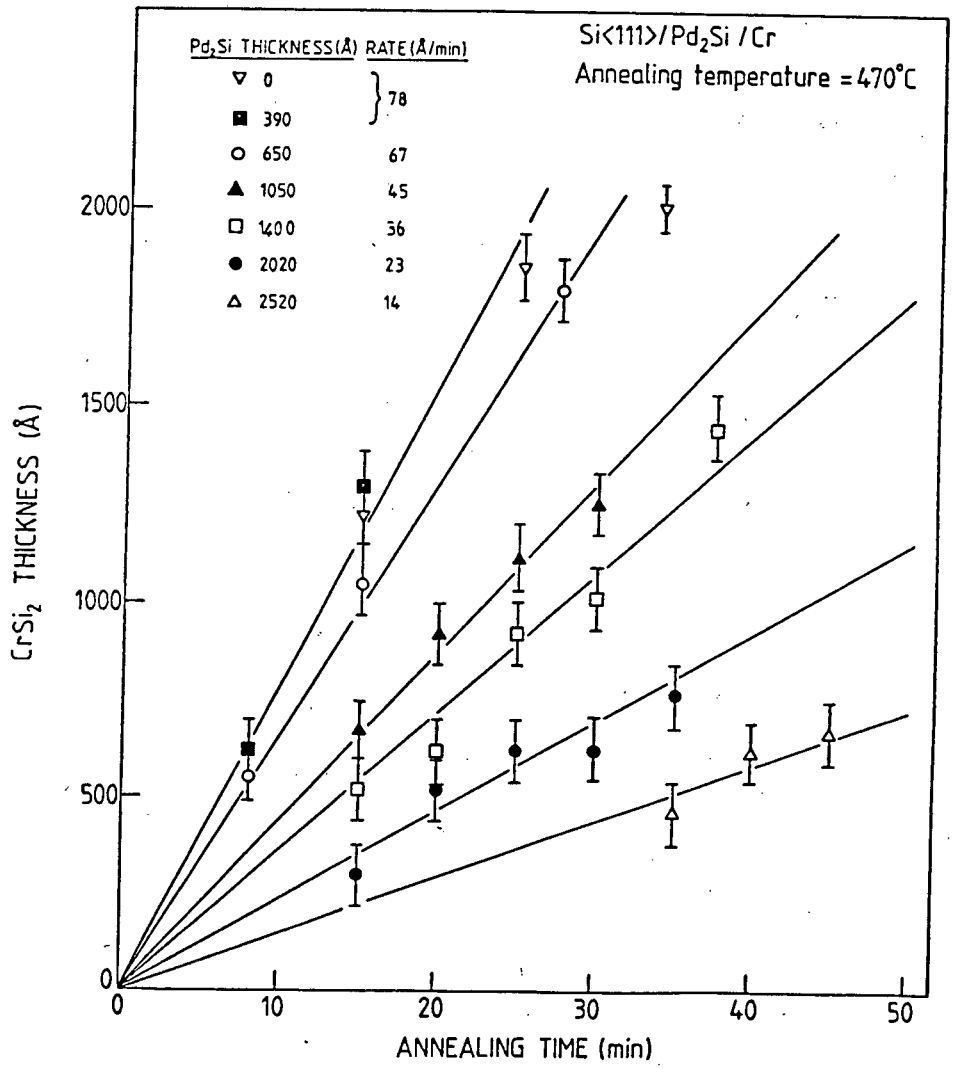

FIG 4-6 Formation of $CrSi_2$ at a fixed temperature of 470°C, for Pd_2Si thicknesses varying between 0 Å and 2520 Å. It should be noticed that the rate of $CrSi_2$ formation is the same for 0 Å and 390 Å of Pd_2Si, while the growth rate decreases for thicker Pd_2Si layers

against the annealing time at 470°C for various thicknesses of the interposed Pd_2Si layer. The thickness of the $CrSi_2$ layer varies linearly with annealing time irrespective of the Pd_2Si thickness while the rate of $CrSi_2$ formation decreases with increase in Pd_2Si thickness.

The Arrhenius plot from which the activation energy, associated with the silicide growth process, can be determined, is usually obtained by plotting the natural log of the silicide growth rate against the inverse of the annealing temperature. Since the thickness of the interposed Pd_2Si layer is found to influence the $CrSi_2$ growth rate, it is necessary to compile Arrhenius plots for constant Pd_2Si layer thicknesses. It proved difficult to prepare a very large number of samples with identical Pd thicknesses, as required for Arrhenius plot compilation. The following normalization procedure was thus adopted. It was predicted in 3.3.4 that a linear relationship should exists between the outer silicide formation rate and the inverse of the interposed silicide layer thickness. The $CrSi_2$ layer growth rate is plotted against the inverse of the Pd_2Si thickness at constant temperature in Figure 4-7. The asterisks indicate $CrSi_2$ growth rates on silicon directly, i.e. without an interposed Pd_2Si layer. Two regions can be distinguished: the rate of $CrSi_2$ growth remains constant for relatively thin layers of Pd_2Si but is inversely proportional to the Pd_2Si layer thickness for thick Pd_2Si layers. The $CrSi_2$ growth rates on Pd_2Si layers of various thicknesses are now read off from Figure 4-7 for Pd_2Si thicknesses of 300, 1000,

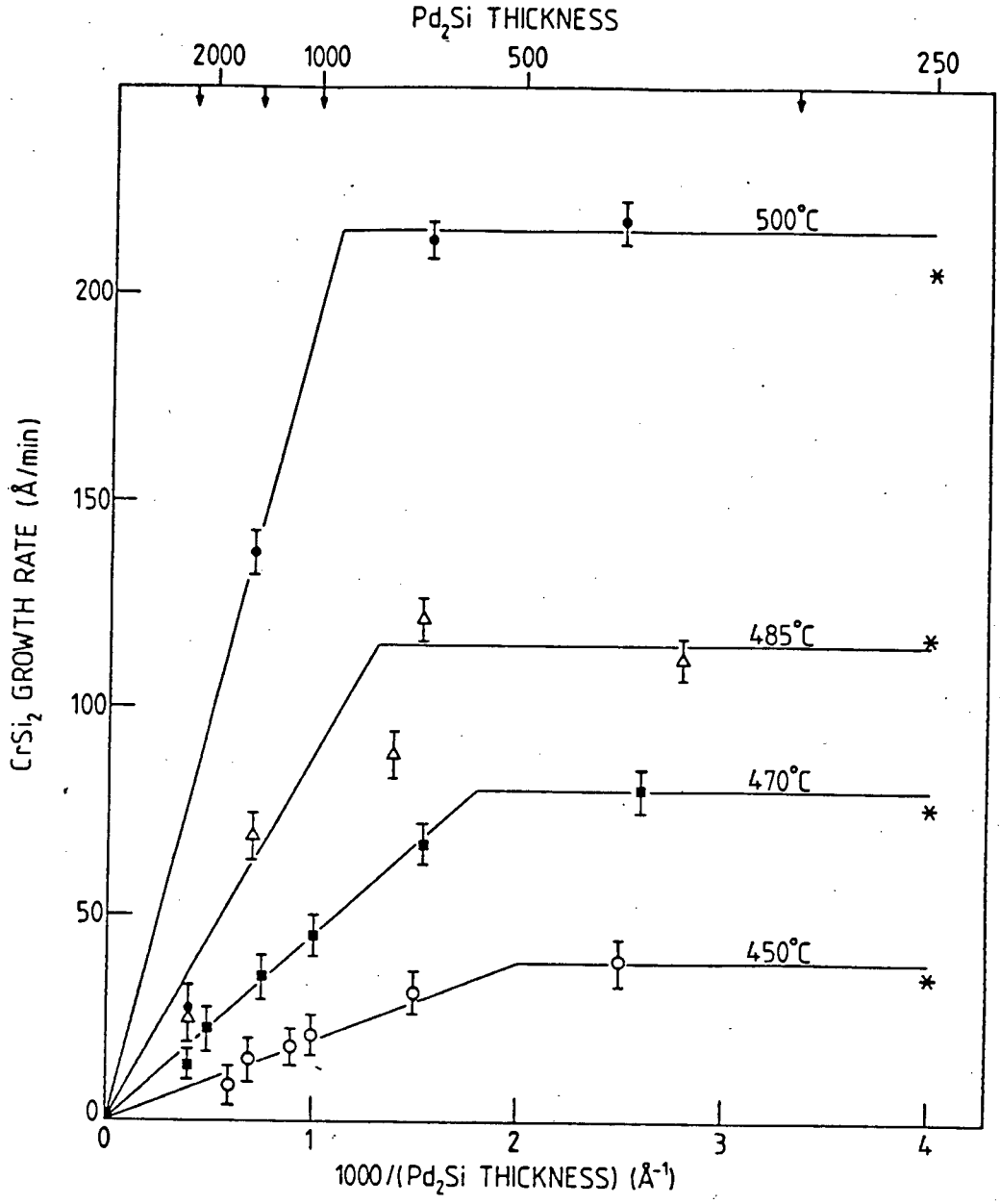

FIG 4-7 The effect of Pd_2Si thickness on $CrSi_2$ growth rate at various annealing temperatures. It can be seen that for thicknesses less than a critical value, the rate of $CrSi_2$ formation is not affected by the interposed Pd_2Si thickness. The asterisks indicate $CrSi_2$ growth rates as measured directly on a silicon substrate, therefore a Pd_2Si thickness of O Å. The arrows on the top scale indicate the Pd_2Si thickness for which Arrhenius plots are given in Figure 4-8.

1400 and and 2500 Å (see arrows along the Pd_2Si thickness axis). The corresponding Arrhenius plots are shown in Figure 4-8.

Two activation energies were obtained, namely 1.6 eV for the relatively thin Pd_2Si layer (300 Å) and 2.2 eV for the thick Pd_2Si layers (1000, 1400 and 2500 Å). The temperature dependence of the parameter $\{R_oY_o\}$ is also shown in Figure 4-8. Values of the parameters R_o and Y_o were obtained from Fig 4-7 where R_o is the $CrSi_2$ growth rate on "thin" Pd_2Si layers and Y_o is the critical thickness of the Pd_2Si layer (see section 3.3.4). An activation energy of 2.2 eV was also obtained from this plot.

4.3.2 Comparison between $CrSi_2$ formation on polycrystalline and epitaxial Pd_2Si respectively

It is well-known that Pd_2Si grows epitaxially on Si<111> and non-epitaxially on Si<100> (see 4.1.2). A comparative study was therefore made of $CrSi_2$ growth on Pd_2Si formed on Si<111> and Si<100> respectively in order to investigate the effect of the microstructure of the Pd_2Si layer.

The growth of $CrSi_2$ on polycrystalline Pd_2Si formed on Si<100> was reported to be linear with time [23], similar to the results presented in 4.3.1. The extent to which the interposed Pd_2Si layer affects $CrSi_2$ growth on it depends on the microstructure of the Pd_2Si layer. Backscattering spectra of identical samples (except for the substrate orientation or Pd_2Si thickness) annealed at 470°C for 25 minutes are shown in Figure 4-9. It is observed that $CrSi_2$ formation is complete

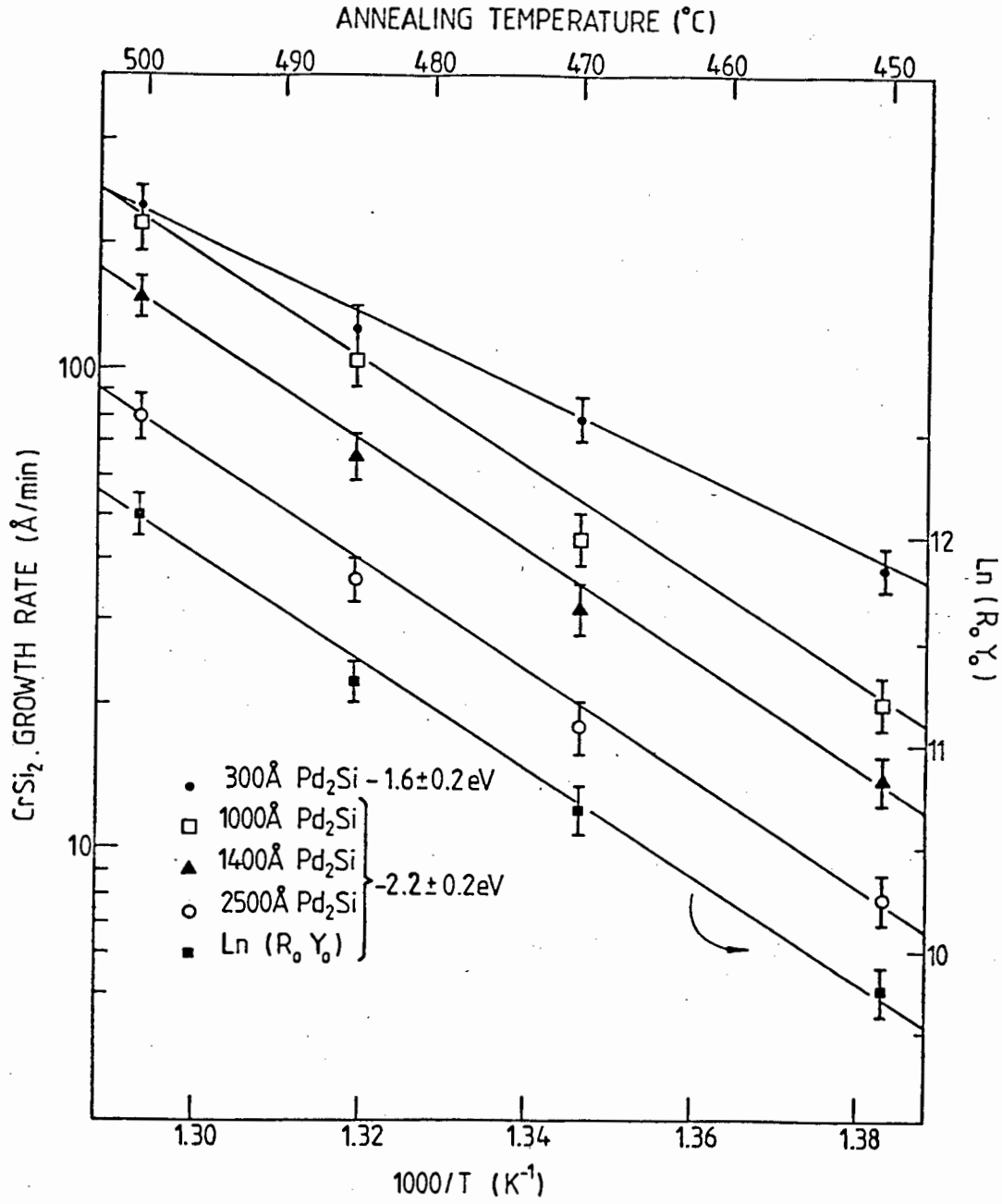

FIG 4-8 Arrhenius plots for $CrSi_2$ formation on different thickness epitaxial of Pd_2Si formed on Si<111> substrates. For a Pd_2Si thickness of 300 Å an activation energy of 1.6 eV is obtained, while a value of 2.2 eV is found for those cases where $CrSi_2$ growth is limited by silicon diffusion through the thicker interposed Pd_2Si layer. The bottom line represents the slope (R_oY_o) of the lines given in Fig 6 as a function of the inverse annealing temperature. The scale for the R_oY_o plot is shown on the right hand side.

in all cases except on relatively thick epitaxial Pd_2Si (Si<111> substrate). This is consistant with the results presented in 4.3.1 where it was shown that "thick" interposed eptaxial Pd_2Si layers reduce the $CrSi_2$ growth rate. From (3-39) it is however expected that any interposed silicide layer, including non-epitaxial Pd_2Si (Si<100> substrate) would influence the rate of $CrSi_2$ formation when the critical thickness Y_o is exceeded.

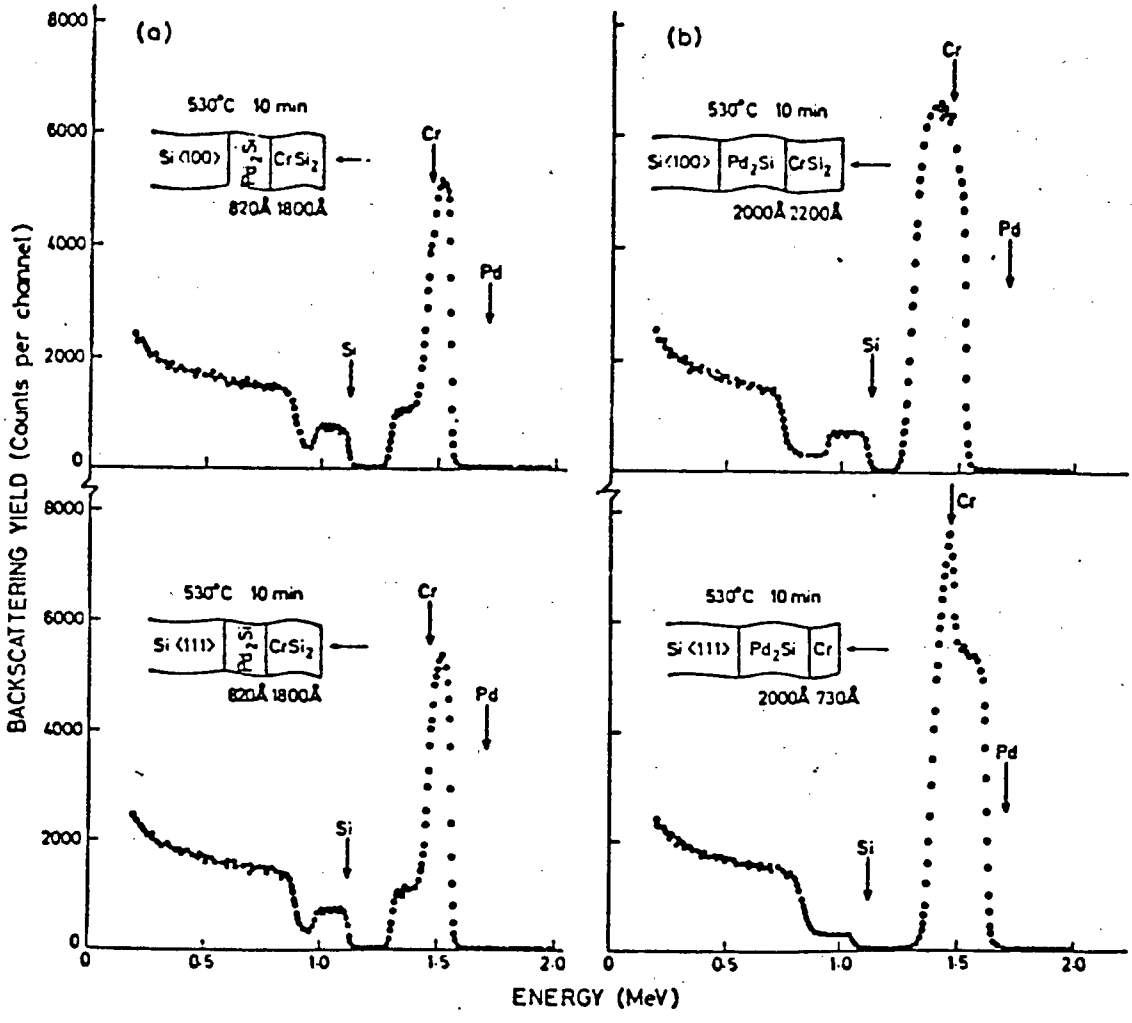

FIG 4-9 Rutherford backscattering spectra illustrating how thick epitaxial Pd_2Si layers inhibit the growth of $CrSi_2$. No thickness effect is seen for Si<100> substrates as the Pd_2Si is not epitaxial.

Such an effect is in fact observed when the polycrystalline Pd_2Si layer thickness approaches 1 µm at temperatures between 400° and 500°C. In Figure 4-10 backscattering spectra of Si<100>/Pd/Cr samples annealed at 440°C for fourty minutes are shown. The two samples differ with respect to the Pd_2Si layer thicknesses (1730 Å and 9530 Å).

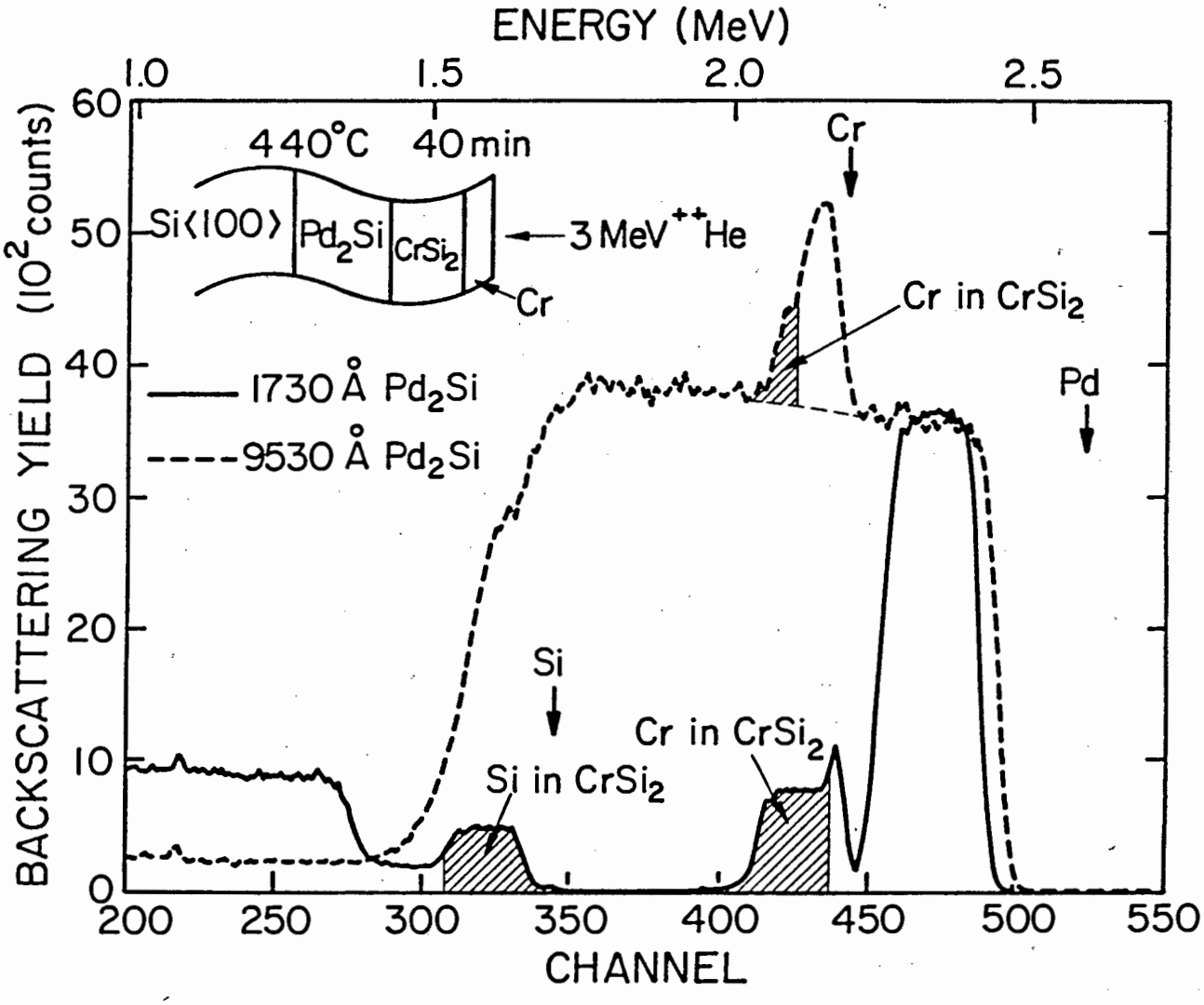

FIG 4-10 Backscattering spectram of Si<100>/Pd/Cr samples annealed at 440°C for 40 min. The step width of the Cr signal representing $CrSi_2$ (hatched area), is much smaller in the case of thick Pd_2Si (9030 Å).

On comparing the Cr signals in the two spectra, it is seen that a thinner layer of $CrSi_2$ has formed on the thick Pd_2Si layer. This is due to the reduced growth rate on thick Pd_2Si. The growth of $CrSi_2$ remains linear with time, similar to $CrSi_2$ growth on epitaxial Pd_2Si (4.3.1) and on thin polycrystalline Pd_2Si [23].

The dependence of the $CrSi_2$ growth rate on the Pd_2Si layer thickness is illustrated in Figure 4-11. The $CrSi_2$ growth rate is seen to be inversely proportional to the Pd_2Si layer thickness for both epitaxial and polycrystalline Pd_2Si. The very thick layers of polycrystalline Pd_2Si necessary to influence the $CrSi_2$ growth rate are ascribed to the higher Si mobility in polycrystalline Pd_2Si compared to that in epitaxial Pd_2Si.

As a result of limited data obtained for $CrSi_2$ growth on polycrystalline Pd_2Si, it was not possible to produce a family of growth rate curves similar to that in Figure 4-7 from which Arrhenius plots were compiled for $CrSi_2$ growth on epitaxial Pd_2Si. A different normalization procedure was therefore followed. From (3-39) it follows that:

$$\frac{dY_2}{dt} \cdot Y_1 = B_{Si} \frac{\Delta G_f^{o\,(CrSi_2)}}{n} \cdot \frac{[Si^{Pd_2Si}]}{[Si^{CrSi_2}]}$$

where $\frac{dY_2}{dt}$ represents the $CrSi_2$ growth rate and Y_1 represents the Pd_2Si layer thickness. It is seen that the temperature

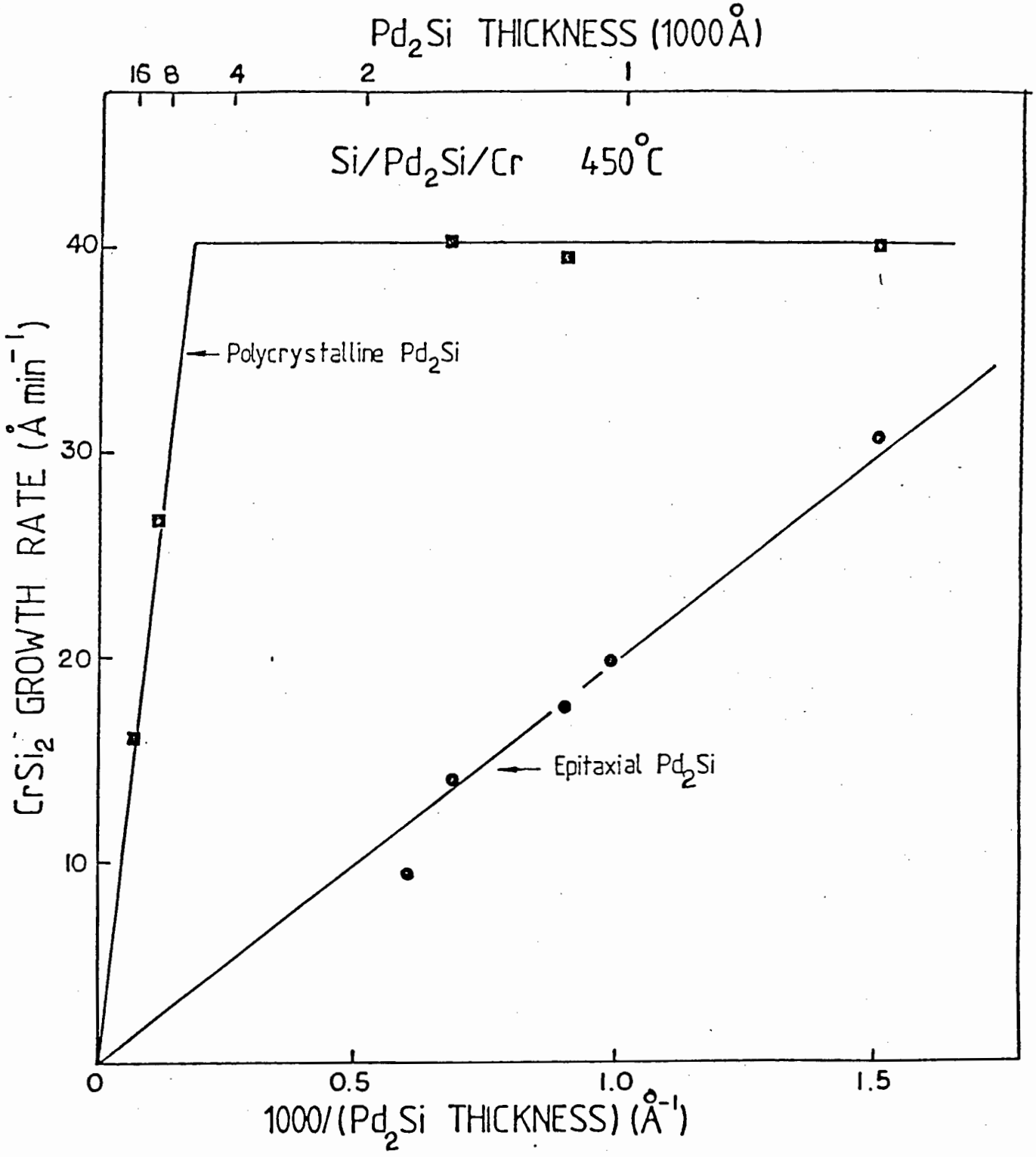

FIG 4-11 The $CrSi_2$ growth rate is inversely proportional to the Pd_2Si layer thickness provided the Pd_2Si layer exceeds a critical thickness. Critical thickness at 450°C is approximately 6700 Å polycrystalline Pd_2Si (position of kink in curve) and 500 Å epitaxial Pd_2Si (see Figure 4.7).

dependence of $\frac{dY_2}{dt}.Y_1$ reflects the temperature dependence of Si in Pd_2Si since all the other parameters on the right hand side are insensitive to temperature changes. The product of the true $CrSi_2$ growth rate and the "thick" interposed Pd_2Si layer thickness is termed the normalized growth rate of $CrSi_2$. An Arrhenius plot of the normalized $CrSi_2$ growth rate against the reciprocal temperature is shown in Figure 4-12. Data used in compiling this curve are summarized in Table 4-1. An activation energy of 1.7 eV is determined from the Arrhenius plot and is associated with the Si transport process through polycrystalline Pd_2Si.

TABLE 4-1 DATA USE FOR COMPILING THE ARRHENIUS PLOT IN FIGURE 4-12

Temperature (°C)	Pd_2Si layer thickness Y_1 (A°)	$CrSi_2$ growth rate $\frac{dY_2}{dt}$ (A°/min)	Normalized $CrSi_2$ growth $Y_1.\frac{dY_2}{dt}$ (10^{-13} Å²/min
420	9 500	0.12	1.14
425	9 500	0.16	1.52
445	9 500	0.45	4.28
445	15 500	0.27	4.19
455	9 500	0.52	4.94
470	9 500	0.85	8.08
470	15 500	0.47	7.39
480	9 500	1.1	10.45

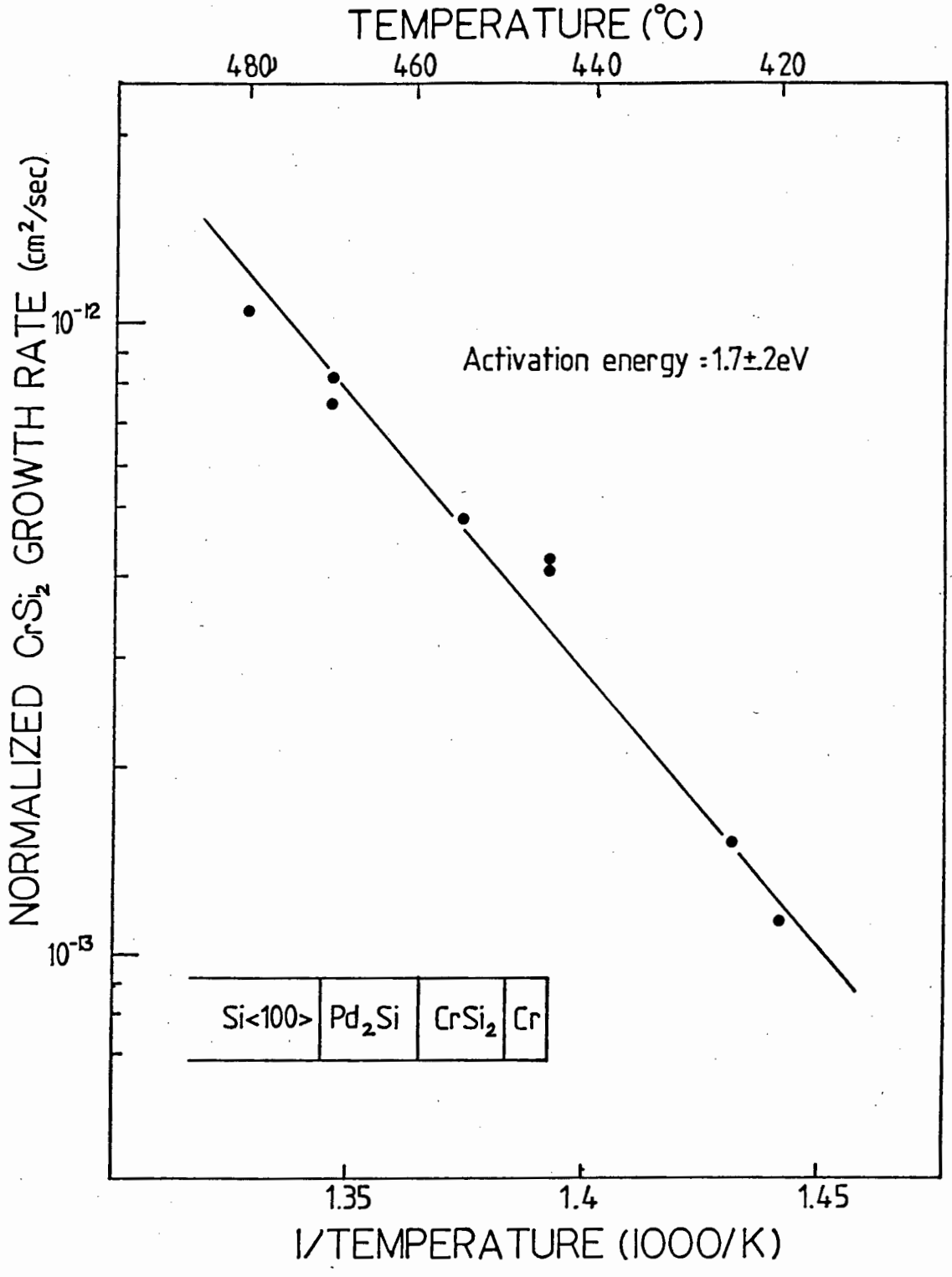

FIG 4-12 Arrhenius plot of the normalized growth rate of $CrSi_2$ formed on polycrystalline Pd_2Si on Si<100> substrates.

4.3.3 Microstructure and morphology

The stoichiometry of the Pd_2Si layer is found to be affected by the $CrSi_2$ growth process. Two spectra of a Si<111>/Pd/Cr sample at various stages of $CrSi_2$ growth are shown in Figure 4-13. The stages represented in the spectra are

(a) after pre-annealing (complete Pd_2Si formation but prior to $CrSi_2$ growth) and

(b) partial $CrSi_2$ growth.

By comparing the plateaus of the Pd and corresponding Si signals in the spectra, it is deduced that the Pd/Si atomic ratio in Pd_2Si is affected by the $CrSi_2$ growth process.

The plateaus of the signals representing Pd and Si in Pd_2Si in Figure 4-13(a) both show the expected gradual increase in height with decrease in energy. This suggests a uniform atomic concentration of Pd and Si in the Pd_2Si film (see 2.2.1). The ratio of the two signal heights indicate that the Pd_2Si layer is roughly stoichrometric (Pd/Si $\approx$ 2). The Pd signal height in the second spectrum (Figure 4-13(b)) shows a decrease with decrease in energy while the corresponding Si signal height increases with decrease in energy. This suggests that the Pd/Si atomic ratio in the Pd_2Si layer decreases with increase in depth below the specimen surface. The Pd_2Si layer is therefore relatively Si-rich near the Si/Pd_2Si interface and relatively Pd-rich near the $Pd_2Si/CrSi_2$

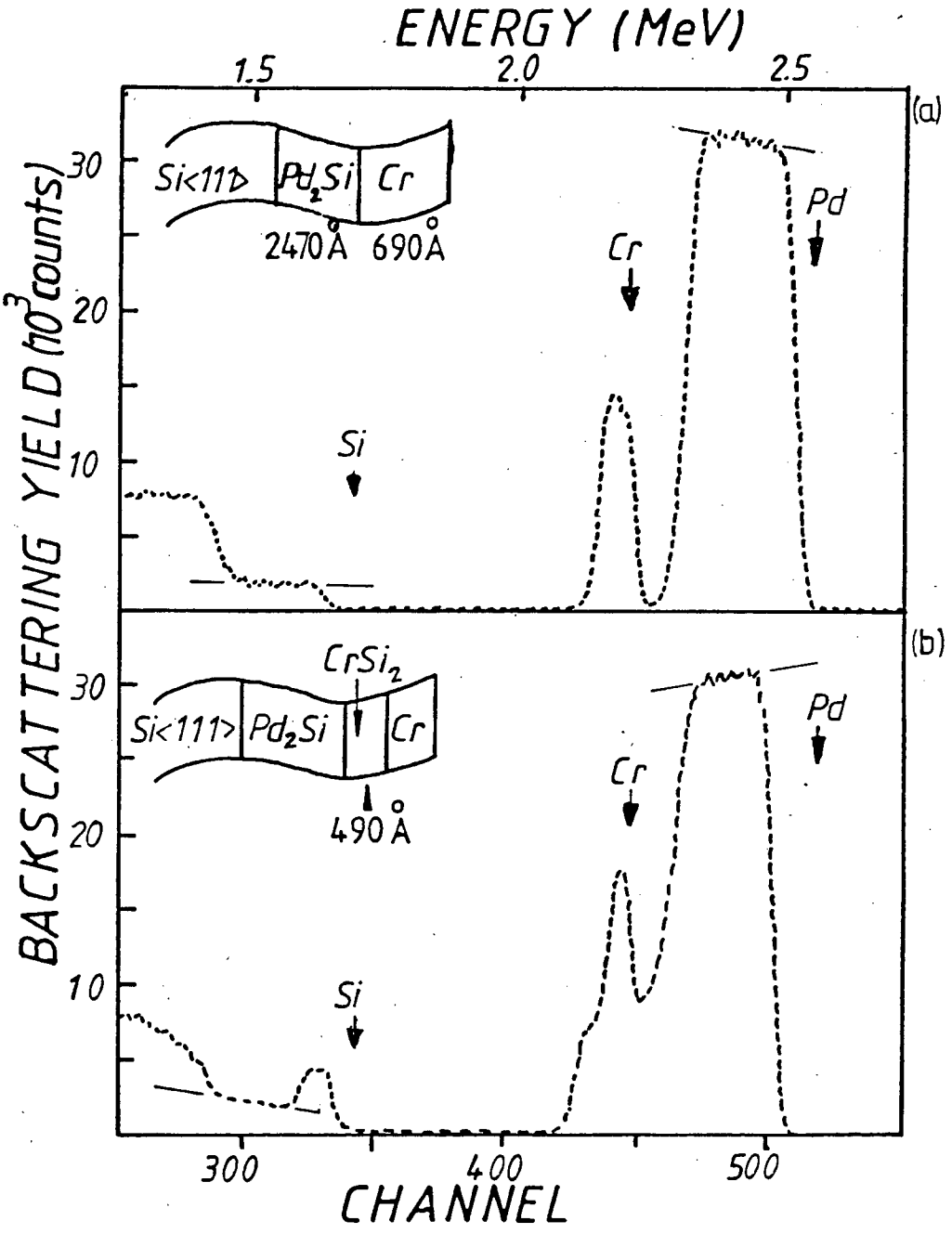

FIG 4-13 Backscattering spectra of Si<111>/Pd_2Si/Cr specimens before (spectrum (a)) and during (spectrum (b)) $CrSi_2$ formation. The plateaus of both Pd (in Pd_2Si) and Si (in Pd_2Si) signals are influenced by the $CrSi_2$ formation process.

interface. It is estimated that the difference in Pd/Si atomic ratio between the Si-rich and Pd-rich regions is in excess of 10%. Spectra of samples in which the $CrSi_2$ formation is complete, indicate that the Pd/Si atomic ratio returns to its uniform value (similar to spectrum (a)) upon termination of the $CrSi_2$ growth process. This phenomenon whereby the $CrSi_2$ growth process affects the stoichiometry of the Pd_2Si layer was also observed in the case of Si<100>/Pd/Cr samples with similar metal layer thicknesses.

The morphology of the Si/Pd_2Si and $Pd_2Si/CrSi_2$ interfaces was examined using scanning electron microscopy. The micrographs of the $Pd_2Si/CrSi_2$ interface of a Si<100>/$Pd_2Si/CrSi_2$ and Si<111>/$Pd_2Si/CrSi_2$ sample are shown in Figure 4-14. These samples were identical with respect to the deposited metal layers, heat treatment and chemical treatment during etching. The two interfaces appear to be equally uniform. Figure 4-15 shows micrographs of the Si/Pd_2Si interface of the same samples as shown in Figure 4-14. The corresponding backscattering spectra of the samples before etching are also shown in the figure. It is obvious that the Si⟨111⟩/Pd_2Si interface is relatively non-uniform. The tail of the low energy edge of the the Pd signal of the corresponding backscattering spectra is indicative of a non-uniform interface, in agreement with the SEM results. Both interfaces of samples with thin interposed layers of epitaxial and polycrystalline Pd_2Si were found to be relatively uniform. This was deduced from scanning electron micrographs as well as backscattering spectra.

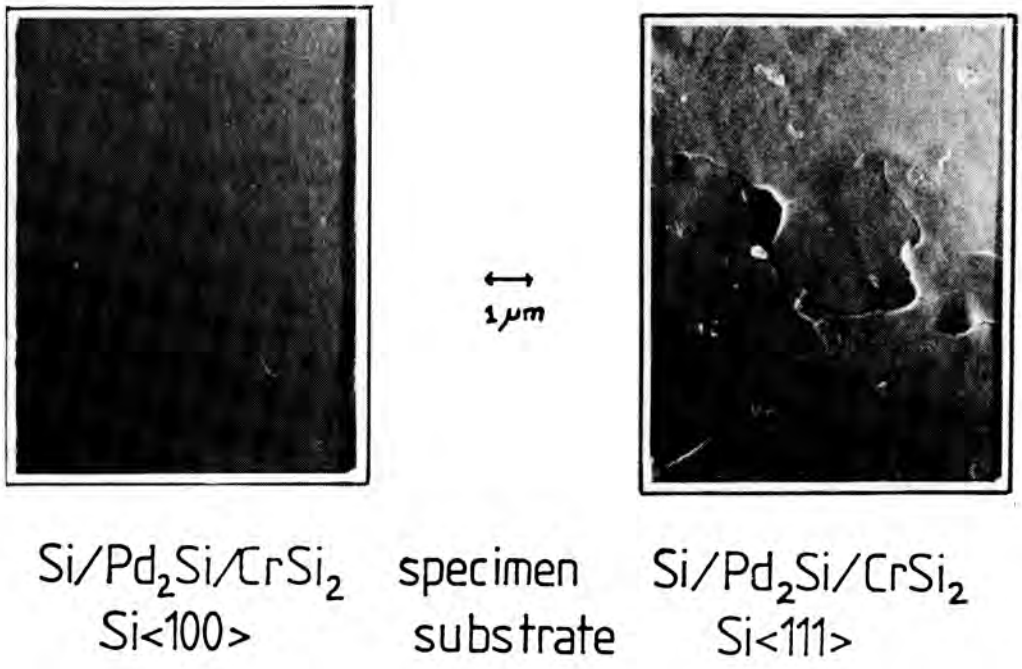

FIG 4.14 Scanning electron micrographs of $Pd_2Si/CrSi_2$ interface morphology of $Si/Pd_2Si/CrSi_2$ specimens. Interface was exposed by etching in HF.

The non-uniformity of the Si<111>/Pd_2Si interface is seen to arise upon Si transport during $CrSi_2$ growth since all the spectra of $Si/Pd_2Si/Cr$ samples (prior to $CrSi_2$ formation but complete Pd_2Si formation) suggest a uniform Si/Pd_2Si interface.

It is known that Pd_2Si grows epitaxially on Si<111> substrates. It is interesting to determine whether Si transport through Pd_2Si affects the degree of epitaxy. The random and aligned spectra of a Si<111>/$Pd_2Si/CrSi_2$/Cr sample are shown in Figure 4-16. The minimum yield is found to be approximately 80%

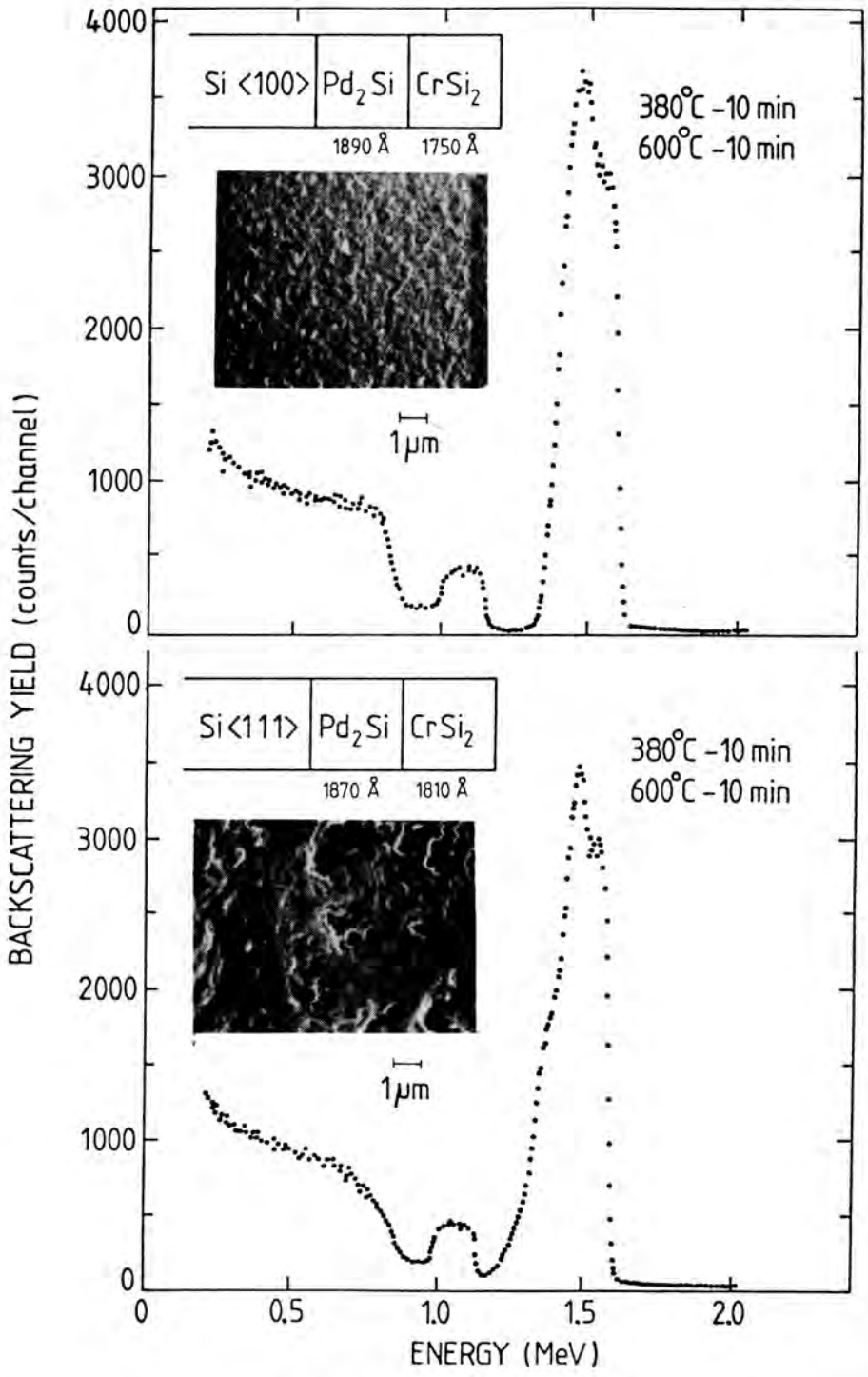

FIG 4-15 Rutherford backscattering spectra of $CrSi_2$ formation on non-epitaxial (top) and epitaxial Pd_2Si (bottom). Scanning electron micrographs of the Si (substrate)/Pd_2Si interface are inserted. Substrates were exposed by etching in HF (removes $CrSi_2$) followed by aqua/regia (removes Pd_2Si).

(Pd signal height in aligned spectrum/Pd signal height in random spectrum). This is a typical value for epitaxial Pd_2Si since it compares well with values reported by Cheung et al.: 80% for Pd_2Si formed at 300°C and 70% for Pd_2Si formed at 400°C [31]. It is assumed that the degree of epitaxy (80% minimum yield) is established during Pd_2Si formation at 380°C and that further annealing at 480°C or Si transport during $CrSi_2$ growth does not affect the epitaxy of the interposed Pd_2Si layer [31].

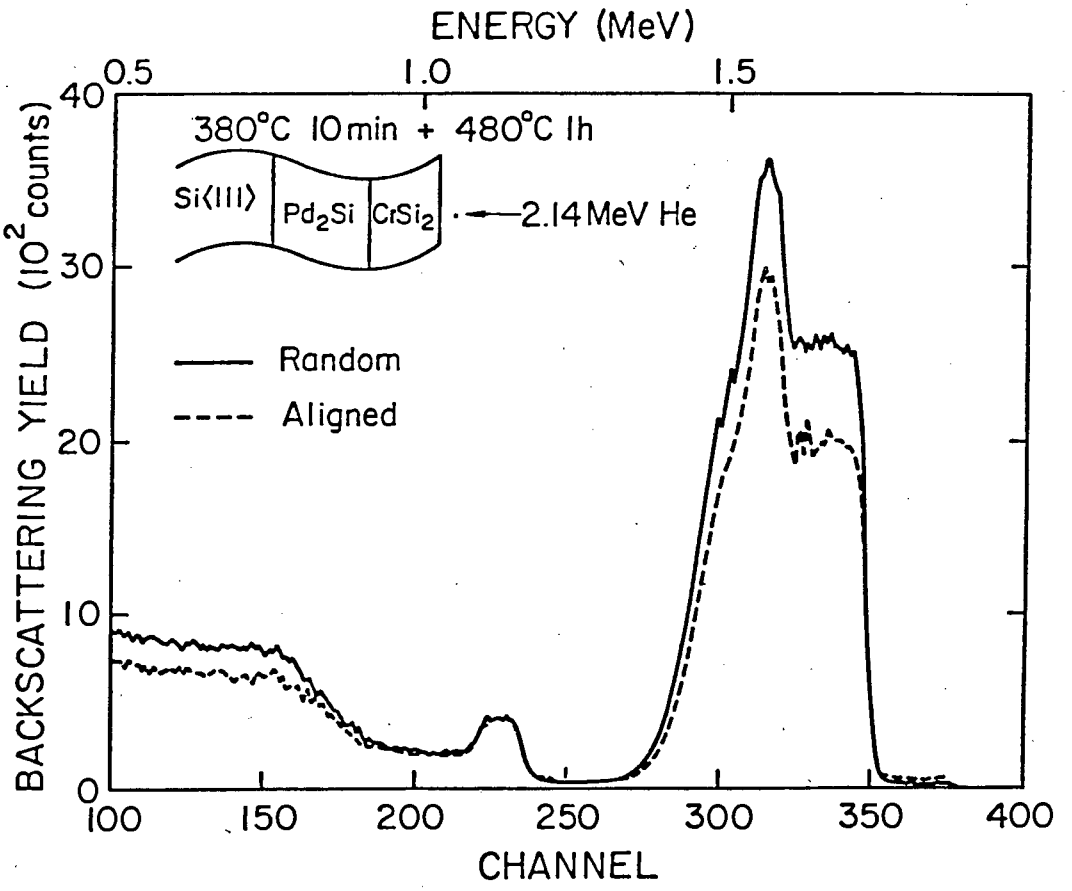

FIG 4-16 Random and aligned backscattering spectra of Si<111>/Pd_2Si/$CrSi_2$ specimen. The reduced height of the Si in Si<111>, Si in Pd_2Si and Pd in Pd_2Si signals in the aligned spectrum indicate that the Pd_2Si layer has grown epitaxially on the Si<111> substrate.

4.4 DISCUSSION

4.4.1 Kinetics

It is interesting to note that the first phase to form during the heat treatment of $Si/Pd_2Si/Cr$ samples is $CrSi_2$, identical to the phase formed during Si-Cr interdiffusion in binary couples. This suggests that the physical and/or chemical characteristics of the Si/Cr interface do not determine which phase ($CrSi_2$, Cr_2Si_3 or CrSi) will form first as such an interface (Si/Cr) is absent in $Si/Pd_2Si/Cr$ samples. Walser and Bené suggested a model to be used in predicting the first phase to nucleate in binary couples [4]. This model is based upon the postulation that a glassy membrane forms at the interface between the components of the couple, most probably during vapour deposition, prior to compound formation. The temperature during the heat treatment of the $Si/Pd_2Si/Cr$ samples never exceed 600°C whereas the lowest eutectic temperature of Si-Cr is 1305°C. It is therefore unlikely that a glassy Si-Cr membrane would have formed at the Pd_2Si/Cr interface prior to $CrSi_2$ formation. This would imply that the first silicide phase to form is not determined by the glassy membrane as was proposed by Walser and Bené.

It has been found that the growth of $CrSi_2$ on epitaxial and polycrystalline Pd_2Si is linear with time. This is in agreement with previous results reported for $CrSi_2$ growth on thin (less than 3000 Å) layers of polycrystalline Pd_2Si [23]. It was pointed out in section 3.3.4 that linear growth in bilayer

metal-silicon systems is not necessarily an indication that the growth is limited by an interfacial reaction. Linear growth in conjunction with an interposed layer thickness effect implies a diffusion limited process.

The model developed in section 3.3 suggests that the thickness of the interposed layer, Y_1, affects the growth rate of the top silicide layer only if Y_1 exceeds a critical value. The results shown in Figures 4-7 and 4-11 are in complete agreement with the model predictions as illustrated in Figure 3-7. The rate of $CrSi_2$ growth is found to be inversely proportional to the Pd_2Si layer thickness when the critical Pd_2Si thickness is exceeded. For thin interposed layers of Pd_2Si, i.e., less than the critical thickness, the $CrSi_2$ growth rate is unaffected by the Pd_2Si layer thickness and similar to that for Si-Cr binary couples. The growth rate of $CrSi_2$ grown on polycrystalline Pd_2Si was reported to be unaffected by the Pd_2Si layer thickness [23]. The reason for this apparent disagreement lies in the fact that the critical polycrystalline Pd_2Si thickness (approximately 6700 Å at 450°C) was not exceeded in the reported study.

It is interesting to note in Figure 4-7 that the critical thickness Y_o increases with increase in temperature. This temperature variation can be interpreted by rewriting (3-39) with $Y_1 = Y_o$ and $\frac{dY_2}{dt} = R_o$:

$$Y_o = B_{Si} \left[\frac{{}_{Si}Pd_2Si}{{}_{Si}CrSi_2}\right] \frac{\Delta G_f^{o}(CrSi_2)}{n R_o} \qquad (4\text{-}1)$$

Although both the mobility B_{Si} and the linear growth rate R_o increase with temperature, an increase of Y_o with temperature indicates that the activation energy associated with the mobility is larger than that associated with the linear rate constant. The fact that the critical thickness of polycrystalline Pd_2Si (approximately 6700 Å at 450°C) is more than ten times the critical thickness of epitaxial Pd_2Si (approximately 500 Å at 450°C) indicates that the Si mobility in polycrystalline Pd_2Si is at least an order of magnitude larger than in epitaxial Pd_2Si. The higher Si mobility is ascribed to the polycrystallinity of the non-epitaxial Pd_2Si. Grain boundary diffusion is expected to contribute to the Si transport process in polycrystalline Pd_2Si whereas in epitaxial Pd_2Si, silicon vacancy diffusion is considered to be the dominant transport mechanism. Grain boundaries can also serve as sources and sinks for Si vacancies [46]. In the case of vacancy sources, the Si vacancy concentration in polycrystalline Pd_2Si is enhanced. Both the above-mentioned effects of grain boundaries would subsequently increase the Si mobility in polycrystalline Pd_2Si.

The activation energy of 1.6 eV obtained from the Arrhenius plot in Figure 4-8 (300 Å Pd_2Si) is in good agreement with the values of 1.7 and 1.5 eV reported for $CrSi_2$ formation directly on Si [23,24]. Since the growth rate of $CrSi_2$ is unaffected by the epitaxial Pd_2Si layer thickness around 300 Å, the linear kinetics and similar activation energy value indicate that the same controlling interfacial reaction is operative during $CrSi_2$

growth with and without interposed Pd_2Si. The only interface which is common to the two systems ($Si/Pd_2Si/CrSi_2/Cr$ and $Si/CrSi_2/Cr$) is the $CrSi_2/Cr$ interface. It can therefore be concluded that the $CrSi_2/Cr$ interfacial reaction controlls the growth of $CrSi_2$ in binary couples in agreement with the speculation in reference 24. The measured activation energy of 1.6 eV is therefore associated with the reaction at the $CrSi_2/Cr$ interface.

Although $CrSi_2$ growth on "thick" Pd_2Si is linear with time, it is not necessarily reaction limited. The growth rate is found to be inversely proportional to the Pd_2Si layer thickness, which, together with the linear growth, indicate that the growth is limited by diffusion of Si through the Pd_2Si layer. The high activation energy of 2.2 eV measured in the cases of 1000, 1400, and 2500 Å Pd_2Si (see Figure 4-8) is associated with the Si transport process as can be deduced from equation (3-39):

$$\ell n\{R_2\} = \ell n\{B_{Si}\} + \ell n \left\{ \frac{\left[{}_{Si}^{Pd_2Si}\right]}{\left[{}_{Si}^{CrSi_2}\right]} \cdot \frac{\Delta G_f^{o(Cr_2Si)}}{n\ Y_1} \right\}$$

The temperature dependence of $\ell n\{R_2\}$ in fact reflects the temperature dependence of $\ell n\{B_{Si}\}$ since the second term on the right hand side is insensitive to temperature variation. The high activation energy of 2.2 eV for $CrSi_2$ growth (R_2) on "thick" epitaxial Pd_2Si therefore represents the activation energy of the Si mobility (B_{Si}) in epitaxial Pd_2Si.

From (3-39) the "normalized" growth rate R_2Y_1 can be expressed as:

$$\ell n\{R_2 Y_1\} = \ell n\{B_{Si}\} + \ell n \left\{ \frac{\left[{}_{Si}^{Pd_2Si}\right]}{\left[{}_{Si}^{CrSi_2}\right]} \cdot \frac{\Delta G_f^{o(CrSi_2)}}{n} \right\}$$

The activation energy of 1.7 eV which was obtained from the Arrhenius plot in Figure 4-12 is therefore that of the Si mobility in polycrystalline Pd_2Si. A similar plot for epitaxial Pd_2Si was included in Figure 4-8 ($\ell n\{R_o Y_o\}$ against 1/T) and yielded 2.2 eV, in agreement with the other curves in the same figure.

The activation energy of 2.2 eV for the mobility of Si in epitaxial Pd_2Si is of the same order as the value of 2.1 eV reported for Si self diffusion in PtSi [47]. Self diffusion takes place predominantly by Si vacancy diffusion. It is therefore concluded that the Si transport mechanism in epitaxial Pd_2Si during $CrSi_2$ growth is also vacancy diffusion. The lower activation energy of 1.7 for Si mobility in polycrystalline Pd_2Si as determined from Figure 4-12 is due to the presence of grain boundaries. The contribution of grain boundaries in providing short circuit diffusion paths and in serving as sources of Si vacancies will be reflected in the lowering of the activation energy. The possible contribution of fast diffusion paths along the grain boundaries is less likely since grain boundary diffusion would generally not lead to the $R_2 \propto \frac{1}{Y_1}$ dependence (see 6.2.2).

The rate of $CrSi_2$ formation directly on Si substrates (i.e., reciprocal Pd_2Si thickness $\rightarrow \infty$) was generally found to be slightly

less than the rate on thin Pd_2Si layers, (see asterisks in Figure 4-7) in accordance with observations by Olowolafe et al. [23]. This observation is believed to be due to a contaminated Si/Cr interface. An interposed Pd layer serves the purpose of "cleaning" the Si/Pd interface during Pd_2Si formation so that subsequent $CrSi_2$ growth is not inhibited by a contaminated interface at the Si substrate.

4.4.2 Microstructure and morphology

The Si transport process through Pd_2Si is not expected to affect the stoichiometry (see Figure 4-13) or the interface morphology (see Figure 4-15) of the Pd_2Si layer unless a lattice diffusion mechanism is operative. It is observed that the stoichiometry of the Pd_2Si layer is uniform after preannealing, i.e., before $CrSi_2$ growth. The stoichiometry of Pd_2Si at this stage is therefore determined by the Si/Pd_2Si interface equilibrium conditions since the Pd_2Si/Cr interface is inactive (no transport across the interface prior to $CrSi_2$ growth). The Pd_2Si layer is therefore expected to be slightly silicon-rich. The Si/Pd atomic ratio corresponds to point B in the imaginary free energy diagram in Figure 3-2.

During $CrSi_2$ growth on Pd_2Si, a gradient in the Pd and/or Si atomic concentration in Pd_2Si developes, as is deduced from Figure 4-13(b). In order to identify the sublattice (Pd or Si) of Pd_2Si which contains the large concentration gradient, it is necessary to determine the absolute densities of Pd and

Si in the Pd_2Si layer. This proves to be difficult when utilizing backscattering spectrometry for sample analysis. Suppose that only Si atoms are displaced in Pd_2Si during $CrSi_2$ growth (see Chapter 5), then it is reasonable to assume that the gradient observed in the backscattering spectrum is due to a gradient in the Si atomic concentration across the Pd_2Si layer. This Si concentration gradient developes as a result of the two interfacial reactions and the diffusion process. Following (3-29) and (3-32), the interfacial reaction equations are:

$$Si^X \rightarrow Si + V_{Si}$$

in the Pd_2Si layer at the $Pd_2Si/CrSi_2$ interface where Si vacancies V_{Si} are created, and;

$$V_{Si} + Si \rightarrow Si^X$$

at the Si/Pd_2Si interface where the Si vacancies are annihilated. In the above equations Si^X represents a silicon atom on a lattice site in Pd_2Si whereas Si represents a free silicon atom. These two reactions establish different Si vacancy concentrations (also different Si atomic concentration), at the two interfaces, resulting in a flow of Si vacancies. A corresponding Si flux in the opposite direction therefore establishes the observed Si concentration gradient across the Pd_2Si layer. The fact that the Si concentration gradient disappears once $CrSi_2$ growth is terminated (Cr completely consumed) indicates that the Si concentration in Pd_2Si is eventually determined by a single interfacial reaction, probably that at the Si/Pd_2Si interface.

The non-uniformity of the Si/Pd_2Si interface only appears when Si is transported through thick epitaxial Pd_2Si for $CrSi_2$ growth. Because of straggling in the case of "thick" polycrystalline Pd_2Si (~1μm) it was impossible to investigate the uniformity of the Si/Pd_2Si interface by means of backscattering spectrometry. Following the arguments below, the $Si<100>/Pd_2Si$ interface uniformity is not expected to be affected by Si transport through thick polycrystalline Pd_2Si. The exact cause of the non-uniformity is not known but the following explanation is proposed: As a result of the misfit (lattice mismatch) between the Si<111> substrate and the epitaxial Pd_2Si layer, the interface is strained. It is known that the interfacial strain energy increases with increase in epitaxial film thickness and is insignificant in the case of polycrystalline films [48 , 49]. The interfacial strain can however be relieved through the development of misfit dislocations [48]. These dislocations could serve as sources and sinks for the generation or trapping of vacancies, thereby creating a favourable chemical environment for nucleation and reaction [50]. The Si-release reaction (Si bond breaking) at the $Si<111>/Pd_2Si$ interface will therefore be enhanced at the sites where these dislocations emerge. It is furthermore expected that the interfacial strain is non-uniform, having its peak values where the expitaxial "grains" meet. These localized high-strain regions represent "weak" spots on the Si<111> substrate where Si bond-breaking will preferably take place. This laterally non-uniform process whereby Si is released for diffusion through

the Pd_2Si layer results in the pitting of the Si<111> substrate which is reflected in the non-uniform Si<111>/Pd_2Si interface in the case of thick interposed epitaxial Pd_2Si layers. The Si<111>/Pd_2Si interface of samples with thin interposed epitaxial Pd_2Si layers remains uniform owing to the small amount of interfacial strain energy (strain energy increases with increase in film thickness [48,49]). The uniformity of the Si<100>/Pd_2Si interface of Si<100>/Pd_2Si/$CrSi_2$ samples is not affected by the Si release process since the strain energy is significant only in the case of isostructural (epitaxial) films [48].

It is interesting to note that the Si<111>/Pd_2Si interface remains relatively uniform during the growth of thick epitaxial Pd_2Si layers from Si<111>-Pd couples, in spite of the expected laterally non-uniform Si-release. It should however be borne in the mind that both Pd and Si diffuse during Pd_2Si growth whereas only Si diffuses through Pd_2Si during $CrSi_2$ growth on it (see Chapter 5). The diffusing palladium atoms which reach the Si/Pd_2Si interface during Pd_2Si growth assist in the silicon bond breaking process by diffusing interstitially into the Si substrate [51]. This leads to a laterally uniform Si-release process and hence results in a uniform Si<111>/Pd_2Si interface.

CHAPTER 5

THE DIFFUSING SPECIES DURING $CrSi_2$ GROWTH ON Pd_2Si

5.1 INTRODUCTION

During $CrSi_2$ growth on Pd_2Si there is an overall displacement of Si with respect to Pd in the Pd_2Si layer. The question to be addressed in this chapter is: what is the specific diffusion mechanism for Si transport through the Pd_2Si layer. Various mechanisms are possible:

1. Silicon diffuses via vacancies in the Si sub-lattice of Pd_2Si.
2. Silicon diffuses interstitially through the Pd_2Si lattice.
3. Silicon diffuses along the grain boundaries in poly-crystalline Pd_2Si.
4. Dissociation of Pd_2Si near the $Pd_2Si/CrSi_2$ interface will release Si for $CrSi_2$ growth. The free Pd atoms subsequently diffuse to the substrate to form new Pd_2Si. The specific mechanism of Pd diffusion is irrelevant in this study.

The diffusion mechanism for Si transport could also be a combination of the processes described above.

Marker experiments have been used extensively to identify the diffusing species and the diffusion mechanism during atomic interdiffusion. Two classes of markers can be distinguished namely inert markers and isotope markers. Inert markers which

do not participate in the diffusion process, reveal the flux ratio of the interdiffusing atomic species. No information regarding the specific diffusion mechanism can be obtained. Isotopic markers (radio-active or stable) participate in the diffusion process since they are chemically identical to one of the diffusing species. Information about the diffusion mechanism can therefore be extracted from the redistribution of the isotopic markers upon interdiffusion. These two techniques are seen to be complementary and a complete picture of the diffusion process can be obtained by applying both techniques to the interdiffusing system.

5.2 RADIO-ACTIVE ^{31}Si TRACER STUDIES OF $CrSi_2$ GROWTH ON Pd_2Si

A radio active ^{31}Si tracer experiment, with the objective of establishing the Si transport mechanism during $CrSi_2$ growth on Pd_2Si, was performed by Pretorius et al. [52]. The significance of the experimental results will become evident after the following detailed description of the experimental procedure. Radioactive silicon (Si*) was deposited on Si<100> substrates on which palladium was predeposited. This was followed by a chromium layer of thickness varying between 300 and 3500 Å. The specimens (Si<100>/Pd/Si*/Cr) were subsequently pre-annealed at 400°C for five minutes to form Pd_2Si by a reaction of Pd with both the activated amorphous Si and the single crystal Si from the substrate. The radioactive Si is therefore imbedded in a Pd_2Si sublayer (Si<100>/Pd_2Si / Pd_2Si^*/Cr). On further annealing at elevated temperatures up to 650°C, $CrSi_2$ was formed. The Si radio-activity of the samples originating from the β-decay

of ^{31}Si, was determined before and after removal of the $CrSi_2$ layer. In Figure 5-1, the percentage activity left in die Pd_2Si layer after etching off $CrSi_2$, is plotted as a function of the D-values (ratio of Si atoms in $CrSi_2$ to Si atoms in the Pd_2Si layer) for various annealing temperatures.

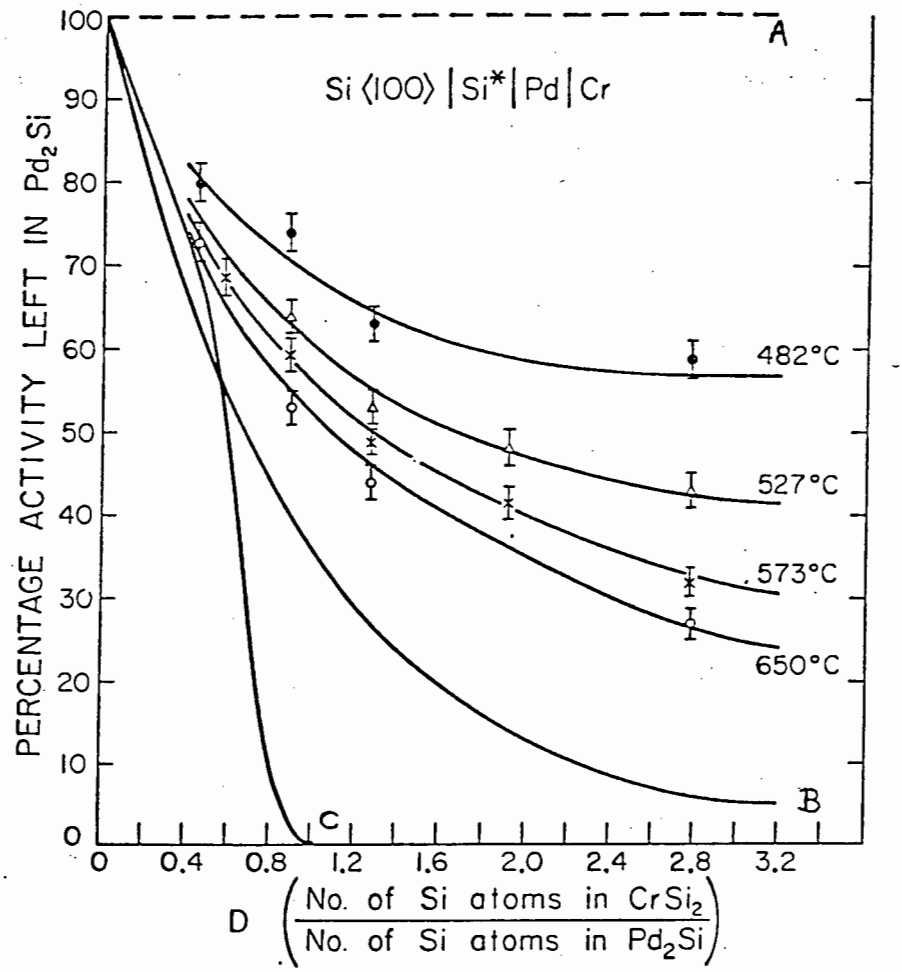

FIG 5-1 Percentage Si^* radio activity left in the Pd_2Si layer after $CrSi_2$ formation, as a function of $CrSi_2$ thickness (D value). Curves A, B and C are calculated for various diffusion mechanisms in Pd_2Si: A, grain boundary or interstitial Si diffusion; B, Si vacancy diffusion with high Si self diffusion in Pd_2Si; C, Si vacancy diffusion with low Si self diffusion in Pd_2Si. (from reference 52).

Theoretical curves are also shown in Figure 5-1. Curve A is obtained if it is assumed that Si is transported along the grain boundaries or via interstitial sites in the Pd_2Si lattice. When calculating curve B, Si vacancy diffusion was considered to be the transport mechanism, with a high Si-self diffusivity in Pd_2Si and low Si self diffusivity in $CrSi_2$. Complete mixing of the radioactive and non-radioactive Si in Pd_2Si is thus obtained. A variation to this mechanism is Si vacancy diffusion through the interposed Pd_2Si layer with relatively low Si self-diffusion in Pd_2Si (little mixing of radioactive and non-radioactive Si in Pd_2Si). This is represented by curve C. In Figure 5-2 the radioactive Si distribution in the Si/Pd/*Si/Cr samples before and after $CrSi_2$ growth, are shown schematically for the three cases, A,B, and C in Figure 5-1. It is shown that specific diffusion mechanisms as mentioned in section 5.1 give rise to specific activity distributions upon complete $CrSi_2$ formation. Silicon vacancy diffusion (mechanism 1) and Pd_2Si dissociation with Pd diffusion (mechanism 4) give rise to the same Si activity distribution after $CrSi_2$ growth. Similarly diffusion of silicon via interstitial sites (mechanism 2) and diffusion along grain boundaries (mechanism 3) give rise to the same Si activity distribution.

The experimental results of interest to this work are the data at temperatures below 500°C. From Figure 5-1 it appears that approximately 50% of the Si is transported via grain boundary or interstititial diffusion. The remainder is transported either via Si vacancy diffusion or Pd diffusion (in conjunction with Pd_2Si dissociation). A decrease in temperature seems to favour

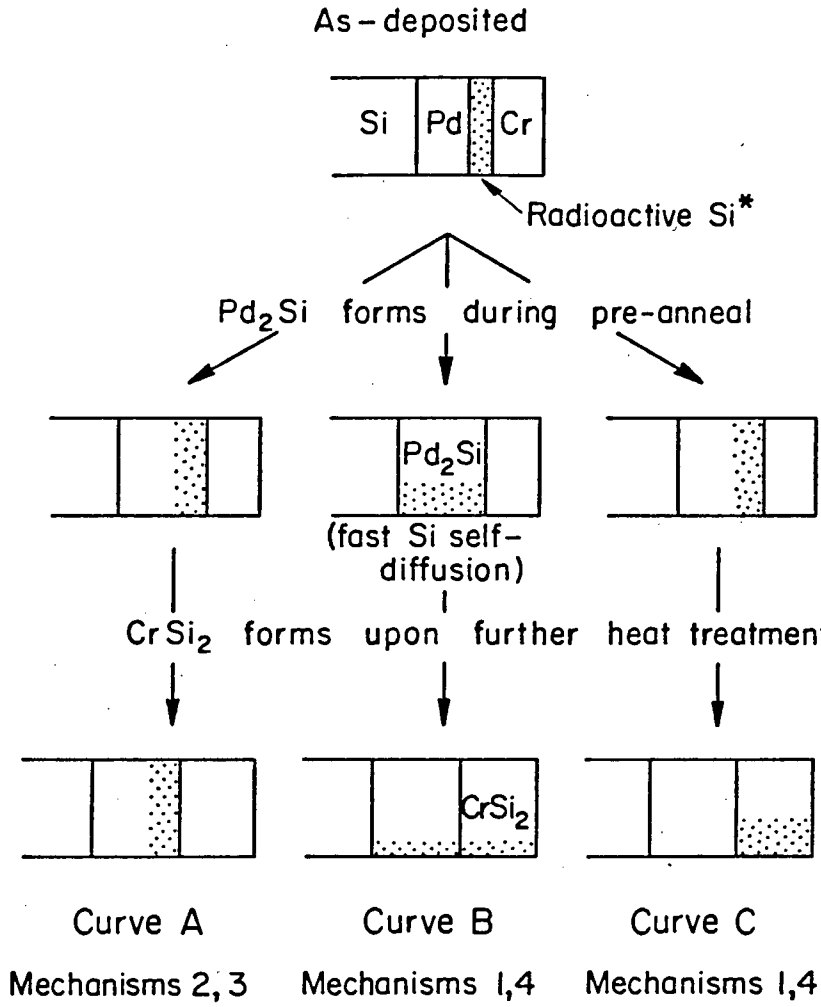

Mechanism 1 Vacancy diffusion of Si through Pd_2Si

Mechanism 2 Interstitial diffusion of Si through Pd_2Si

Mechanism 3 Grain boundary diffusion of Si through polycrystalline Pd_2Si

Mechanism 4 Dissociation of Pd_2Si with Pd diffusion through Pd_2Si

FIG 5-2 Redistribution of radioactive Si as a result of $CrSi_2$ formation. Fast Si self diffusion in $CrSi_2$ has been assumed [26]. The curves A, B and C which are being referred to, are shown in Figure 5-1 and the corresponding diffusion mechanisms are illustrated in the above figure.

grain boundary and interstitial diffusion as could be expected from thermodynamic considerations. It should be pointed out that these measurements reflect the Si transport mechanism (during $CrSi_2$ growth) through Pd_2Si, which has been formed through the interaction of Pd with amorphous (radioactive) silicon. The grain size of Pd_2Si formed on amorphous Si substrates is found to be significantly smaller than that on Si<100> substrates [31,53]. The contribution from Si grain boundary diffusion to Si transport through Pd_2Si on Si<100> will therefore be smaller than is implied in Figure 5-1. In the case of epitaxial Pd_2Si, grain boundary diffusion of Si can be largely disregarded. Although these results do not provide an unambiguous picture of the diffusion mechanism for Si transport in Pd_2Si during $CrSi_2$ growth, they tend to suggest that Si vacancy diffusion and/or Pd diffusion are the dominant mechanisms. It is therefore necessary to use radioactive Pd tracer atoms or inert markers to complement these results so as to identify the diffusing species.

5.3 TUNGSTEN MARKER IN Si/Pd/Cr SYSTEM

5.3.1 Introduction

Inert markers were first used by Kirkendal in bulk Cu-Zn couples [54]. Since then the marker technique has been widely applied to various interdiffusing systems including thin films. The dominant diffusing species during thin film metal silicide formation have been established for a large number of systems, using this method [24,55]. Inert noble gas marker atoms (Ar, Xe, or Kr) are usually implanted in the metal or Si layer prior to

interdiffusion. An analytical technique such as RBS is then used to monitor the position of the marker with respect to the moving interfaces during silicide formation. The flux ratio of the interdiffusing atomic species is determined from the relative displacement of the marker atoms with respect to the moving interfaces.

In order to provide reliable results with unambiguous interpretations, the inert marker has to fulfill a number of requirements:

1. It should not partake in the diffusion, nor react with any of the components [56].
2. The presence of the marker should not influence the diffusion process through becoming a diffusion barrier to one or both interdiffusing components.
3. The marker layer thickness should be relatively small compared to the total diffusion layer thickness.
4. The marker atoms should not be dragged along by the moving interface [57].

Implanted inert markers satisfy most of the above requirements. The ideal situation is when the inert marker is imbedded in the partially formed silicide layer. This would avoid interface drag.

Recently W has been used as a marker during metal silicide formation and oxidation [56-58]. An advantage of using W is

the ease with which it can be introduced into the thin film system, using the usual deposition techniques. This eliminates the use of an implanter. Another advantage is the well defined distribution of deposited W compared to implanted inert atoms. It is anticipated that W would form compounds such as WSi_2 with the Si atoms. Because of the high thermal stability of this compound these silicide molecules (clusters) will be relatively inert so that W can be considered as a pseudo-inert marker. In order to limit the influence of W on the diffusion process, the tungsten layer should be discontinuous. It is assumed that very thin layers of W (<10°A) will result in incomplete coverage, thereby limiting the interference caused by the marker atoms.

In the following sections experimental results of W marker studies of Pd_2Si growth and $CrSi_2$ growth on Pd_2Si are presented.

5.3.2 Atomic flux ratio during Pd_2Si growth

Thin film structures consisting of Si/Pd/W/Pd were prepared in the usual manner. Both Si<100> and Si<111> substrates were used. The thickness of the various layers were approximately 20 Å Pd, 5 Å W, and 1000 Å Pd. The thin Pd layer between Si and W ensures that the initial Si/Pd interface does not affect the movement of the W marker. It also provides Pd_2Si nucleation seeds for epitaxial growth on Si<111> substrates. The samples were subsequently annealed at various temperatures between 200 and 400°C.

Backscattering spectra of a Si<100>/Pd/W/Pd sample, before and after Pd_2Si growth, are shown in Figure 5-3. On comparing the spectra it is seen that the W signal position is not affected by the Pd_2Si growth process. The broadening of the

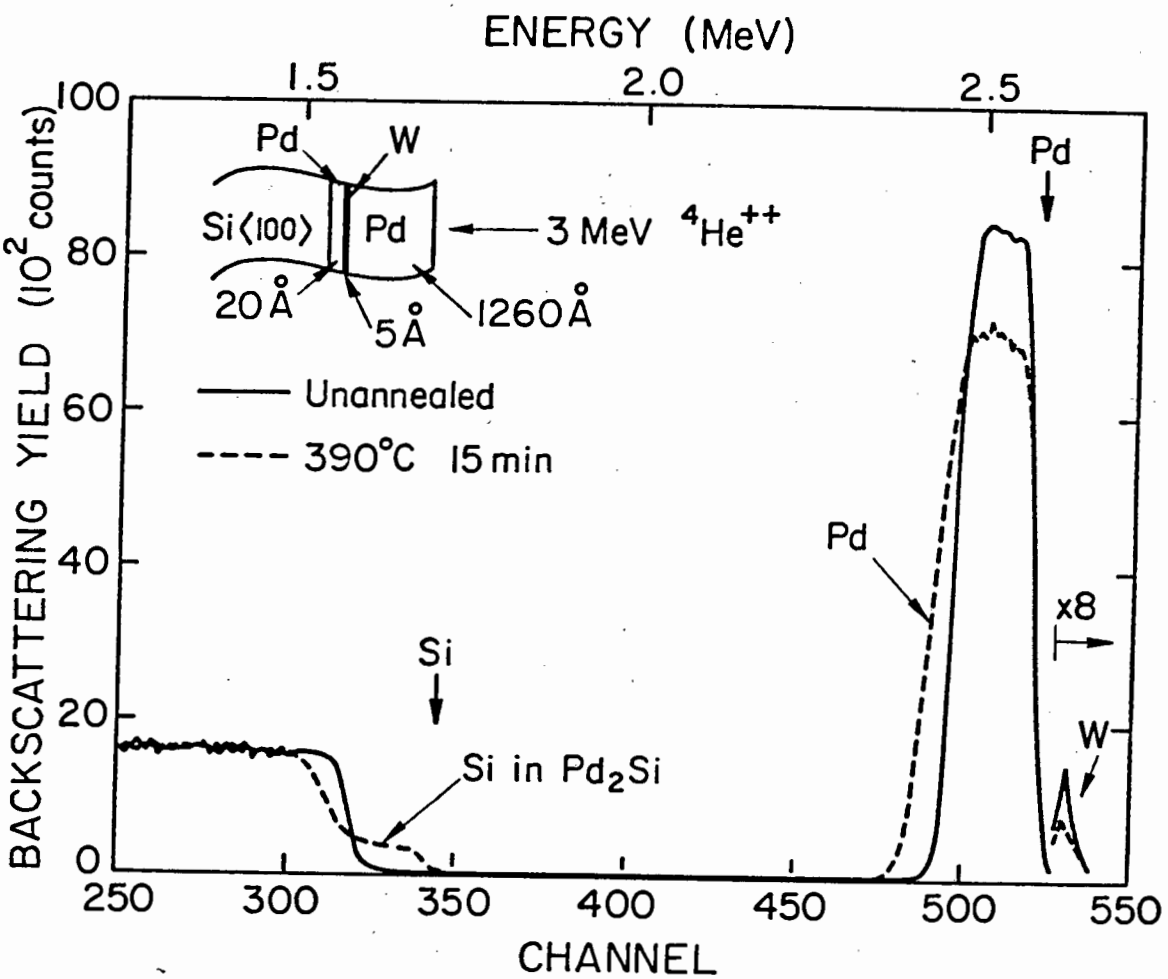

FIG 5-3 Backscattering spectra of a Si<100>/Pd/W/Pd sample before and after Pd_2Si formation. The position of the W signal is unaffected by Pd_2Si growth.

Pd signal and the step in the Si signal are indicative of Pd_2Si formation. The relatively narrow W peak before annealing is seen to be spread out after Pd_2Si growth. This would suggest that the W atoms partake in the diffusion process to a limited extent. A similar behaviour has been reported

for implanted inert atoms during silicide growth [55].

Although the position of the W signal in Figure 5-3 is not affected by the silicide formation, it actually represents a shift in the position of the W layer with respect to the Si/Pd_2Si (originally Si/Pd) interface. The relative displacement of the W layer from which the Si/Pd atomic flux ratio is calculated is determined from energy loss considerations.

Consider a Si-Pd couple with the W marker atoms originally at the Si/Pd interface. This is illustrated in Figure 5-4(a).

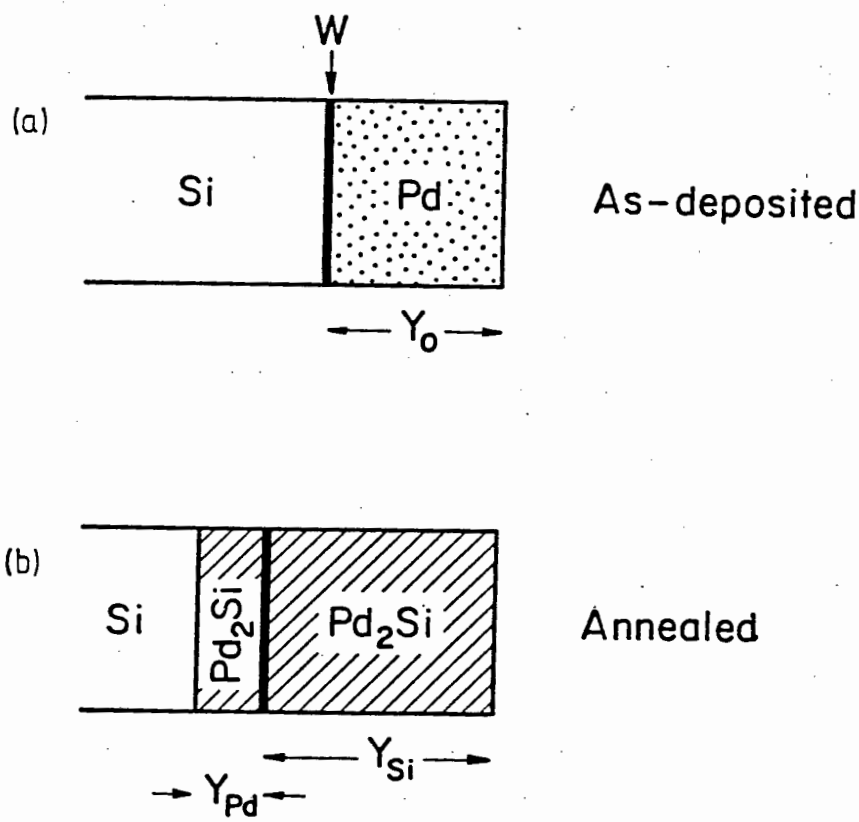

FIG 5-4 Schematic of a Si-Pd couple with W marker atoms originally near the Si/Pd interface. After Pd_2Si growth the W marker atoms are imbedded in the Pd_2Si layer.

The thickness of the Pd layer is Y_o. If both Si and Pd diffuse during Pd_2Si growth, then the position of the W marker atoms with respect to the Pd_2Si layer will be as illustrated in Figure 5-4(b). The number of silicon atoms which have diffused past the marker atoms is given by $Y_{Si}[Si^{Pd_2Si}]$ where $[Si^{Pd_2Si}]$ is the silicon concentration in Pd_2Si and Y_{Si} is the depth of the W marker atoms below the specimen surface. Similarly the number of palladium atoms which have diffused past the marker atoms are given by $Y_{Pd}[Pd^{Pd_2Si}]$ where $[Pd^{Pd_2Si}]$ is the palladium concentration in Pd_2Si and Y_{Pd} is the distance from the W atoms to the Si/Pd_2Si interface. The Si/Pd atomic flux ratio is now given by

$$\frac{\text{Si flux}}{\text{Pd flux}} = \frac{Y_{Si}[Si^{Pd_2Si}]}{Y_{Pd}[Pd^{Pd_2Si}]} \qquad (5\text{-}1)$$

The parameter Y_{Si} is determined from the energy shift ΔE of the W signal in the two backscattering spectra in Figure 5-3

$$\Delta E_W = Y_o[\varepsilon]^{Pd}_{Pd}[Pd^{Pd}] - Y_{Si}\left\{[\varepsilon]^{Pd_2Si}_{Si}[Si^{Pd_2Si}] + [\varepsilon]^{Pd_2Si}_{Pd}[Pd^{Pd_2Si}]\right\} \qquad (5\text{-}2)$$

where $[\varepsilon]^{Pd_2Si}_{Si}$ is the stopping cross-section factor of Si in Pd_2Si, and

$[Si^{Pd_2Si}]$ is the concentration of silicon in Pd_2Si.

The parameter Y_{Pd} is determined from the conservation of mass principle:

$$Y_o[Pd]^{Pd} = (Y_{Pd} + Y_{Si})[Pd]^{Pd_2Si} \qquad (5\text{-}3)$$

Using the following experimental data (ΔE and Y_o) and published values for the stopping cross-section factors and concentrations in conjunction with the three equations above, the Si/Pd flux ratio was determined.

Experimental:

$\Delta E_W = 0$ (no significant energy shift of W signal observed in Figure 5-3)

$Y_o = 1260$ Å

From reference [9] :

$$[\varepsilon]^{Pd}_{Pd} = 154 \times 10^{-15} \text{ eV cm}^2$$

$$[\varepsilon]^{Pd_2Si}_{Pd} = 154 \times 10^{-15} \text{ eV cm}^2$$

$$[\varepsilon]^{Pd_2Si}_{Si} = 77 \times 10^{-15} \text{ eV cm}^2$$

From reference [6] :

$$[Pd]^{Pd} = 6.8 \times 10^{22} \text{ atoms cm}^{-3}$$

$$[Pd]^{Pd_2Si} = 4 \times 10^{22} \text{ atoms cm}^{-3}$$

$$[Si]^{Pd_2Si} = 2 \times 10^{22} \text{ atoms cm}^{-3}$$

The values of Y_{Si} and Y_{Pd} were found to be:

$$Y_{Si} = 1720 \text{ Å}$$

$$Y_{Pd} = 420 \text{ Å}$$

From these values of Y_{Si} and Y_{Pd} it is seen that upon Pd_2Si growth, the marker atoms are positioned approximately $\frac{1}{5}$th $\left[\frac{Y_{Pd}}{(Y_{Pd} + Y_{Si})}\right]$ of the Pd_2Si layer thickness away from the Si/Pd_2Si interface. The Si/Pd atomic flux ratio was thus found to be 2.0 ± 0.6. The large uncertainly in the value for the flux ratio is a consequence of the poor depth resolution of the backscattering technique (typically 200 Å).

The temperature of Pd_2Si formation was not found to have a significant influence on the atomic flux ratio. This suggests that the Si and Pd flux are coupled through a diffusion mechanism which is characteristic of the particular crystal structure. If Si and Pd were to diffuse independently, the temperature would be expected to influence the atom flux ratio if it is assumed that the respective mobilities are associated with different activation energies. The Si/Pd flux ratio was found to be very similar (within experimental error) for epitaxial and polycrystalline Pd_2Si growth, in spite of the fact that the diffusion mechanisms are probably slightly different. This indicates that the contribution from grain boundary diffusion to the growth of polycrystalline Pd_2Si is relatively small compared to lattice diffusion. The small difference in activation energies reported for epitaxial and polycrystalline

Pd_2Si growth (0.95 ± 0.1 eV polycrystalline and 1,05 ± 0.1 eV epitaxial [31]) suggest similar diffusion mechanisms in the two cases. Since grain boundary diffusion in epitaxial Pd_2Si is limited, the similar activation energies suggest little grain boundary diffusion also in the case of polycrystalline Pd_2Si.

It is thus concluded that both Si and Pd diffuse through Pd_2Si during its growth and their atom fluxes are comparable. Inert marker atoms, originally near the Si/Pd interface, will be positioned near the Si/Pd_2Si interface (approximately $\frac{1}{5}$th of Pd_2Si layer thickness), after Pd_2Si growth, irrespective of the formation temperature or Si substrate orientation.

5.3.3 Atom flux during $CrSi_2$ growth on Pd_2Si

The diffusion mechanism during $CrSi_2$ growth in Si/Cr couples has been carefully examined [24,26]. The results indicate that Si diffuses via vacancies. It is assumed that the interposed Pd_2Si layer in $Si/Pd_2Si/Cr$ samples does not influence the diffusion mechanism in $CrSi_2$ during its growth on Pd_2Si. In order to elucidate the relative Pd and Si fluxes in Pd_2Si during $CrSi_2$ growth, a W marker experiment similar to that described in 5.3.2 was performed. The pseudo-inert W atoms, imbedded in the Pd_2Si layer, delineate a reference plane across which the flux of Si and Pd is monitored.

Samples, similar to those described in section 5.3.2 except for an additional Cr layer on the surface, were used in the study. After preannealing these samples at 390°C for fifteen minutes, the W is positioned in the Pd_2Si layer. This is

illustrated in Figure 5-5 where the backscattering spectra of Si/Pd/W/Pd/Cr samples, before and after pre-annealing, are shown. The position of the W peak is seen to be relatively unaffected by the formation of Pd_2Si, similar to the case without Cr, discussed in section 5.3.2. On further annealing at elevated temperatures, $CrSi_2$ forms. Backscattering spectra

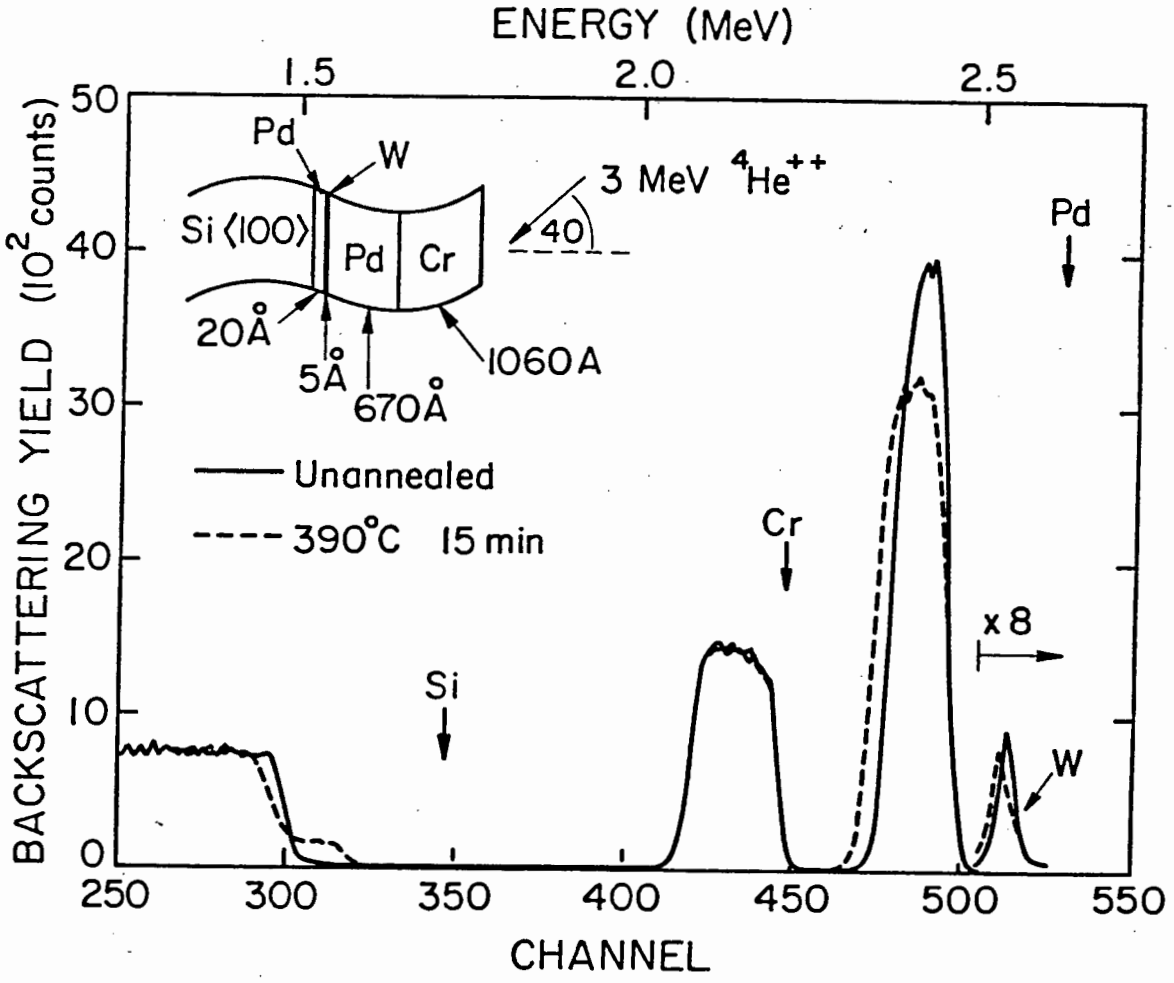

FIG 5-5 Backscattering spectra of a Si<100>/Pd/W/Pd/Cr specimen before and after heat treatment at 390°C. The position of the W signal is seen to be relatively unaffected by the heat treatment.

of a sample prior and subsequent to annealing at 480°C are shown in Figure 5-6. Both the Pd and W peaks are seen to be shifted to lower energy positions while the relative position of the W peak with respect to the Pd peak remains the same. This indicates that the W atoms, after becoming embedded in the Pd_2Si layer during Pd_2Si growth, do not move

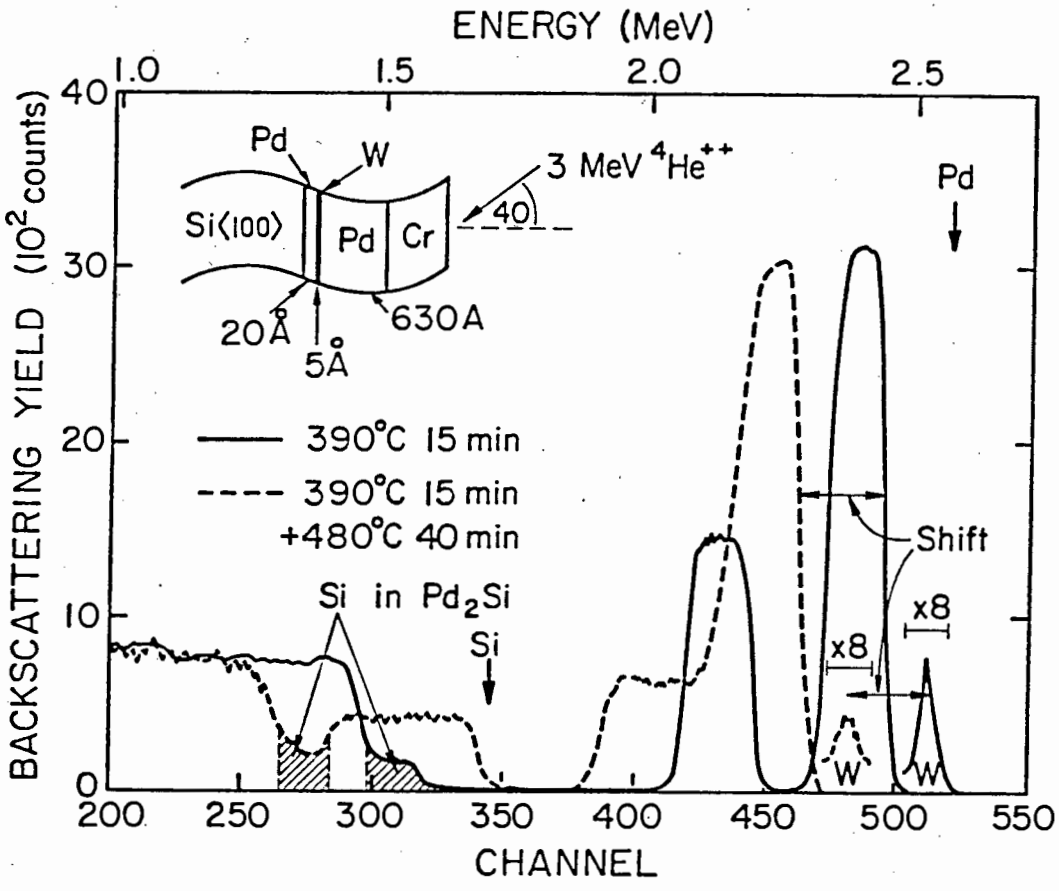

FIG 5-6 Backscattering spectra of a Si 100 /Pd/W/Pd/Cr specimen before and after $CrSi_2$ growth at 480°C. The shifts in the W and Pd signals to lower energies are equal.

relative to the Pd atoms during $CrSi_2$ growth. During silicon transport from the Si substrate, through the Pd_2Si layer, to the $CrSi_2$ layer, Si atoms thus migrate relative to both the W and Pd atoms. The orientation of the Si substrate, pre-annealing temperature and $CrSi_2$ formation temperature were all found to have no significant effect on the observed relative shifts of the W and Pd peaks during $CrSi_2$ growth.

5.4 DISCUSSION

The pseudo-inert W marker experiment has shown that both Pd and Si diffuse through Pd_2Si during its growth. The limited depth resolution of the backscattering analysis technique makes it difficult to determine the atom flux ratios with great accuracy. It is therefore concluded that the magnitude of the Pd and Si fluxes during Pd_2Si growth are comparable. This is in agreement with results from radioactive Si tracer experiments [33] and the redistribution of interfacial oxide layers studies [35,36] . It is however in disagreement with W marker studies by Bartur et al. [58] who concluded that Si is the only diffusing species. Their results are questionable because of the particular sample configuration used in the investigation. The composition of the unannealed sample was reported to be Si<100>/W/680 Å Si/1200 Å Pd. During the initial Pd_2Si formation stage, the deposited Si layer will be consumed, resulting in the following structure: Si<100>/W/1650 Å Pd_2S/200 Å Pd. Upon further heat treatment (complete Pd_2Si formation) the structure is transformed to the following: Si<100>/1980 Å Pd_2Si. The Pd_2Si layer which can possibly

affect the position of the W marker atoms is buried under 1650 Å Pd_2Si. The final position of the W marker atom is expected to be 66 Å ($\frac{1}{5}$th of 330 Å) from the Si/Pd_2Si interface which is well below the depth resolution of backscattering. Although the final position of the W marker atoms is near the Si/Pd_2Si interface (from which fact they concluded that Si is the only diffusing species), both Pd and Si diffusion have in fact influenced the position of the W marker atoms.

During $CrSi_2$ growth on Pd_2Si, W marker experiments have thus shown that Pd_2Si does not dissociate but that Si diffuses through the Pd_2Si layer. In a similar W marker experiment, it was also found that Si is the only diffusing species in Pd_2Si during its oxidation at 750°C [58]. The Pd_2Si layer merely serves as a membrane through which Si diffuses to form SiO_2 on the Pd_2Si layer. The passive nature of Pd in Pd_2Si during $CrSi_2$ growth is not surprising, considering the large energy barrier for dissociation at the Pd_2Si/Cr interface. The following two equations together with the associated enthalpy change are expected to reflect the interaction at the Pd_2Si/Cr interface. Dissociation of two moles of Pd_2Si:

$$2(Pd_2Si) \rightarrow 2(2Pd + Si) \qquad \Delta H_f^o = 2 \times 56{,}5$$

$$2Pd_2Si \rightarrow 4Pd + 2Si \qquad = 113 \text{ k cal}$$

Formation of one mole of $CrSi_2$:

$$2Si + Cr \rightarrow CrSi_2 \qquad \Delta H_f^o = -29 \text{ k cal}$$

The heats of formation ΔH_f^o are obtained from reference [6]. The effective energy barrier is 84 k cal (3.7 eV). On diffusing to the Si/Pd_2Si interface, Pd would however combine with Si to form new Pd_2Si according to the equation below:

$$2(2Pd + Si) \rightarrow 2(Pd_2Si) \qquad \Delta H_f^o = 2(-56.5)$$

or

$$4Pd + 2Si \rightarrow 2Pd_2Si \qquad = -113 \text{ k cal}$$

Although the total enthalpy change is ΔH^o = -29 k cal (84-113) which indicates an energetically favourable process, the large energy barrier (3.7 eV) for dissociation at the Pd_2Si/Cr interface makes the dissociation mechanism improbable. The enthalpy has been used instead of the free energy since free energy data is not available. The entropy term (difference between free energy and enthalpy) is however expected to be insignificant.

The reliability of the W marker results depends on the extent to which W is a diffusion barrier to either of Pd and Si. Since it was shown in section 5.3.1 that both Si and Pd permeate the W marker layer, it is concluded that the thin W layer does not act as a diffusion barrier and thus does not perturb the diffusion mechanism in the Pd_2Si layer during $CrSi_2$ growth on it. Silicon is therefore the only diffusing species during $CrSi_2$ formation on Pd_2Si.

The results of radio-active Si tracer experiments shown in Figure 5-1, suggest that Si vacancy diffusion and/or Pd diffusion

can account for approximately 50% of the Si transport. It was however argued that in the case of Pd_2Si formed on Si<100> or Si<111> substrates in contrast to Pd_2Si formed with amorphous Si (as was the case for the radioactive silicon tracer experiment), the fraction of Si transport via Si vacancy diffusion or Pd diffusion is expected to be significantly higher. The W marker experiments have shown that Si rather than Pd diffuses through Pd_2Si during $CrSi_2$ growth. It is therefore concluded that when $CrSi_2$ grows on Pd_2Si which was formed on single crystal Si, silicon diffuses through the Pd_2Si layer mainly via silicon vacancies.

CHAPTER 6

DIFFUSION MEMBRANE TECHNIQUE

6.1 INTRODUCTION

The atomic mobility of the components of a compound is a measure for its stability with respect to interdiffusion. The mobility is therefore of importance for reliability considerations of electronic devices fabricated from these compound materials. Few techniques have been exploited to determine the atomic mobility of the components (metal and silicon) in thin film metal silicides. The measuring techniques are limited through the fact that the silicide system should be subjected to a driving force during mobility measurements. Self-diffusion experiments, by virtue of their nature, do not involve driving forces for diffusion and as such do not provide measures for the mobility (stability). Before describing the diffusion membrane method, two other measuring techniques of which only one has been reported, will be discussed.

6.1.1 Growth kinetics technique

When a metal silicide forms by the interdiffusion of a metal/silicon couple, the mobility of one of the components can be determined from the growth kinetics of the metal silicide phase. This method is applicable only to systems satisfying the following conditions:

(1) The silicide layer growth is limited by diffusion.

(2) A single phase is growing.

(3) Only one of the two components (metal or silicon) diffuses during phase growth.

(4) The chemical potential gradient of the diffusing species in the growing layer is known. This provides a measure for the driving force for diffusion.

A brief outline of the procedure for calculating the mobility follows. From (3-27) the mobility B is given in terms of the parabolic rate constant $\tilde{B}$ and the chemical potential difference across the growing layer:

$$B = -\tilde{B}/\Delta\mu^{e}_{Si}$$

With the appropriate equation in (3-13), it follows that:

$$B = -\tilde{B}n / \Delta G^{o}_{f}$$

where n is the stoichiometric atomic fraction of the diffusing species in the compound layer. The entropy does not contribute significantly to the free energy at temperatures common in these investigations so that the free energy change ΔG^{o}_{f} can be replaced by the enthalpy change ΔH^{o}_{f}. The parabolic rate constant is defined in (3-2) as $\frac{L^2}{2t}$ where L is the thickness of the growing layer formed in time t. The mobility is therefore given by:

$$B = -nL^2/2t\Delta H^{o}_{f} \qquad (6\text{-}1)$$

The mobility can therefore be calculated from the parabolic rate constant, the stoichiometric atomic fraction of the diffusing component in the silicide and the standard free energy of formation of the silicide. Only a few metal silicides satisfy the requirements for using (6-1). In Table 6-1, the mobility values for the diffusing species during Ni_2Si, Pt_2Si, Co_2Si and $TiSi_2$ growth are given at a particular temperature. The parabolic rate constants and free energy of formation were obtained from the literature. The activation energies reported by the various authors for the respective parabolic rate constants are necessarily the activation energy associated with the respective mobilities.

More general methods are however necessary for determining the mobility, since this particular approach is applicable to very few silicide systems.

6.1.2 Inert marker technique

The inert marker technique for determining the atomic flux ratio of the interdiffusing components of a compound was discussed in 5.3. By combining the results of such experiments with the growth kinetics measurements, the respective mobilities of the two components can be unravelled. This method, as was the case in the previously described approach, is applicable only to systems in which the compound growth is limited by diffusion. The advantage of this technique however is that the mobility can be determined even when both components diffuse.

TABLE 6-1 DATA USED FOR CALCULATING THE ATOMIC MOBILITY

Compound	Pt_2Si	Ni_2Si	Co_2Si	$TiSi_2$
L (A°)	b) 1 000	c) 1 000	d) 1 500	e) 300
t (min)	b) 80	c) 25	d) 58	e) 55
Parabolic rate constant $\tilde{B} = L^2/2t$ ($A^{\circ 2}$/min) (Effective mobility	$0.6X10^4$	$2.0X10^4$	$1.9X10^4$	$0.08X10^4$
Temp. (°C)	250	250	468	475
Atomic ratio n	$^2/_3$	$^2/_3$	$^2/_3$	$^2/_3$
a) ΔH°_f (kcal/mol)	51	35.4	27.6	32
Mobility B (cm^2 mol/sec kcal)	$1.4X10^{-16}$	$6.3X10^{-16}$	$7.8X10^{-16}$	$2.8X10^{-17}$
Species	Pt	Ni	Co	Si

$$B = -nL^2/2t\ \Delta H^\circ_f$$

(a) reference 6
(b) reference 59
(c) reference 60
(d) reference 61
(e) reference 62

On this basis an attempt was made to extend Darken's analysis of marker motion [63], to implanted Xe marker motion in Ni_2Si during its growth [57]. The incorrect application of certain physical principles resulted in an unrealistic ratio for the mobility of Si and Ni. A simple analysis was recently suggested for determining "diffusion coefficients" from the relative motion of an inert marker with respect to the two moving interfaces during compound growth [64]. The ease with which this analysis can be applied makes it very attractive. It is evident that with this technique, the mobility is determined and not the diffusivity as is incorrectly suggested by the authors.

6.2 PRINCIPLE OF MOBILITY AND DIFFUSIVITY MEASUREMENTS

6.2.1 Diffusion membrane technique

The diffusion membrane technique to be described, is proposed as a method for determining the mobility of the components in a compound. It is also possible to extend this method for measuring the mobility of foreign atoms under certain special conditions.

Consider a Pd_2Si layer as a membrane. A substrate of A atoms (A for Si, Pd or foreign atoms) serves as a source region. The flux of A through Pd_2Si can now be monitored with the aid of a suitably chosen layer of material B on the other side of the Pd_2Si layer. This layer serves as a sink for the diffusing atoms (see Figure 6-1(a)). On diffusing through the Pd_2Si layer, the A atoms react with B to form a compound A_xB. The

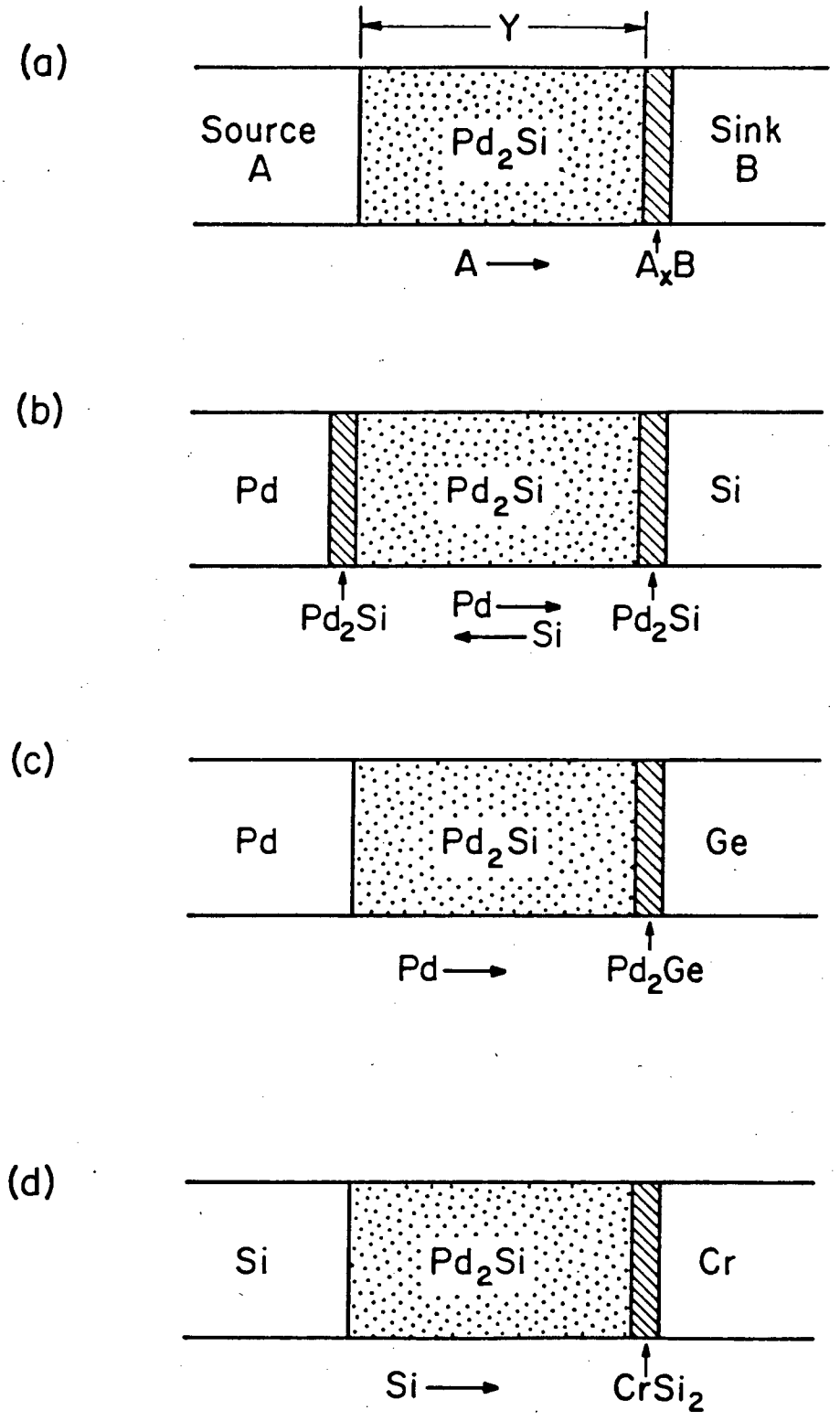

FIG 6-1 Schematic of thin film combinations illustrating
(a) the diffusion membrane principle,
(b) the analogy with Pd_2Si growth,
(c) the configuration for Pd mobility measurements
and (d) the configuration for Si mobility measurements.

described arrangment of chemically and physically different phase boundaries gives rise to a chemical potential gradient of A in the Pd_2Si membrane. Following equation (3-39), the flux of A through Pd_2Si, J_A, can be expressed in terms of the chemical potential difference of A across Pd_2Si, $\Delta\mu_A$, and the mobility of A in Pd_2Si, B_A.

$$J_A = -B_A \, [A^{Pd_2Si}] \frac{\Delta\mu_A}{Y} \qquad (6\text{-}2)$$

where $[A^{Pd_2Si}]$ is the concentration of A in Pd_2Si and Y is the thickness of the Pd_2Si layer. The effective mobility $\bar{B}$ is now defined as:

$$\bar{B}_A = -B_A \, \Delta\mu_A$$

In equation (6-2) and in the definition for the effective mobility, $-\Delta\mu_A$ represents the <u>magnitude</u> of the chemical potential difference. By convention the chemical potential difference is negative (since ΔG_f^o in equation 3-15 is negative). The flux equation (6-2) becomes:

$$J_A = \bar{B}_A \, \frac{[A^{Pd_2Si}]}{Y} \qquad (6\text{-}3)$$

The rate of A_xB formation R_{A_xB}, is expressed in terms of the flux according to (2-38):

$$R_{A_xB} = \frac{J_A}{[_A{}^{A_xB}]}$$

so that

$$R_{A_xB} = \bar{B}_A \frac{[A^{Pd_2Si}]}{[A^{A_xB}]\,Y} \qquad (6\text{-}4)$$

which can be rewritten as:

$$\bar{B}_A = R_{A_xB} \frac{Y[A^{A_xB}]}{[A^{Pd_2Si}]} \qquad (6\text{-}5)$$

The effective mobility $\bar{B}_A$ is not equivalent to the intrinsic diffusivity of A in Pd_2Si, since A is subjected to a driving force $\Delta\mu_A$, but it is comparable to the parabolic rate constant $\tilde{B}_{Pd_2Si}$ as determined from the growth kinetics of Pd_2Si (see equation (3-26)).

Equation (6-5) offers a means of calculating the effective mobility of component A in Pd_2Si when the various parameters are known. This measuring technique where the Pd_2Si serves as a membrane through which the atoms diffuse, is to be referred to as the diffusion membrane technique.

In chosing suitable sinks for the various source atoms, the following guidelines should be used:

(1) The sink atoms should not diffuse into the membrane or react with the components of the membrane compound except when forming the A_xB compound.

(2) The reaction whereby A_xB is formed should be relatively rapid so that the transport of A through the membrane is not limited by the interaction between A and B.

From Figure 6-1(b) it is seen that in the Pd-Si binary couple, Pd serves as a sink for Si and vice versa, because both Pd and Si diffuse during Pd_2Si formation (see chapter 5). Since the growth regions cannot be distinguished from the membrane, this configuration is not suitable for mobility measurements.

The following multi-layer combinations were used for determining Pd and Si mobility in Pd_2Si:

(1) Pd mobility: $Pd/Pd_2Si/Ge$
The Ge layer serves as a sink for Pd and the compound Pd_2Ge is formed at the Pd_2Si/Ge interface (see Figure 6-1(c).

(2) Si mobility: $Si/Pd_2Si/Cr$
The Cr layer which serves as a sink for Si yields $CrSi_2$ which is formed at the Pd_2Si/Cr interface (see Figure 6-1(d)).

When applying the diffusion membrane technique to a particular system, one has to realize that the driving force (chemical potential difference) which is characteristic of the system, influences the measured values of the effective mobility. Care should therefore be taken when comparing effective mobility

values. The applicability of this technique is based on the fact that the growth of the A_xB layer is limited by diffusion of A through Pd_2Si. In order to verify it, the following properties of A_xB layer growth should be investigated.

(1) It should grow linear with time since $t^{\frac{1}{2}}$-kinetics would imply growth controlled by diffusion through a layer which grows with time, that being A_xB (see section 3.3.3).

(2) Equation (6-4) predicts that $R_{A_xB} \alpha 1/Y$. The rate of A_xB growth should therefore be inversely proportional to the thickness of the interposed Pd_2Si layer.

In the event that the thickness of the interposed Pd_2Si does not affect the growth rate of A_xB one of the interfaces or diffusion through the A_xB layer controls the growth so that the diffusion membrane technique is not applicable. When the mobility depends on the membrane thickness (e.g., when the transport mechanism through Pd_2Si is grain boundary diffusion), the growth rate of A_xB is affected more strongly by the Pd_2Si thickness so that instead, the following thickness dependence will be found:

$$R_{A_xB} \alpha 1/Y^p \qquad \text{(see (6-8))}$$

where $p > 1$ and typically $p \simeq 2$, as will be shown in the following section where grain boundary diffusion will be treated.

6.2.2 Surface accumulation tehcnique

There are fundamental differences between the diffusion membrane technique (6.2.1) and the surface accumulation method to be described here, although the two techniques are similar in principle. The prime difference is that the diffusivity is determined by means of the surface accumulation method whereas the mobility is determined using the diffusion membrane technique. The surface accumulation method for studying the diffusion of atoms along grain boundaries and dislocations is well documented [65-70]. Typically, a polycrystalline film (diffusion matrix A) is deposited on a substrate (B) which also serves as the source. The accumulation of B atoms on the free surface of A after diffusion through A (see Figure 6-2(a))

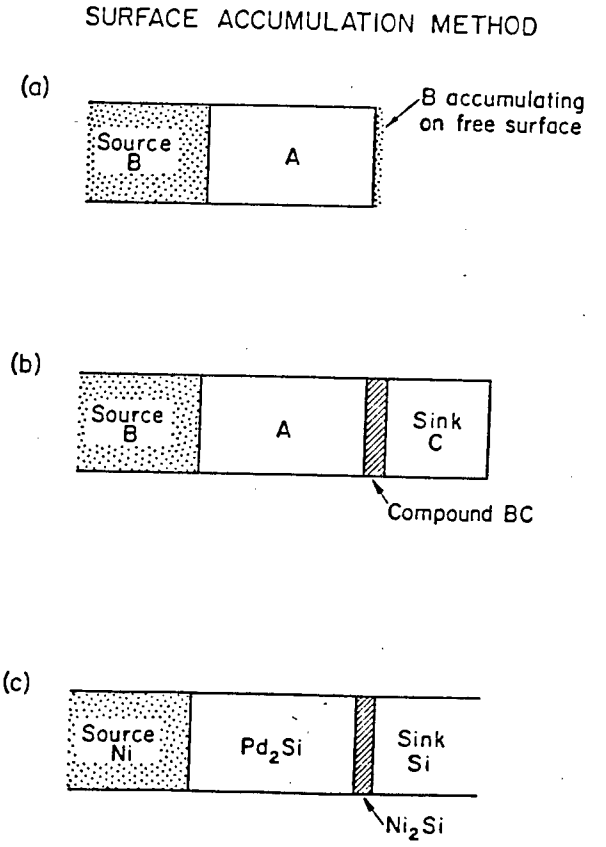

FIG 6-2 Schematic of sample configurations for surface accumulation experiments.

is monitored by various techniques such as AES, (Auger electron spectrometry) RBS (Rutherford backscattering spectrometry) or ESCA (electron spectroscopy for chemical analysis). It is also common to provide a sink for B atoms at the free surface of A so that the B atoms are consumed through a reaction upon arriving on the surface. An oxidizing ambient [67] or a layer of material C deposited on B as in Figure 6-2(b) could act as a sink. This is similar to the diffusion membrane configuration (see Figure 6-1(a)).

The analysis of data obtained from surface accumulation experiments is discussed in references [69] and [70]. A simple approximate solution of the associated mathematical problem is obtained when certain conditions are satisfied:

(a) For an infinite source the concentration of the diffusant at the entrance to the grain boundary remains constant and equal to α_o.

(b) If an infinite sink is available (the case where B and C readily react to form a compound) then the diffusant concentration at the exit of the grain boundaries remains zero.

(c) The loss of diffusant from the grain boundary into the grain is negligible.

The surface accumulation of B atoms, Q, is then given by equation (9) of reference [69]:

$$Q/\alpha_o L = \nu(\dot{\eta}^2 t - 1/6 - 2/\pi^2 \sum_{j=1}^{\infty} (-1)^j/j^2 \exp(-n^2 j^2 \pi^2 t)) \qquad (6\text{-}6)$$

where Q : amount (atoms/cm^2) of diffusant accumulated on the surface;

α_o : concentration of diffusant at the entrance to the grain boundaries;

L : thickness of layer A;

ν : density of grain boundaries;

D_{gb} : grain boundary diffusion coefficient

$\dot{\eta}^2$: D_{gb}/L^2

t : time

The three conditions above (a,b and c) are necessary in order to postulate a concentration gradient in the grain boundary. The use of the grain boundary diffusion coefficient D_{gb} to characterize the flux of atoms along the grain boundary is therefore justified.

A graphical representation of the above equation approaches a constant slope for sufficiently large values of $\dot{\eta}^2 t$, i.e., for large values of t for which quasi-steady state diffusion is established in the grain boundaries. Equation (6-6) becomes:

$$Q/\alpha_o L = \nu\dot{\eta}^2 t$$

$$Q/\alpha_o L = \nu D_{gb}\, t/L^2 \qquad (6\text{-}7)$$

If we assume a constant grain boundary width w, and cylindrical grains with grain size d, then the grain boundary density, ν is approximately given by $2w/d$. The grain size is usually dependent on the film thickness [71]. Suppose the relation between grain size and film thickness is given by

$$d = \beta L^{p-1} \qquad (6\text{-}8)$$

where β and p are constants, then from (6-7), (6-8) and ($\nu = 2w/d$), the accumulation dependence is expressed as:

$$Q \propto D_{gb}\, t/L^{p} \qquad (6\text{-}9)$$

The accumulation Q is therefore linear with time for constant D_{gb} (constant temperature) and constant L (same layer thickness). By rewriting (6-9) in the form

$$D_{gb} \propto QL^{p}/t \qquad (6\text{-}10)$$

it is seen that QL^{p}/t is a measure for the grain boundary diffusion coefficient. The ratio Q/t is referred to as the accumulation rate and QL^{p}/t is referred to as the "normalized" rate of accumulation.

Since the grain size is usually directly proportional to the layer thickness, the value of p is typically 2 (since $p - 1 = 1$ in (6-8)). The proportionality constant in (6-9) or (6-10) depends on α_o, w and β. In the event that these parameters are not known, it is impossible to obtain quantitative values for the diffusion coefficient from (6-10). It

should be pointed out that the diffusivity is determined by means of the surface accumulation method using this specific analysis, whereas the mobility is determined using the diffusion membrane technique. There are no stoichiometric restrictions on the concentration of foreign atoms in the grain boundaries as there are on the concentration of the components of a compound in the grains. A concentration can therefore be assumed so that the use of Fick's diffusion laws in reference [69], where equation (6-6) was derived, is justified.

The Ni/Pd_2Si/Si system was chosen to study grain boundary diffusion of Ni through Pd_2Si. The Ni layer serves as an infinite source while the Si substrate acts as an infinite sink for Ni (see Figure 6-2(c)). It will be shown that this system satisfies the conditions necessary for applying the above analysis. The experimental results are presented in section 6.3.3 .

6.3 RESULTS

6.3.1 Si mobility in Pd_2Si

The mobility of Si in epitaxial and polycrystalline Pd_2Si was determined by using Si<111>/Pd_2Si/Cr and Si<100>/Pd_2Si/Cr thin film structures respectively. The experimental data necessary to calculate the mobility according to equation (6-5) have been discussed in Chapter 4. It was shown that $CrSi_2$ growth on both epitaxial and polycrystalline Pd_2Si is linear and the rate is inversely proportional to the Pd_2Si

thickness provided a critical Pd_2Si layer thickness is exceeded. The conditions for applying the diffusion membrane technique are therefore satisfied provided the Pd_2Si membrane is sufficiently thick.

The experimental data used for mobility calculations are summarized in Table 6-2. A single epitaxial Pd_2Si layer thickness and corresponding $CrSi_2$ growth rate have been selected for each temperature from the data represented in the curves in Figure 4-7. The data for the polycrystalline Pd_2Si membrane are in essence the data contained in Table 4-1. The effective mobility values for Si in Pd_2Si are shown graphically in an Arrhenius plot in Figure 6-3. The microstructure of the Pd_2Si layer is seen to have a drastic effect on the mobility. A lower activation energy 1.7 ± 0.2 eV and higher mobility is measured for polycrystalline Pd_2Si compared to an activation energy of 2.1 ± 0.2 eV for epitaxial Pd_2Si. The difference is ascribed to the presence of the grain boundaries in polycrystalline Pd_2Si which offer additional diffusion paths and serve as point defect sources.

6.3.2 Pd mobility in Pd_2Si

The utilization of $Pd/Pd_2Si/Ge$ structures for Pd mobility measurements makes it impossible to vary the microstructure of the Pd_2Si membrane as in the case of Si mobility measurements. These structures were obtained by preannealing the multi-layer structures Ge/Si/Pd deposited on an inert substrate SiO_2, at temperatures around 200°C. Backscattering

TABLE 6-2 DATA USED IN CALCULATING THE EFFECTIVE MOBILITY ACCORDING TO:

$$\overline{B} = R_{A_xB} \cdot Y \cdot \frac{[A^{A_xB}]}{[A^{Pd_2Si}]}$$

Diffusing species	Temp. (°C)	Y Pd_2Si thickness (Å)	R_{A_xB} A_xB growth rate (Å/sec)	$\overline{B}$ Effective mobility (10^{-13} cm²/sec)
Si through epitaxial Pd_2Si to form $CrSi_2$	450	1 100	0.3	0.77
	470	1 000	0.75	1.75
	485	1 420	1.14	3.8
	500	1 420	2.9	7.6
Si through polycrystalline Pd_2Si to form $CrSi_2$	420	9 500	0.12	2.7
	425	9 500	0.16	3.6
	445	9 500	0.45	9.9
	445	15 500	0.27	9.8
	455	9 500	0.52	11.6
	470	9 500	0.85	19.0
	470	15 500	0.47	17.2
	480	9 500	1.1	25.0
Pd through polycrystalline Pd_2Si to form Pd_2Ge	200	1 600	0.022	0.23
	220	1 600	0.083	0.13

$$\frac{[Si^{CrSi_2}]}{[Si^{Pd_2Si}]} = 2.35 \qquad \frac{[Pd^{Pd_2Ge}]}{[Pd^{Pd_2Si}]} = 0.96$$

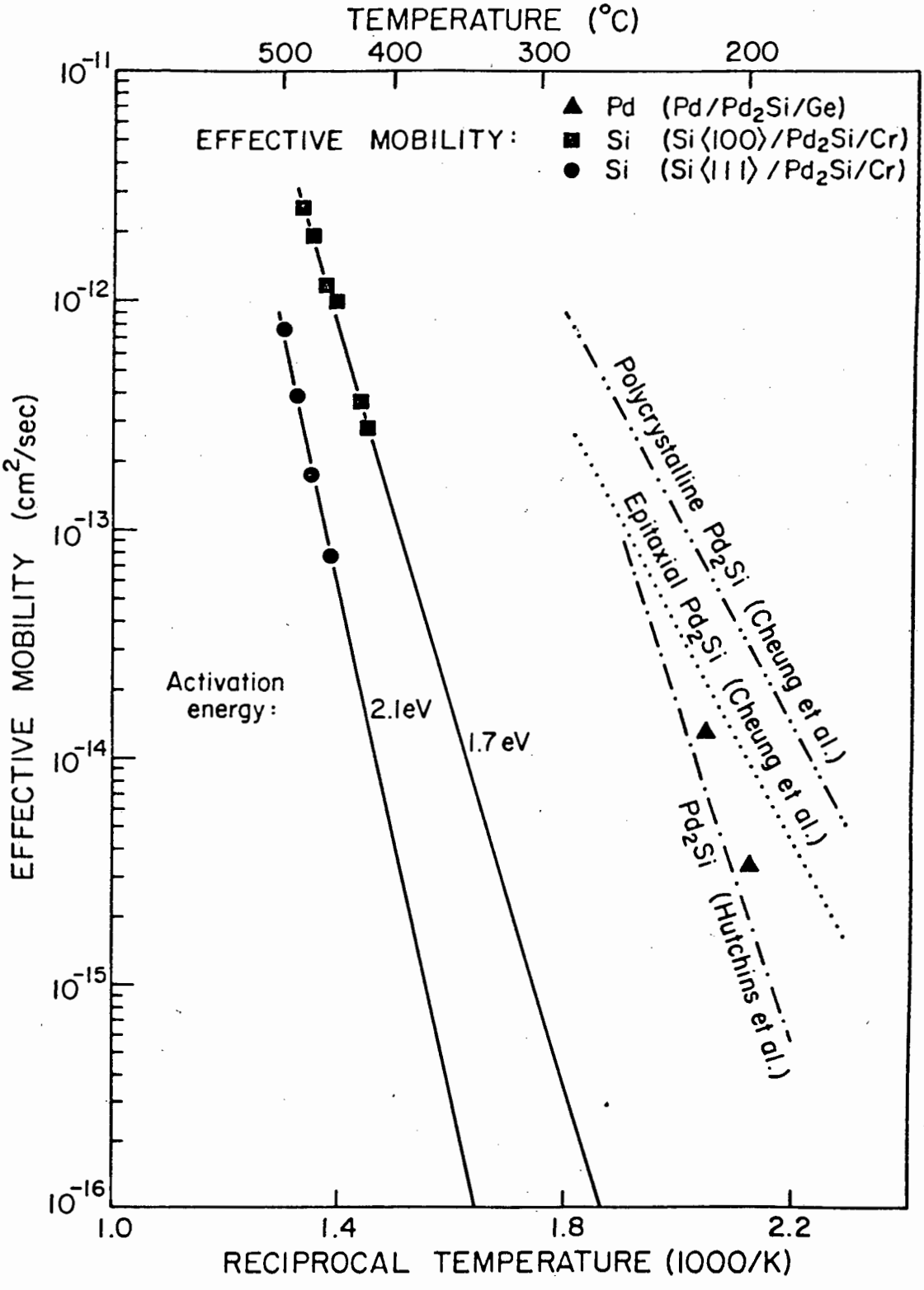

FIG 6-3 Effective mobility of Pd and Si in Pd_2Si. Also shown are parabolic rate constant plots for Pd_2Si growth as reported by Cheung et al. [31] and Hutchins [29].

spectra of an unannealed and preannealed sample are shown in Figure 6-4(a). On comparing the two spectra, a broadening of the Si signal as well as a step in the Pd signal are observed. This indicates that Pd_2Si, which was confirmed by X-ray diffraction, has formed. The Ge signal around channel 430 has remained unchanged, indicating that no Ge compounds have formed on preannealing at 220°C for one hour.

After further annealing the sample at 220°C for three hours, a change in the Ge signal is observed. (see spectrum in Figure 6-4(b)). The decrease in height and the broadening of the Ge signal as well as the increase in the step of the Pd signal are indicative of Pd_2Ge that has formed. This was confirmed by X-ray diffraction. Since it is difficult to distinguish the Pd_2Si and Pd_2Ge regions of the Pd signal, the thickness of the unreacted Pd was determined and from that the thickness of the Pd_2Ge layer was deduced. The width of the signal originating from Ge in Pd_2Ge is also a measure for the thickness of Pd_2Ge.

The growth of Pd_2Ge at 200°C is illustrated in Figure 6-5. Linear thickness and time scales are used in this figure in order to illustrate the dramatic effect of interposed Pd_2Si on the Pd_2Ge growth. It is observed that Pd_2Ge growth on Pd_2Si is linear with time whereas it is parabolic (linear, when the thickness is plotted against the square root of the annealing time) when grown during Pd/Ge binary couple interdiffusion. It was pointed out in 3.3.4 that linear growth in

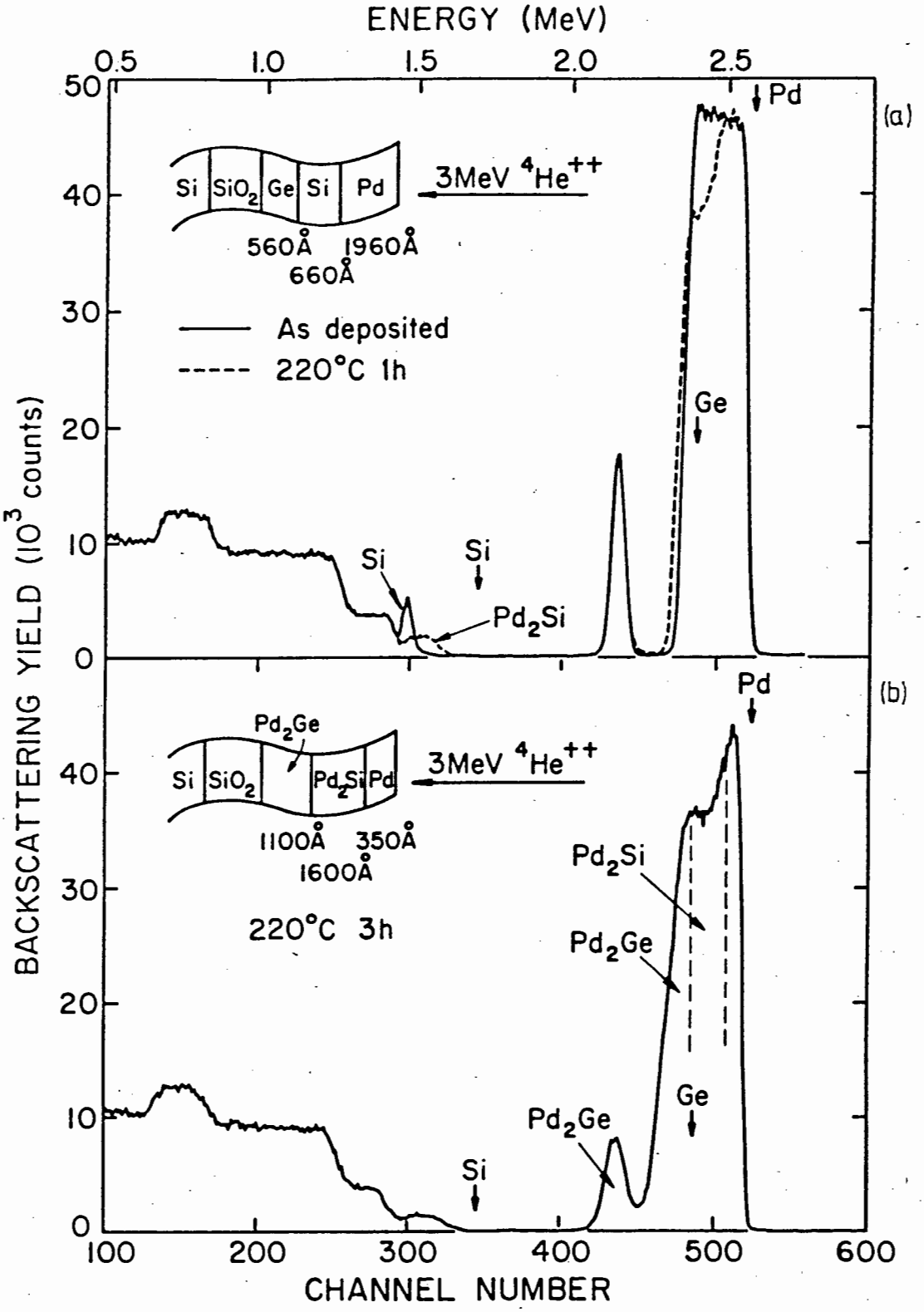

FIG 6-4 Backscattering spectra of a Ge/Si/Pd structure on SiO_2.

(a) After heat treatment for 1h, Pd_2Si is formed.

(b) Upon further annealing Pd_2Ge forms as result of Pd diffusing through Pd_2Si.

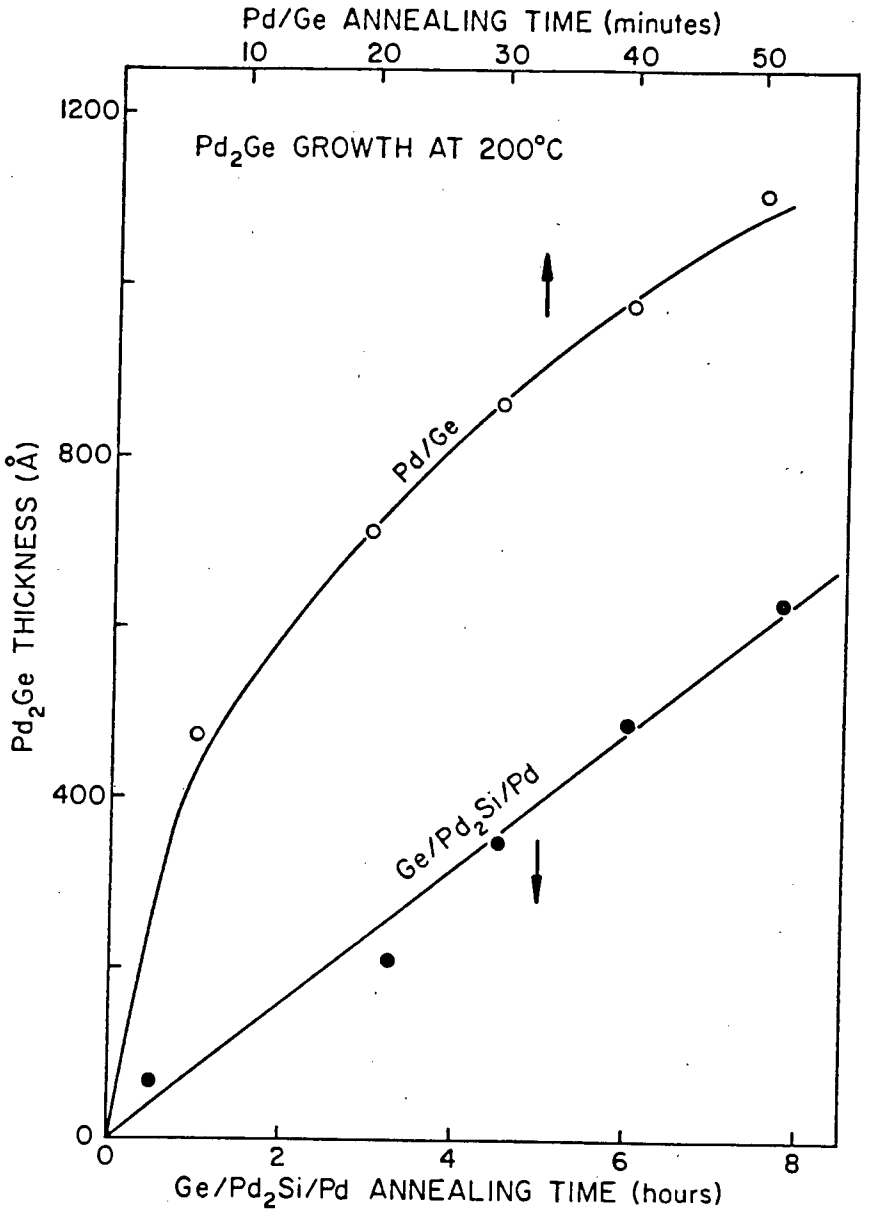

FIG 6-5 The kinetics of Pd_2Ge formation, with and without an interposed Pd_2Si layer. Growth of Pd_2Ge from Pd/Ge couples is parabolic (time scale at top). With interposed Pd_2Si the growth is linear (time scale at bottom).

multi-layer compound forming systems is no longer indicative of interfacial reaction controlled growth. The Pd_2Ge growth on Pd_2Si is in fact limited by diffusion of Pd through the Pd_2Si layer, the thickness of which remains constant with time.

The effective mobility of Pd in Pd_2Si at 200 and 220°C are also shown in Figure 6-3. The data used for calculating these values are given in Table 6-1. Because insufficient data is available, the activation energy has not been determined. The Pd mobility is seen to be orders of magnitude larger than the Si mobility when extrapolated down to about 200°C. Plots representing the parabolic rate constant for Pd_2Si growth from Si-Pd couples (from literature) are also shown in Figure 6-3. It is observed that the Pd effective mobility is of the same order of magnitude as the parabolic rate constant.

6.3.3 Ni grain boundary diffusion in Pd_2Si

The diffusion of Ni along the grain boundaries of polycrystalline Pd_2Si was monitored by studying the thermal behaviour of Si/Pd/Ni thin film structures. Since Pd_2Si growth is rapid compared to Pd/Ni interdiffusion, the system is transformed to Si/Pd_2Si/Ni during the initial stage of the heat treatment. It is known that Pd_2Si grows epitaxial on Si<111> and non-epitaxial on Si<100> substrates [30,31]. Grain boundary effects can therefore be distinguished by using both substrate orientations for the Si/Pd/Ni samples. The Si/Pd/Ni deposited samples were preannealed at 250°C to form Pd_2Si without Ni/Pd or Ni/Pd_2Si interdiffusion. Subsequently, the samples were annealed at elevated temperatures for various periods of time.

Typical backscattering spectra of a Si<100>/Pd/Ni sample are shown in Figure 6-6. The two overlayed spectra in Figure 6-6(a) are of the sample before and after being pre-annealed at 250°C. The change in the Pd signal and the step appearing in the Si signal are indicative of Pd_2Si formation. Similar backscattering spectra were obtained for samples with identical metal layers deposited onto Si<111> substrates. After further heat treatment at 350°C, no significant change is observed in the Pd and Si signals (see Figure 6-6(b)). A second Ni peak is however observed around channel 415. The position of this peak corresponds to that of the Si<100>/Pd_2Si interface. The backscattering spectrum of a Si<111>/Pd_2Si/Ni sample subjected to the same heat treatment as a Si<100>/Pd_2Si/Ni sample, does not show a second Ni peak (i.e. no Ni at the Si<111>/Pd_2Si interface). This dramatic effect of the Si substrate orientation is illustrated in Figure 6-7 where backscattering spectra of a Si<100>/Pd_2Si/Ni and a Si<111>/Pd_2Si/Ni sample are shown. Nickel is seen to diffuse into the bulk of the epitaxial Pd_2Si layer (high energy step in Pd signal and low energy step in Ni signal).

The accumulation of Ni at the Si<100>/Pd_2Si interface is seen to occur without a significantly high concentration of Ni in the Pd_2Si layer. This indicates that Ni is transported through Pd_2Si by grain boundary or interstitial diffusion. The concentration of Ni in Pd_2Si is estimated at approximately 1.0 at. %. Since no Ni accumulation is observed at the Si<111>/Pd_2Si interface, we conclude that Ni diffuses through

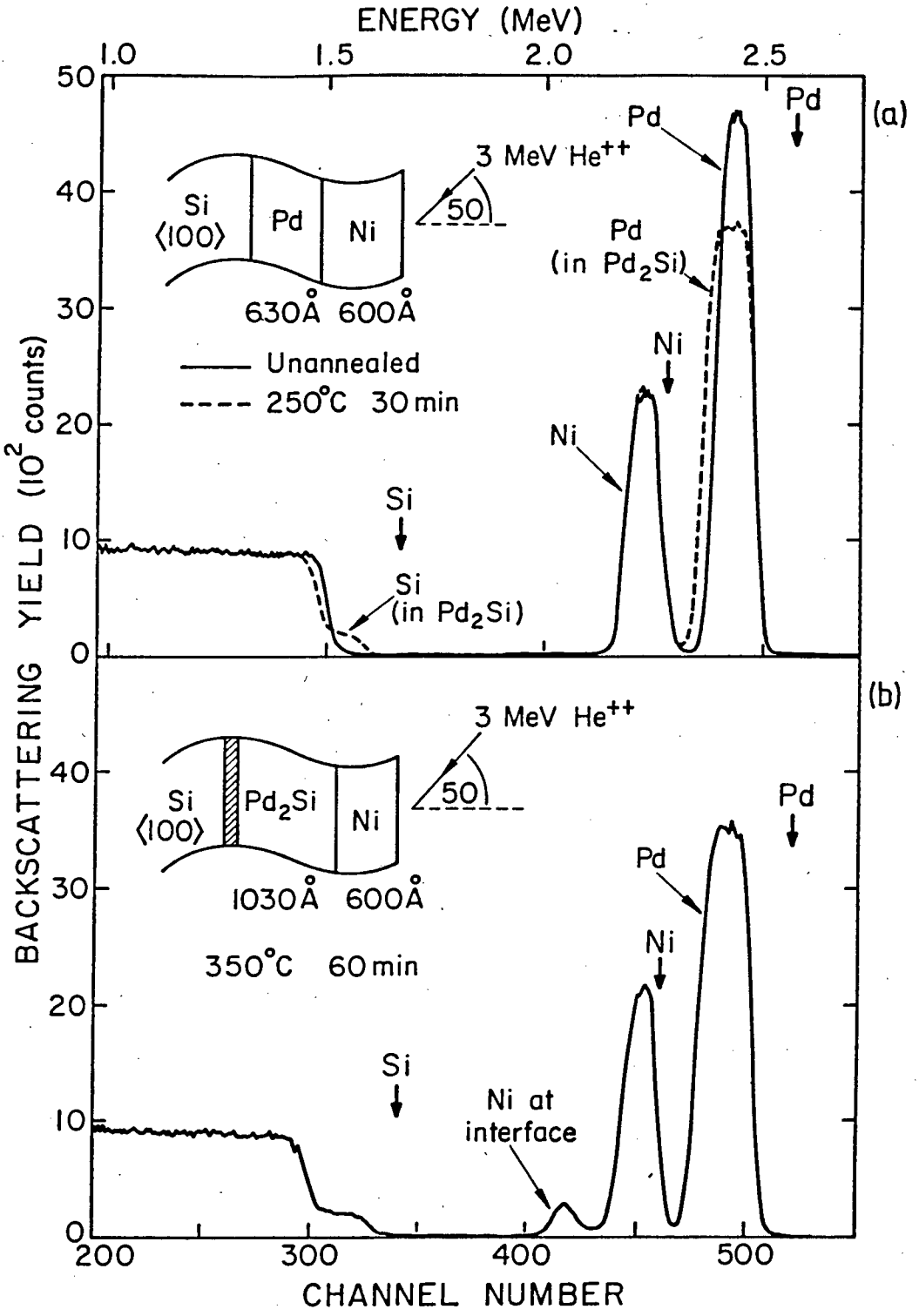

FIG 6-6 Backscattering spectra of a Si<100>/Pd/Ni sample.
(a) Upon pre-annealing at 250°C, Pd_2Si forms.
(b) On furthe rannealing, Ni diffuses through Pd_2Si and accumulates at the Si<100>/Pd_2Si interface.

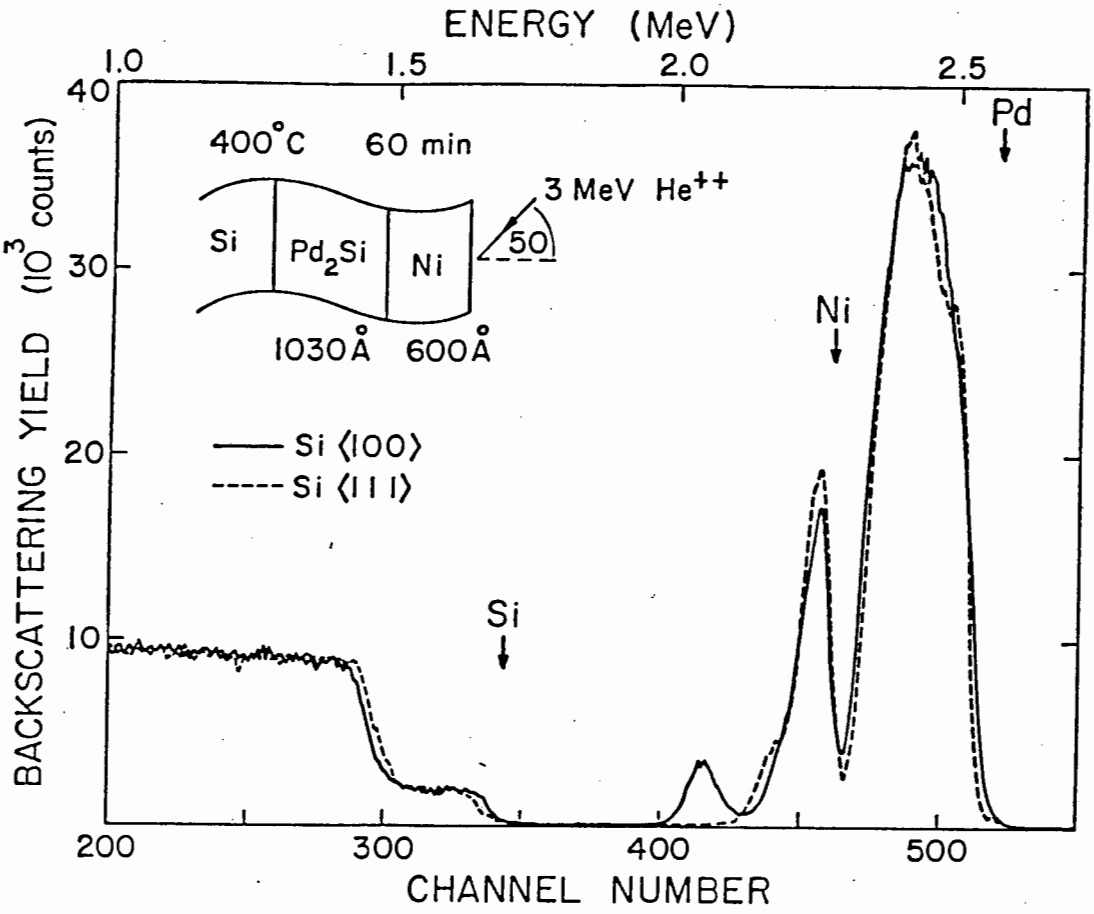

FIG 6-7 Backscattering spectra of $Si/Pd_2Si/Ni$ samples. The second Ni peak observed for $Si<100>/Pd_2Si/Ni$ sample is absent in the $Si<100>/Pd_2Si/Ni$ specimen spectrum. Note step in Ni signal in the case of $Si<111>/Pd_2Si/Ni$ sample.

polycrystalline Pd_2Si (on $Si<100>$) predominantly along the grain boundaries. Very similar diffusion behaviour of Pt through Ni_2Si was reported by Finstad [72].

The fact that Ni accumulates at the $Si<100>/Pd_2Si$ interface without any significant amount of nickel silicide being formed at the Pd_2Si/Ni interface indicates that Ni diffusion along the grain boundaries is faster than Si diffusion through Pd_2Si (lattice or grain boundary).

Figure 6-8 shows the backscattering spectra of samples subjected to isothermal anneals at 350°C for various periods of time. The area under the second Ni peak is seen to increase with time. A small decrease in the width of the surface Ni

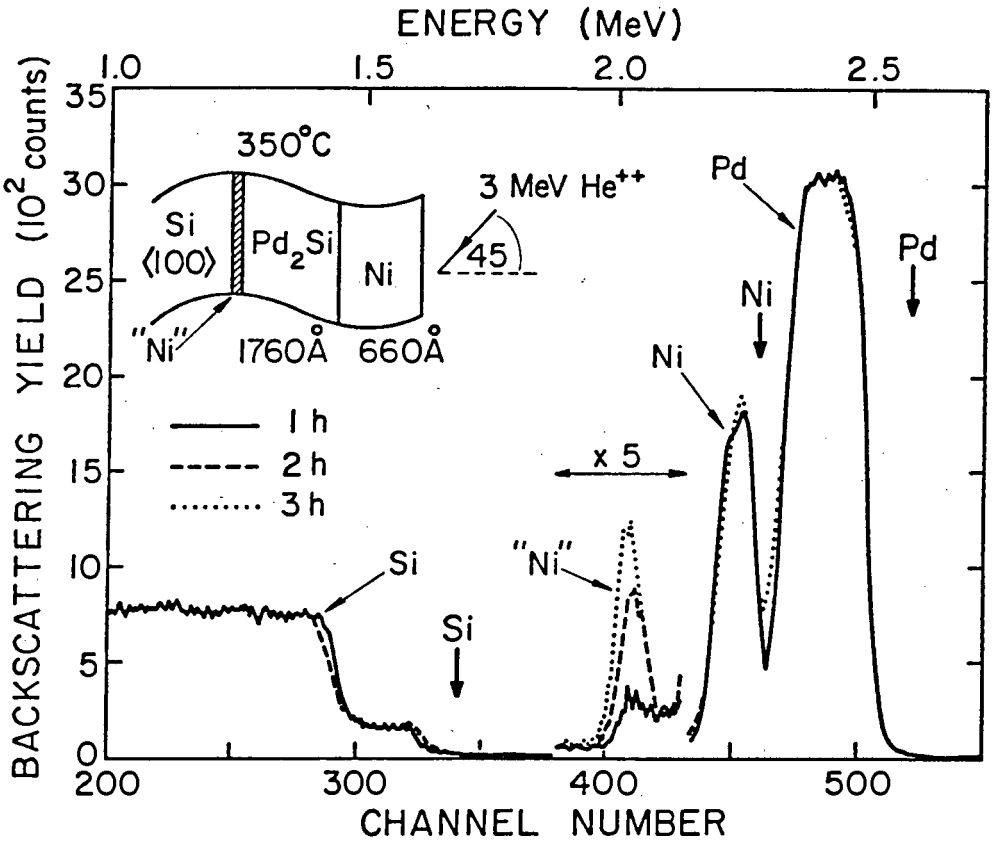

FIG 6-8 Backscattering spectra of a Si<100>/Pd_2Si/Ni showing the accumulation of "Ni" at the Si 100 /Pd_2Si interface (development of the "Ni" signal).

peak is observed. This is consistent with the loss of Ni to the Si<100>/Pd_2Si interface. The area under the second Ni peak represents the density (atoms/cm²) of the Ni accumulated at the Si<100>/Pd_2Si interface but is expressed as an "effective" thickness of accumulated Ni. Although the phase of the accumulated Ni (indicated as "Ni" in Figure 6-8) has not been established because of insufficient amounts present, it is

expected to be Ni_2Si. The particular phase of "Ni" (Ni, Ni_2Si or NiSi) does not affect the analysis and interpretation of the results. In Figure 6-9, the effective thickness of accumulated Ni is plotted against the annealing time for three different temperatures. The accumulation rate is seen to be constant at constant temperature but increases with temperature.

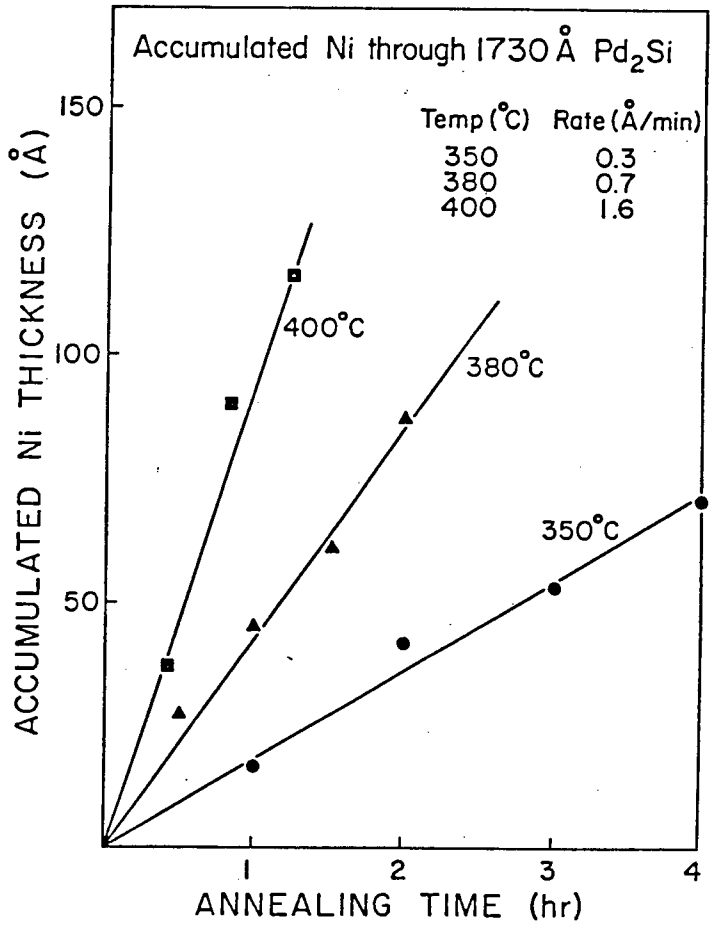

FIG 6-9 The accumulation of Ni at the Si<100>/Pd_2Si interface is seen to increase linearly with increase in annealing time.

The thickness of the Pd_2Si layer is found to affect the rate of Ni accumulation at the interface. This is illustrated in Figure 6-10, where the Ni accumulation rate $\frac{Q}{t}$, is plotted against the Pd_2Si layer thickness L for various temperatures. Since a logarithmic scale is used, the slope of the curves represents the thickness dependence of $\frac{Q}{t}$. The average slope of -1,8 implies that $Q/t \propto L^{-1.8}$ and from (6-9) it follows that p = 1.8. The value of 1.8 obtained for p implies that $d \propto L^{.8}$ (see (6-8)), indicating that the grain size is almost proportional to the Pd_2Si layer thickness. This was confirmed by grain size measurements by means of TEM.

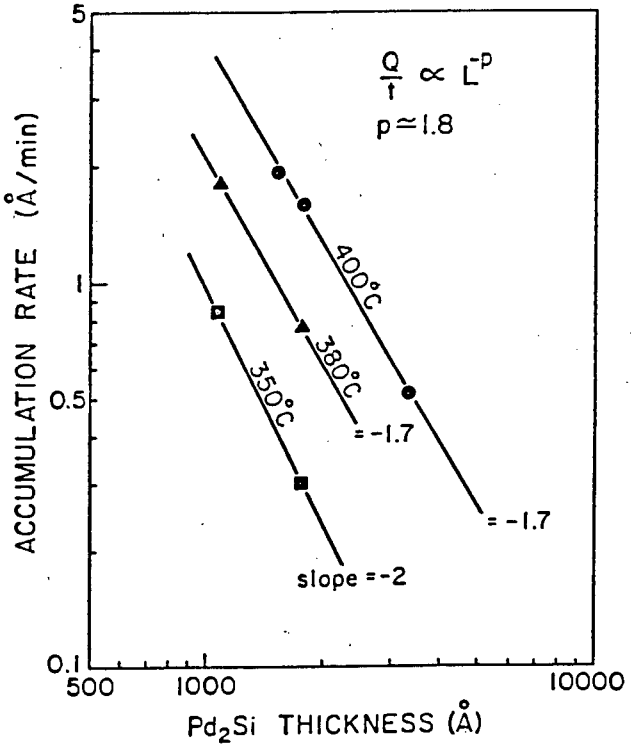

FIG 6-10 The rate of Ni accumulation (log scale) as a function of the Pd_2Si layer thickness (log scale) for Si<100>/Pd_2Si/Ni structures.

The constant rate of accumulation at constant temperature and the particular value of p indicate that the grain boundary diffusion measurement principle as described in 6.2.2 is applicable. Figure 6-11 shows the Arrhenius plot of the normalized accumulation rate ($^{QL^p}/_t$) against the reciprocal temperature. The slope of this curve represents an activation energy of 1.2 eV which is associated with the diffusion of Ni along Pd_2Si grain boundaries.

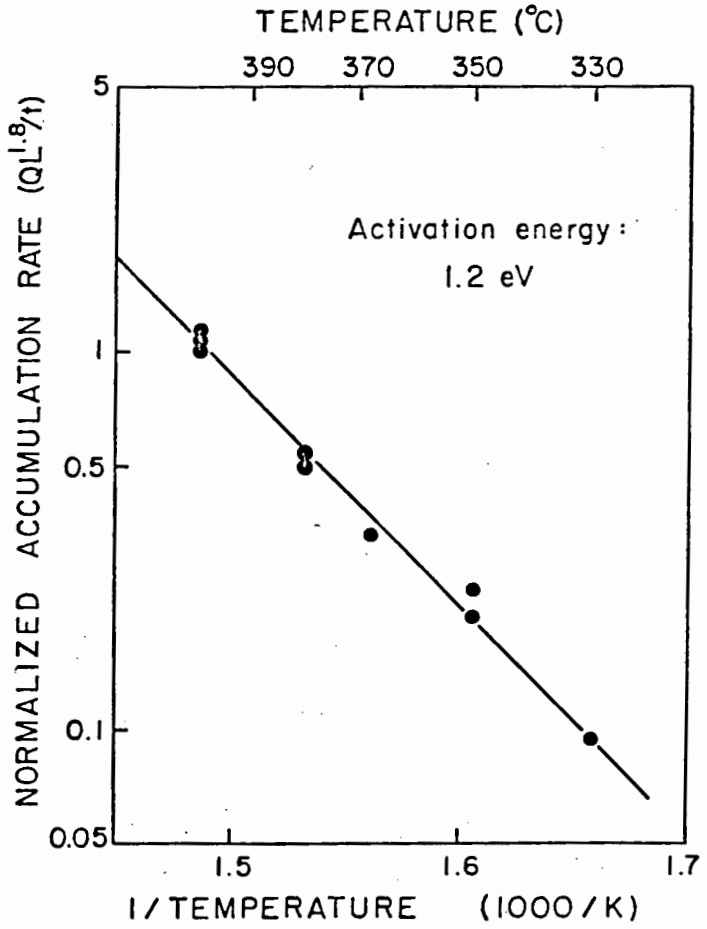

FIG 6-11 Arrhenius plot for the normalized accumulation rate of Ni on Pd_2Si. The activation energy of 1.2 eV is associated with the grain boundary diffusion process.

6.4 DISCUSSION

The prime objective of the mobility measurements was to obtain a more comprehensive understanding of the interdiffusion of Pd and Si during Pd_2Si growth. It was shown in section 3.2.5 that the effective mobility is equivalent to the parabolic rate constant. A comparison of these two parameters is therefore very instructive. The validity of such a comparison is based on the assumption that the chemical potential differences for the diffusing atoms across the Pd_2Si layer is not very different in the various cases (multi-layer film combinations). The chemical potential difference for the diffusing atoms across the Pd_2Si layer is related to the heat of formation of the growing compound layer (see section 3.3.3). Since the heats of formation of silicides are of the same order of magnitude [6] and since Pd_2Ge is expected to have a heat of formation of similar magnitude, it is reasonable to assume that the driving forces for diffusion in the various diffusion membrane configurations (b,c and d in Figure 6-1) are of the same order of magnitude.

The Si and Pd effective mobilities are graphically compared to published values for the parabolic rate constant of Pd_2Si growth from Pd/Si couples, in Figure 6-3. The good agreement between the effective mobility of Pd and the parabolic rate constant suggests that the Pd mobility is sufficiently high to account for the Pd_2Si growth. The spectrum in Figure 6-4(b) and other spectra of similar samples show detectable amounts of Ge diffusion into the Pd_2Si layer. It is well documented that

impurities in films can influence the diffusion of atoms through it [72-75]. The extent to which impurities enhance or inhibit diffusion depends on their interaction with the matrix and diffusing atoms and on the diffusion mechanism. Germanium does not differ much from silicon with respect to its chemistry and atomic volume. The presence of Ge in the Pd_2Si layer is therefore not expected to have an appreciable influence on the diffusion of Pd through the Pd_2Si layer.

When the Si effective mobility curves are extrapolated down to about 200°C, the values are found to be orders of magnitude lower than the Pd effective mobility and the parabolic rate constant for both epitaxial and polycrystalline Pd_2Si growth. The Si mobility is therefore far too low to account for the Pd_2Si growth. Considering the fact that the effective mobility of Pd is found to be sufficiently high, this would suggest that Pd atoms are the dominant diffusing species during Pd_2Si growth, in disagreement with the results in section 5.3.2 where it was shown that Pd and Si have comparable flux magnitudes.

The high activation energy of 2.1 eV obtained for Si mobility in epitaxial Pd_2Si is characteristic of lattice diffusion via vacancies. Similar values have been reported for Si self diffusion in PtSi (2.1 eV) and NiSi (2.3 eV) [47, 76]. The activation energy associated with Pd_2Si growth (epitaxial and polycrystalline) was reported to be approximately 1.0 eV [31]. The large difference in activation energy between the Pd_2Si parabolic growth rate constant and Si mobility implies that Si

is not the only diffusing species during Pd_2Si growth since the parabolic rate constant and mobility are directly proportional (see section 3.2.5).

The apparent disagreement between the mobility results presented here and the flux ratio results presented in section 5.3.2 can be explained if it is assumed that the Si diffusion mechanism in the two cases (Pd_2Si growth, and $CrSi_2$ growth on Pd_2Si), is different. The reason for assuming different mechanisms lies in the particular crystal structure of Pd_2Si which is schematically illustrated in Figure 6-12. It is seen to consist of two alternating planes, the basal plane with hexagonal symmetry. The planar growth of Pd_2Si (epitaxial and polycrystalline) is usually perpendicular to this plane [30] which suggests that rapid diffusion is possible in this direction relative to other possible directions of diffusion (anisotropic). The Pd_2Si crystal has a closed pack structure so that interstitial diffusion of Pd or Si is unlikely [77]. In Figure 6-12 the relative position of a Si atom in the plane above or plane below is indicated by the broken circle. It is observed that these Si atoms do not have immediate Si atom neighbours in the adjacent planes. Vacancy diffusion in the Si lattice (normal to these planes) is therefore associated with a large migration energy during $CrSi_2$ growth on Pd_2Si. In Figure 6-13, the Pd_2Si crystal structure is shown once more but with certain Pd atoms removed, thus representing Pd vacancies (indicated by V in figure). The

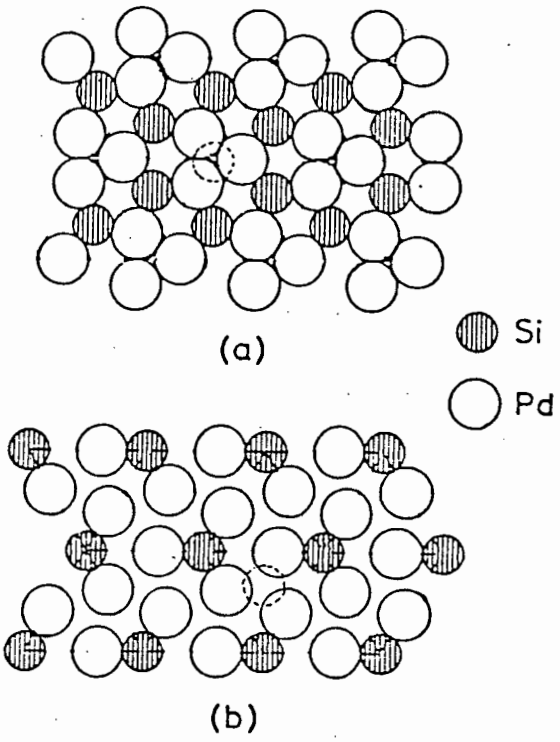

FIG 6-12 The two alternating atomic planes normal to the c_o axis in Pd_2Si and parallel to the Si substrate surface. The large clear circles are Pd atoms and the smaller mottled circles represent Si.
(a) is the base plane of the hexagonal unit cell while
(b) is a plane half way along the c_o axis. The broken circle indicates the position of a Si atom in the plane above or plane below. (From reference 78)

mobility of Si atoms between the neighbouring planes (assuming Si vacancies are present) is seen to be drastically enhanced in the neighbourhood of a Pd vacancy (see arrow indicating migration of Si past a Pd vacancy in Figure 6-13). Therefore, if we assume that Pd diffuses via Pd vacancies during Pd_2Si growth, the presence of the Pd vacancies will drastically increase the mobility of Si atoms (reducing the Si vacancy migration energy) so that both Pd and Si will diffuse.

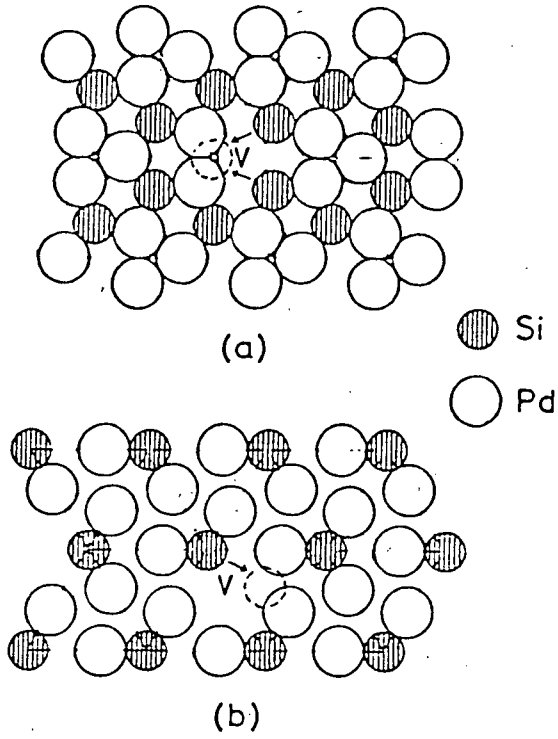

FIG 6-13 A palladium atom has been removed from the lattice (Pd vacancy shown by V). Migration of Si between adjacent planes is facilitated when Si atom moves along arrow.

During $CrSi_2$ growth on Pd_2Si, Pd atoms do not diffuse (therefore few Pd vacancies) so that the mobility of Si is relatively low.

The $Si/Pd_2Si/Ni$ structure used in the study of Ni grain boundary diffusion is analogous to the $Si/Pd_2Si/Cr$ structure used for Si mobility measurements (Pd_2Si membrane sanwiched between Si and Ni sink layers). It is therefore expected that silicon transport through the Pd_2Si membrane would result in Ni_2Si or NiSi being formed at the Pd_2Si/Ni interface. It is rather surprising that both spectra in Figure 6-7 show that no significant Ni_2Si or NiSi has formed on Pd_2Si (polycrystal-

line and epitaxial) in $Si/Pd_2Si/Ni$ specimens annealed for 60 minutes at 400°C. Interdiffusion in Si-Ni binary couples (no interposed Pd_2Si) usually produces Ni_2Si at temperatures around 250°C (see Table 6-1 and refence 60).

Now assume that Si is the only diffusing species during Pd_2Si growth (around 200°C) then the effective mobility ($\bar{B}_{Si}$) of Si in Pd_2Si should be approximately 10^{-13} cm²/sec (maximum parabolic rate constant at 200°C in Figure 6-3). Using equation (6-4), the expected rate of Ni_2Si growth on Pd_2Si formed on Si at 200°C can be calculated:

$$R_{Ni_2Si} = \frac{\bar{B}_{Si}[Si^{Pd_2Si}]}{Y_{Pd_2Si}[Si^{Ni_2Si}]}$$

where Y_{Pd_2Si}: is the Pd_2Si layer thickness

= 1 030 A° (from Figure 6-7),

$[Si^{Ni_2Si}]$ is the concentration of Si in Ni_2Si

$= 2.2 \times 10^{22}$ atoms/cm³

$[Si^{Pd_2Si}]$ is the concentration of Si in Pd_2Si

$= 2 \times 10^{22}$ atom/cm³

$\therefore R_{Ni_2Si} = 1$ Å/sec

Assuming linear Ni_2Si growth, 3 600 A° Ni_2Si is expected to form after 60 minutes at 200°C. Since the mobility of Si is expected to increase with increase in temperature, the thickness of Ni_2Si formed on Pd_2Si is expected to exceed

3 600 A° after 60 minutes at 400°C. Experimental evidence shows that the Ni_2Si formation on Pd_2Si is limited (not detected) so that it can be concluded that the effective mobility of Si in Pd_2Si is orders of magnitude lower than the parabolic rate constant of Pd_2Si growth, in agreement with the results from the diffusion membrane experiments.

The Ni grain boundary diffusion data is interesting in itself but it is more important to relate it to Si and Pd diffusion in Pd_2Si. It is expected that a pair of elements from the same column of the periodic table will display very similar behaviour in a diffusion system. This assumption was exploited in using the interface between the two metal layers as a marker during silicide formation [79]. Although the binary couples Ni/Pd, Ni/Pt and Pd/Pt form continuous series of solid solution [80], the respective crystal structures of the near-noble metal silicides are different: Ni_2Si orthorhombic, Pd_2Si hexagonal and Pt_2Si tetragonal [6]. Substitutional diffusion of one metal (say Ni) into another metal silicide (say Pd_2Si) is therefore expected to be limited.

Grain boundary or interstitial diffusion is not expected to be influenced by the tendency of the diffusing atom to form a silicide with a crystal structure different to that of the matrix. Information about grain boundary and interstitial diffusion can therefore be obtained by probing the silicide with a different metal but from the same column of the periodic table. It was shown that Ni diffuses through polycrystalline

Pd_2Si predominantly via grain boundaries. The Ni grain boundary diffusion in Pd_2Si is therefore a measure for Pd grain boundary diffusion. It was found that the Ni transport along the grain boundaries is more rapid than Si transport along the grain boundaries or through the lattice of Pd_2Si. If we assume that Ni and Pd have similar behaviour in identical diffusion systems, then it is reasonable to conclude that Pd diffuses faster than Si along the Pd_2Si grain boundaries. The activation energy of Pd grain boundary diffusion in Pd_2Si is therefore expexted to be 1.2 eV, as measured for Ni grain boundary.

The grain boundary diffusion of predominantly Pd as deduced from the Ni diffusion experimental results is supported by reported observations during Pd_2Si growth studies. The parabolic rate constant for Pd_2Si growth on Si<100> (polycrystalline Pd_2Si) was found to be slightly higher than that for epitaxial growth on Si<111>[31]. This is due to diffusion along the grain boundaries contributing only in the case of polycrystallinity. It was observed by Cheung et al. that voids were present along the Pd_2Si/Pd interface of partially reacted Si<100>/Pd couples [31]. Although the authors explained the presence of the voids in terms of a large flux of Pd across the Pd_2Si/Pd interface (not necessarily via grain boundaries), it is believed that the cause of the voids is the following: grain boundary diffusion of only Pd causes the Pd layer to be depleted (pitted) around the entrance to the grain boundaries without any silicide

being formed there to compensate for the loss of material. This is illustrated in Figure 6-14. Voids were not observed at the Pd_2Si/Pd interface of partially grown expitaxial Pd_2Si specimens ($Si<111>/Pd_2Si/Pd$) [31]. This is consistent with the void forming mechanism proposed above since grain boundary diffusion in epitaxial layers is negligible.

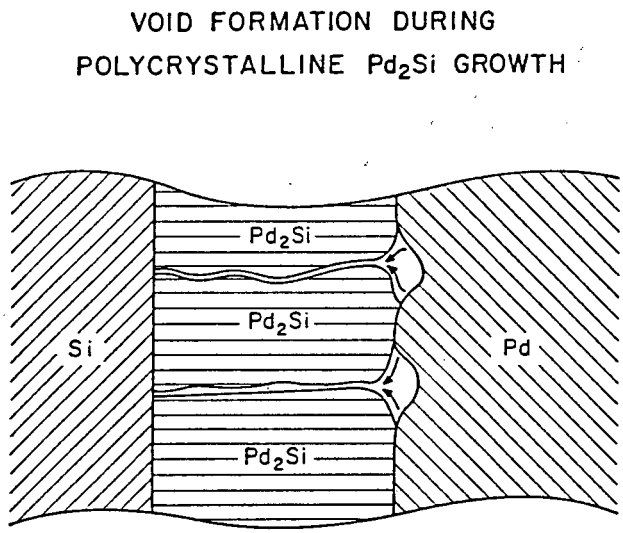

FIG 6-14 Schematic of $Si/Pd_2Si/Pd$ structure showing void formation as result of Pd release from Pd layer and subsequent diffusion along Pd_2Si grain boundaries.

When considering the analogy between the $Si/Pd_2Si/Cr$ and $Si/Pd_2Si/Ni$ structures once more, it is surprising that Cr is not found to diffuse along the Pd_2Si grain boundaries towards the Si substate to form $CrSi_2$ at the Si/Pd_2Si interface, as was found in the case of Ni. The explanation for the difference in thermal behaviour should be sought in the chemical properties of Ni and Cr in relation to those of Pd. Palladium and nickel are similar(near noble metals from the same column in the periodic table) where as chromium is very different in its

chemical behaviour (refractory metal). It was argued earlier that the grain boundary diffusional behaviour of two chemically similar elements will be similar. Chromium, which will be a chemically foreign atom in Pd_2Si, is therefore expected to have a very small tendency to diffuse along the Pd_2Si grain boundaries or through the Pd_2Si lattice.

Considering the mobility and diffusivity results presented in this chapter and the atomic flux ratio results presented in section 5.3.2., the following diffusion model for Pd_2Si growth is proposed. Both palladium and silicon diffuse via a vacancy mechanism through Pd_2Si (epitaxial or polycrystalline). Since the mobility of Si was shown (postulated) to depend on the presence of Pd vacancies, the Si and Pd atomic fluxes are expected to be coupled (Pd mobility also depends on Pd vacancy concentration). This is in agreement with the fact that the Pd/Si atomic flux ratio was found to be independent of temperature. In addition to the lattice diffusion of both Pd and Si, palladium also diffuses along the grain boundaries in polycrystalline Pd_2Si.

CHAPTER 7

LATERAL DIFFUSION

7.1 INTRODUCTION

Metal silicides such as Pd_2Si and PtSi have long been used in contact with lightly doped silicon in fabricating Schottky barrier devices [68]. These silicides have also been considered as candidates for fabricating ohmic contacts to heavily doped silicon. As device dimensions are being scaled down in VLSI (very large scale integration) technology, suppression of metallurgical erosion effects to shallow junctions become increasingly important. During IC fabrication, a metal layer is usually deposited over the contact opening (Figure 7-1(a)). The depth of this silicide layer is usually limited by the stringent conditions laid down by VLSI considerations (see Figure 7-1(b)). Prolonged heating results in the erosion of the silicide/silicon contact as a result of lateral diffusion of the metal and the silicon, as illustrated in Figure 7-1(c). The silicide spike thus shorts the p-n junction. This is similar to the well-known spiking effect in Si/Al contacts [29]. Both lateral and vertical design limits of the contacts are therefore exceeded. A knowledge of lateral diffusion in silicides is therefore essential in order to prevent or limit the erosion of silicide/silicon contacts.

It is often claimed that thin film behaviour is very different to bulk behaviour with regard to interdiffusion and compound formation. By using lateral diffusion couples, it is possible to perform diffusion studies in thin films in the micron

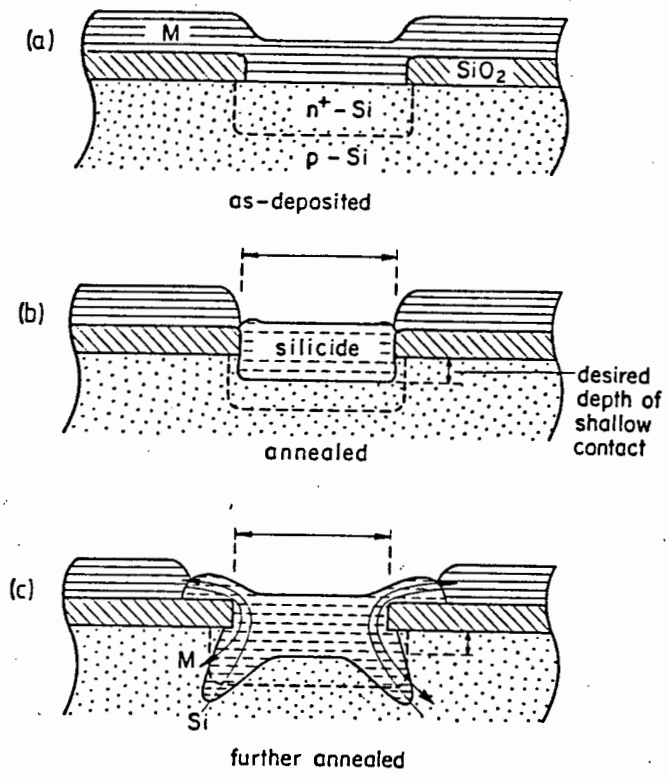

FIG 7-1 Schematic of a contact opening in an IC. Silicide spikes penetate the boundary between p- and n^+-Si regions, thereby short-circuiting the p-n junction.

regime which approaches the typical dimensions of diffusion regions in bulk couples. It will be shown that lateral diffusion couples are ideal for determining the atomic mobility of the components, especially in cases where both components diffuse during compound growth (e.g. Pd_2Si). There is therefore considerable interest attached to the study of lateral diffusion from an academic point of view as well as from the point of view of electronic device manufacturing.

7.2 Lateral diffusion couple geometry

Various thin film sample geometries have been found suitable for lateral diffusion studies [81 - 83]. Three different geometries are shown in Figure 7-2. The characteristic features of these geomeries are:

(1) An inert substrate or layer such as SiO_2 or Al_2O_3 prevents vertical diffusion in the lateral diffusion zone.

(2) A source region which is rich in either Si or metal, is laterally well defined.

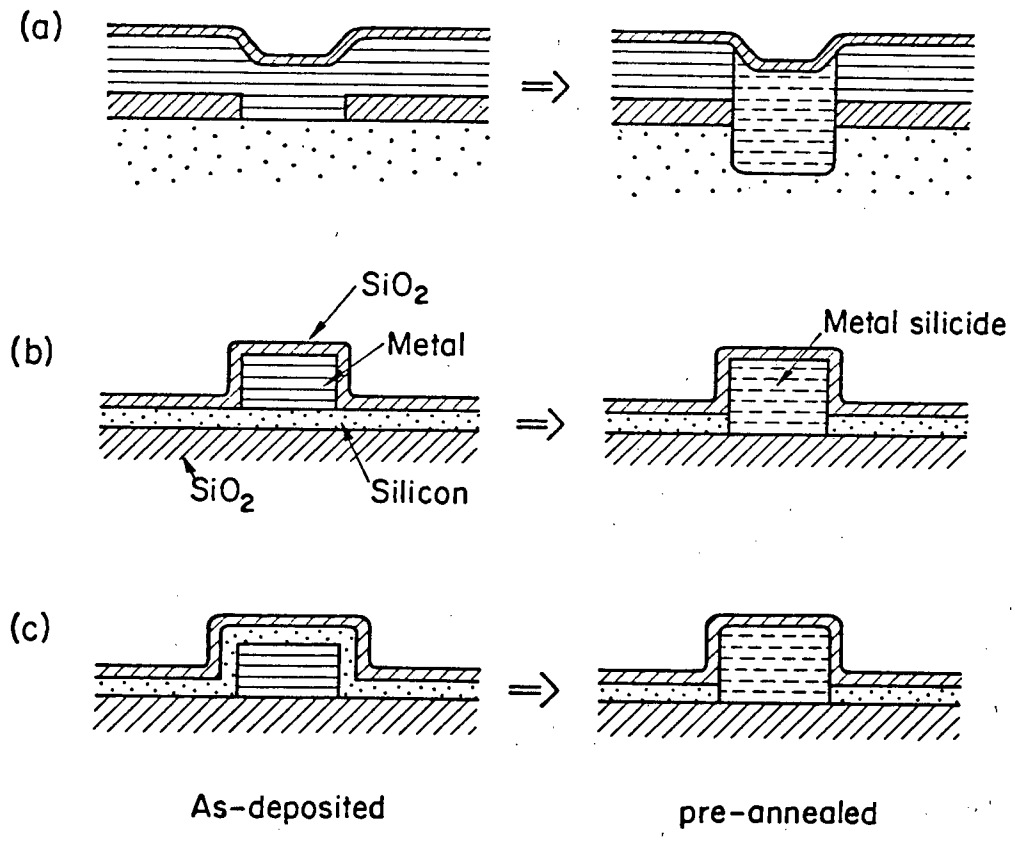

FIG 7-2 Sample geometry of lateral diffusion couples before and after the pre-annealing stage. Cases (b) and (c) are identical after being pre-annealed.

(3) A planar region exists through which the diffusing atoms (Si and/or metal) move laterally.

The purpose of the covering SiO_2 layer is to reduce or eliminate surface diffusion which could overshadow lateral diffusion effects. In Figure 7-2(a), the substrate acts as a source, supplying the diffusant through the etched window. This geometry is the device structure. The geometries in Figures 7-2(b) and 7-2(c) are essentially the same, (after being pre-annealed) differing only in the sequence in which the two layers (metal and silicon) are deposited. This particular sample configuration is referred to as the island structure.

In Figure 7-3 the development of the lateral diffusion zone is illustrated. A single sample geometry is used (Figure 7-2(b) without the covering SiO_2 layer). Two different configurations are obtained by interchanging the metal and silicon. The well defined island of metal (or silicon) becomes a metal-rich (or silicon-rich) source region after pre-annealing. On further annealing, the diffusion regions which develope (lateral extent L) are due to either metal (or silicon atoms) diffusing laterally form the source region, as indicated in the figure. The lateral diffusion technique therefore offers the advantage of isolating the contribution to diffusional growth, of the respective components of the couple.

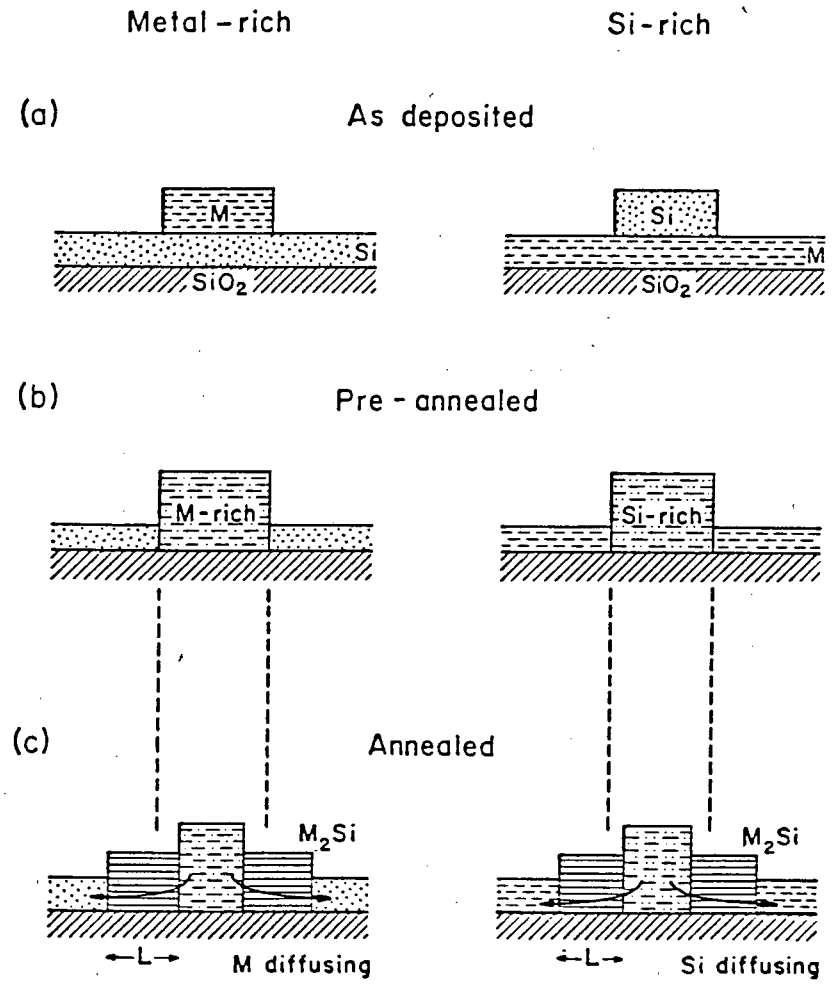

FIG 7-3 Two different configurations of island structures illustrating the diffusing species during lateral growth.

It is however possible that both silicon and metal diffuse (in opposite directions) in the same sample. It is illustrated in Figure 7-4 that the movement of species towards the source region does not affect the lateral extent of the diffusion region but drastically affects the thickness of the region. Three different cases are shown where the silicon/metal flux ratio (silicon/metal mobility ratio) is different in each case. The lengths of the arrows reflect the relative mobilities of the silicon and metal atoms.

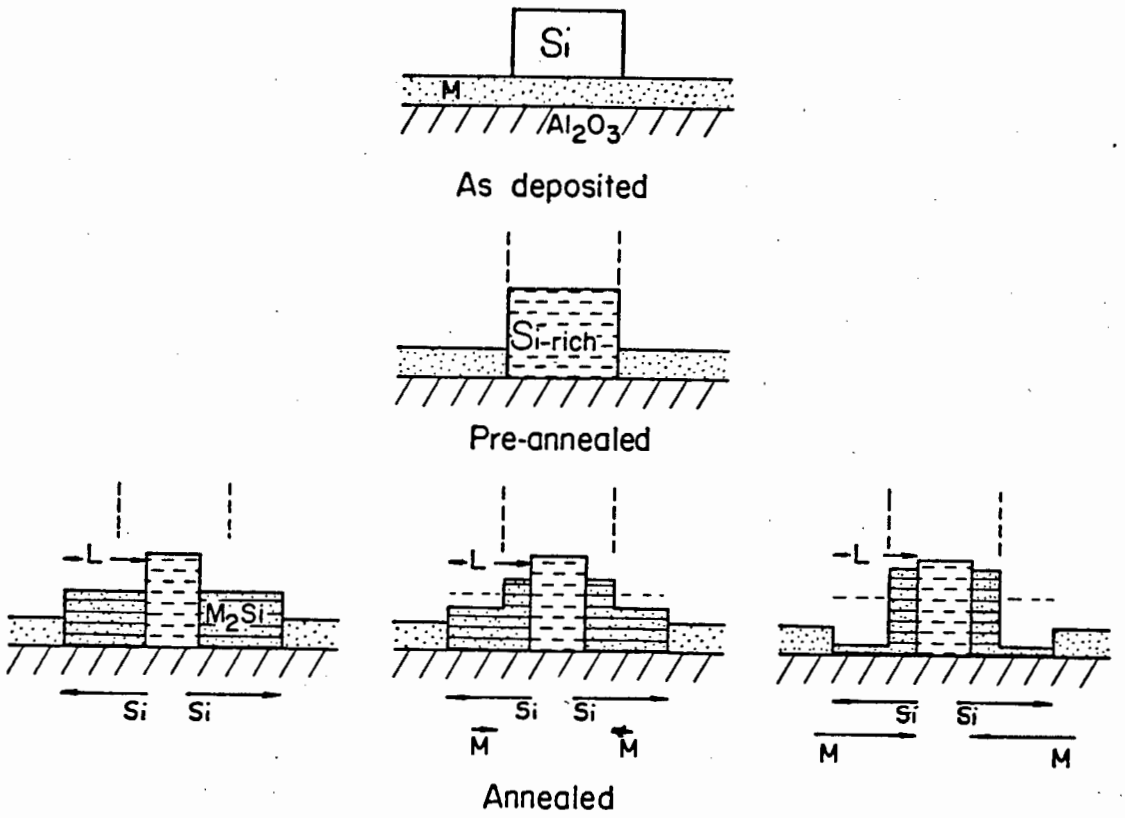

FIG 7-4 Length of the arrows below represent the relative magnitude of Si and M mobility respectively.

The lateral extent of the diffusion zone is therefore entirely determined by the mobility of the species diffusing from the source region.

7.3 Mobility of the diffusing species

Consider the geometry of a sample as illustrated in Figure 7-5. A metal rich source provides metal atoms to diffuse outwards. The original interface between the source and silicon region now divides the diffusion zone (length L) into two regions which are referred to as the inside region (length d_i) and outside region (length d_o) respectively. The outside region is the true growth region resulting from metal having diffused

through the already formed silicide zone and reacting with the silicon. The inside region is effectively formed by depleting the source of the excess metal.

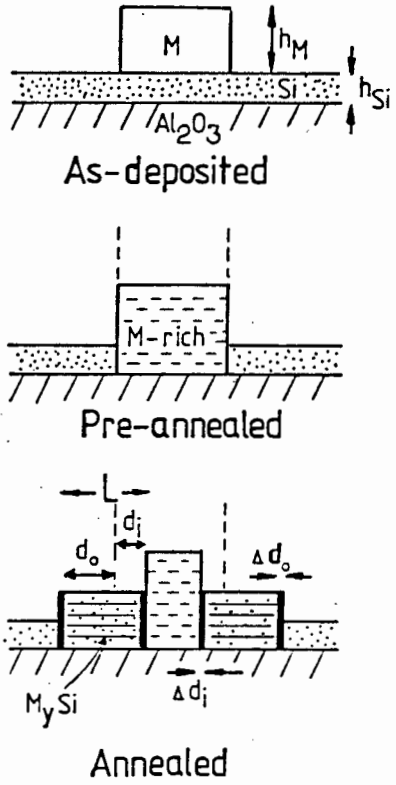

FIG 7-5 Progress of the lateral silicide growth process showing all the relevant parameters.

The lateral extent of the entire diffusion zone is L and a uniform silicide phase M_ySi is assumed. The inside region of length d_i will increase by Δd_i during infinitessimally short time interval $\Delta\tau$ whereas the outside region of length d_o will increase by Δd_o. A flux balance during time interval $\Delta\tau$ is set up. The number of metal atoms crossing a unit area at the silicide/silicon interface (diffusing outwards) during time interval $\Delta\tau$ is ΔN_M while the number of silicon atoms crossing the same interface (diffusing inwards) is ΔN_{Si}.

The metal atoms diffusing outwards across the silicide-silicon interface are incorporated in the newly-formed silicide region of length Δd.

$$\therefore \quad \Delta N_M = \{\text{number of metal atoms incorporated in the silicide region of length } \Delta d_o\}.$$

If y is the ratio of metal to silicon atoms in the stoichiometric compound M_ySi, then

$$\Delta N_M = y\ \{\text{number of Si atoms incorporated in the silicide layer of length } \Delta d_o\}.$$

These silicon atoms however represent only a fraction of the silicon atoms originally present (as deposited) in the region (length Δd_o).

$$\therefore \quad \Delta N_M = y\ \{\text{number of Si atoms orginally present in the deposited silicon layer of thickness } h_{Si} \text{ and length } \Delta d_o \text{ - number of silicon atoms diffusing into the source}\}.$$

If $[Si]^{Si}$ is the atomic concentration of silicon in silicon, then

$$\Delta N_M = y\{[Si^{Si}]\ h_{Si}\Delta d_o - \Delta N_{Si}\} \qquad (7\text{-}1)$$

The metal atoms diffusing outwards originate from the source region with an original (as-deposited) metal layer thickness h_M.

$\therefore \Delta N_M$ = {number of metal atoms in the deposited metal layer of thickness h_M and length Δd_i - number of metal atoms incorporated in the silicide layer of length Δd_i}.

The silicide layer on the "inside" is formed through metal reacting with the silicon in the deposited layer (thickness h_{Si}) and with silicon diffusing inwards (ΔN_{Si}).

$\therefore \Delta N_M$ = {number of metal atoms in the deposited metal layer of thickness h_M and length Δd_i} - y {number of silicon atoms in the deposited Si layer of thickness h_{Si} and length $\Delta d_i + \Delta N_{Si}$}.

$$\therefore \Delta N_M = [M^M]\, h_M \Delta d_i - y([Si^{Si}]\, h_{Si} \Delta d_i + \Delta N_{Si}) \qquad (7\text{-}2)$$

Equating (7-1) and (7-2)

$$y[Si^{Si}]\, h_{Si} \Delta d_o = [M^M]\, h_M \Delta d_i - y[Si^{Si}]\, h_{Si} \Delta d_i$$

$$\therefore \quad \frac{\Delta d_o}{\Delta d_i} = \frac{[M^M]\, h_M}{y[Si^{Si}] h_{Si}} - 1 \qquad (7\text{-}3)$$

Upon integration, (7-3) becomes:

$$\frac{d_o}{d_i} = \frac{[M^M] h_M}{y[Si^{Si}] h_{Si}} - 1 \qquad (7\text{-}4)$$

The significance of (7-4) is that the ratio of the inside and outside regions of the diffusion zone, is determined by the thicknesses of the deposited layers h_M and h_{Si}. It is unaffected by the diffusion of Si into the source, on the assumption that the phases of the inside and outside regions are identical.

It will now be shown that the effective mobility of the atoms diffusing outwards, in this case the metal atoms, can be determined from the lateral growth kinetics of the diffusion zone. Let the total length of the zone be L and the increase in length during the time interval $\Delta\tau$ be ΔL. Then:

$$\Delta L = \Delta d_o + \Delta d_i$$

Using (7-3):

$$\Delta L = \Delta d_o \left\{ 1 + \frac{y[Si^{Si}]h_{Si}}{[M^{M}]h_M - y[Si^{Si}]h_{Si}} \right\} \qquad (7\text{-}5)$$

If $\Delta\mu_M$ is the chemical potential difference of M across the diffusion zone then the flux of metal atoms in the diffusion zone J_M, is given by:

$$J_M = B_M[M^{M_ySi}].\Delta\mu_M/L$$

where B_M is the mobility of M in M_ySi. (similar to (3-21)). The lateral growth of the outside region is a direct result of the metal flux. See (3-22):

$$J_M = [M^{M_ySi}]. \frac{\Delta d_o}{\Delta \tau}$$

where $\frac{\Delta d_o}{\Delta \tau}$ is the rate at which the outside region advances.

Therefore:

$$\frac{\Delta d_o}{\Delta \tau} = B_M \frac{\Delta \mu_M}{L}$$

The effective mobility $\bar{B}_M$ is defined as

$$\bar{B}_M = -B_M \Delta \mu_M$$

so that:

$$\frac{\Delta d_o}{\Delta \tau} = \frac{\bar{B}_M}{L} \qquad (7\text{-}6)$$

From [7-5] and [7-6]:

$$\frac{\Delta L}{\Delta \tau} = \frac{\bar{B}_M}{L} \left\{ 1 + \frac{y[Si^{Si}]h_{Si}}{[M^M]h_M - y[Si^{Si}]h_{Si}} \right\}$$

Upon integration:

$$\bar{B}_M = \frac{L^2}{2t} \cdot \left\{ 1 - \frac{y[Si^{Si}]h_{Si}}{[M^M]h_M} \right\} \qquad (7\text{-}7)$$

The effective mobility is therefore very closely related to the parabolic rate constant for lateral growth $\frac{L^2}{2t}$. It was shown in section 3.2.5 that the effective mobility is equal to the parabolic rate constant for conventional compound growth provided only one of the components diffuse. Care should therefore be taken when comparing the parabolic rate constant for lateral growth to that for conventional thin film growth of the corresponding silicide, as the factor in brackets in

(7-7) could be significant. This factor however approaches unity as the metal to silicon thickness ratio increases so that the ideal sample geometry is a very thick metal layer onto a very thin Si layer. From (7-7) it is seen that the ratio $\frac{L^2}{2t}$ (parabolic rate constant for lateral diffusion) is determined solely by the effective mobility of the out-diffusing metal atoms ($\frac{L^2}{2t}$ not dependent on $\bar{B}_{Si}$ in this configuration). The lateral diffusion techique is therefore ideal for separating the diffusion contributions of the components of a couple without introducing foreign atoms (inert marker atoms) into the system.

7.4 RESULTS

In this study of lateral diffusion in Pd-Si couples various sample geometries, as described in section 7.2, were used. The specimens were annealed at temperatures between 350 and 650°C for periods of time up to 30 h. The pre-annealing stage (pre-annealing around 300°C during which the Pd-rich or Si-rich source region developes) was omitted in most of the specimens since it was found that it did not have a significant effect on the developement of the lateral diffusion zone during the final heat treatment (source region developes within the first few minutes of the final heat treatment).

Extensive lateral diffusional growth of Pd_2Si was observed only in structures with Pd-rich source regions, i.e. only in cases where the lateral diffusion zone developed as result of Pd diffusion from Pd-rich source regions. The structures with

Si-rich source regions showed limited lateral diffusional growth (approximately 1 μm). In Figure 7-6 scanning electron micrographs of the surface topography of Si-rich structures are shown. Both device structure (a) and island structure (b) configuration are shown in Figure 7-6. The limited diffusional growth is seen to be very irregular (spike-like). The Pd thickness (area of Pd signal) from EDS of these spikes was found to be less than the Pd layer thickness of the surrounding areas (deposited Pd layer thickness). This indicates that Pd diffused into the source region from these spike-like areas. Cracks are also observed along the perifery of the source region. This fact, together with the observation that Pd diffuses inwards, suggests that the mobility of Pd in Pd_2Si is much greater than the mobility of Si. (see Figure 7-4).

Typical scanning electron micrographs of island structures with Pd-rich source regions are shown in Figure 7-7. The advancing interface is seen to be relatively uniform. The composition of the inside and outside diffusion zones was established as Pd_2Si from the yield of electron-induced X-rays (EDS). The phase was identified as Pd_2Si by means of transmission electron diffraction in thin samples, prepared specifically for transmission electron microscopy studies. Diffraction patterns characteristic of Pd_3Si were also obtained from the inside region of the diffusion zone especially near the original interface separating the inside and outside diffusion regions. The phase of the Pd-rich source region is expected to depend on the thickness ratio of the deposited Si layer and Pd island as well

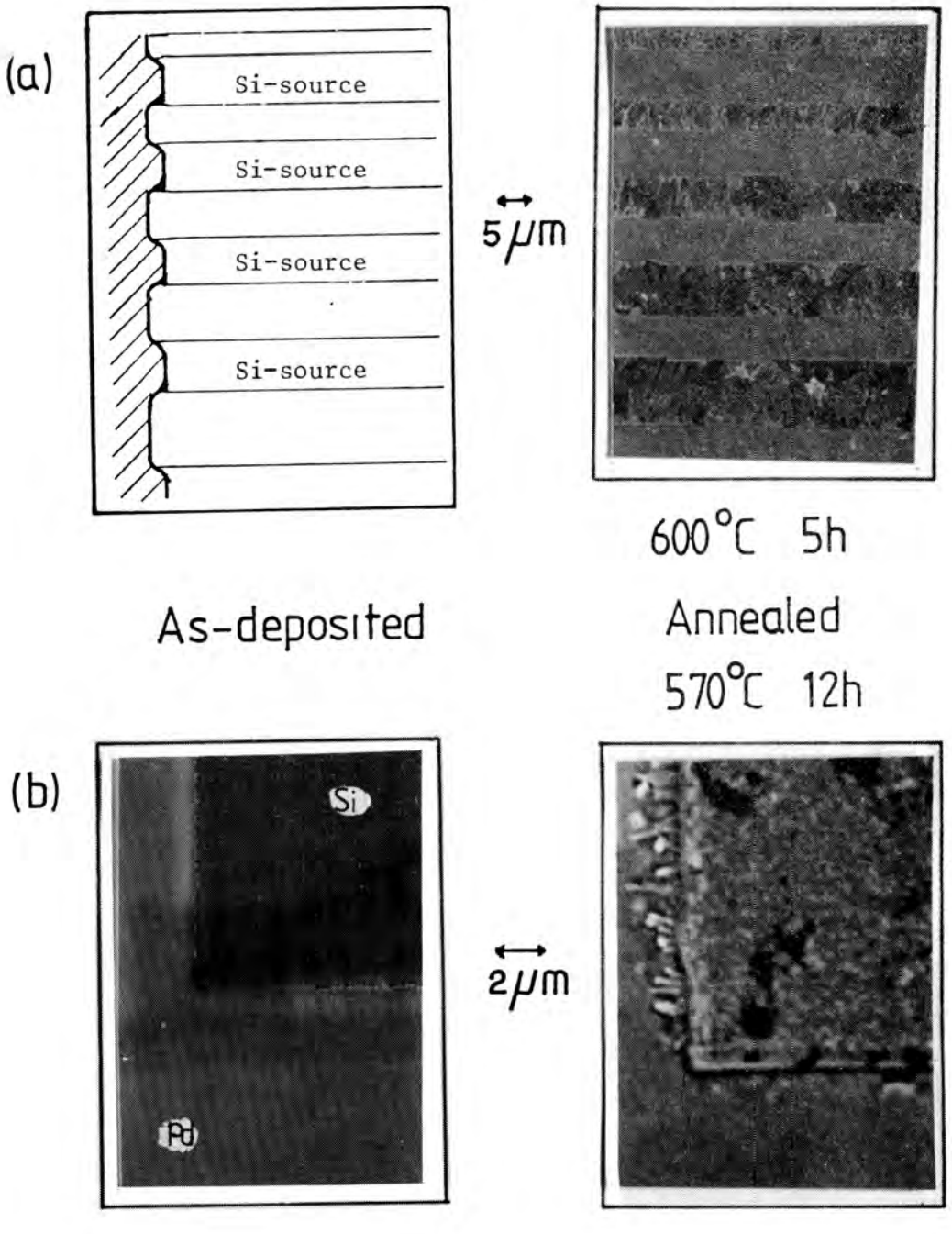

FIG 7-6 Scanning electron micrographs of device structure and Si-rich island structure specimens. The as-deposited device structure specimen is not suitable for S E M due to relatively featureless surface topography.

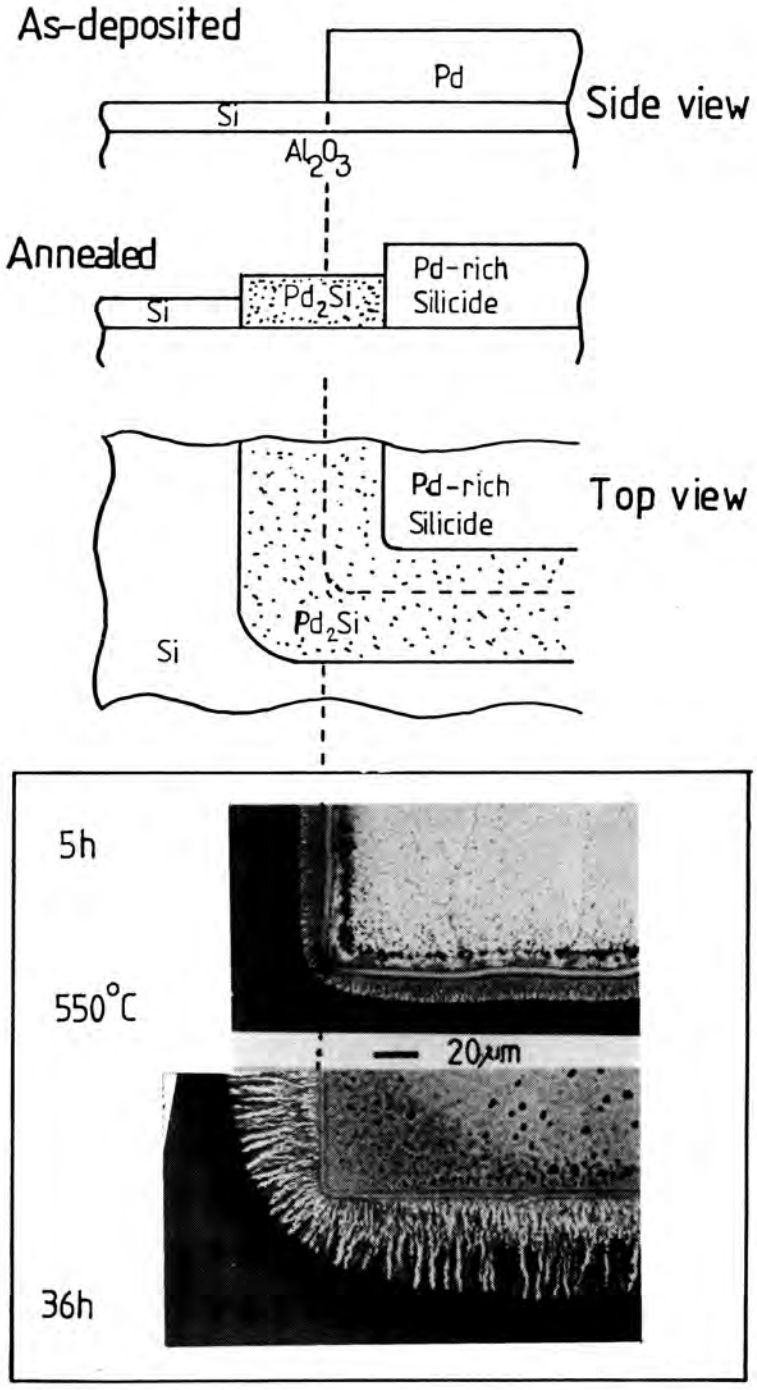

FIG 7-7 Scanning electron micrographs of Pd-rich island structure specimens.

as the annealing temperature. In most of the specimens the phase of the source region is expected to be Pd_3Si plus excess Pd (Pd/Si thickness ratio of specimens greater than 3 and temperature above 300°C). This is based on the results of a study of Pd-rich silicide formation by Canali et. al [85]. It is possible that the phase of the source regions of some specimens (annealing temperature around 600°C) is Pd_4Si. (see reference 85.) Due to the thickness of the source region it is impossible to identify its phase with TED.

The lateral extent of the diffusion zone (inside + outside regions) was found to increase with time at constant temperature. The square of the diffusion zone length L^2 is plotted against the annealing time t in Figure 7-8. The observed linear relation is characteristic of diffusion limited growth in phase forming binary couples. The parabolic growth rate constant $L^2/2t$ is plotted in Figure 7-9 against the reciprocal temperature. The activation energy obtained from the slope of the curve (Arrhenius plot) is 1.1 ± 0.2 eV. This activation energy is associated with the mobility of Pd in Pd_2Si (Figure 7-7) and is of the same order of magnitude as that published for Pd_2Si growth from conventional Pd-Si couples [31]. When extrapolating to lower temperatures, the parabolic rate constant is seen to be of the same order of magnitude as that of conventional Pd_2Si growth as shown in Figure 7-9. This would suggest that the diffusion mechanism in both conventional and lateral diffusion processes is the same.

Figure 7-10 is a composite transmission electron micrograph of the diffusion zone of a Pd-rich specimen. The Pd_2Si grain size

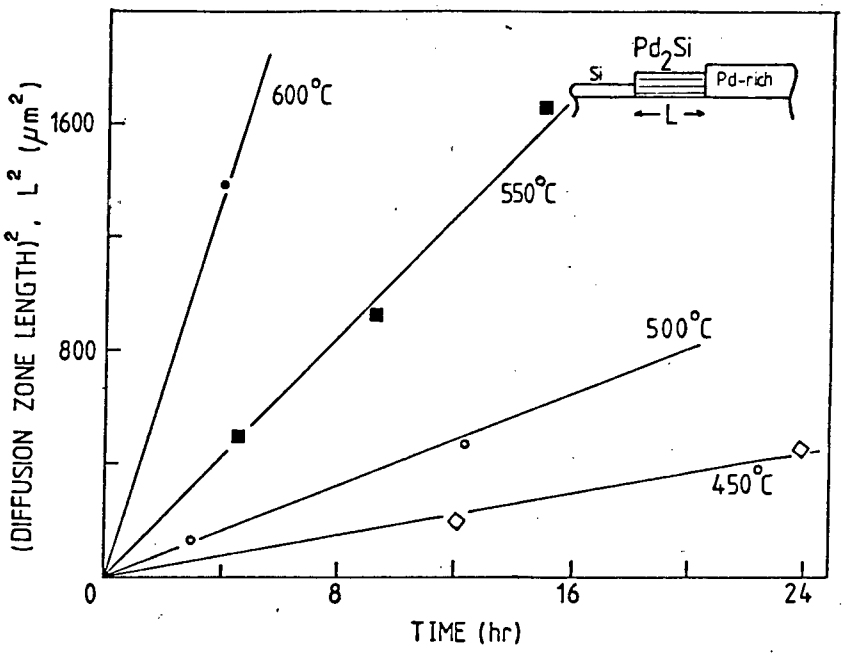

FIG 7-8 Parabolic growth of Pd_2Si in lateral diffusion couples.

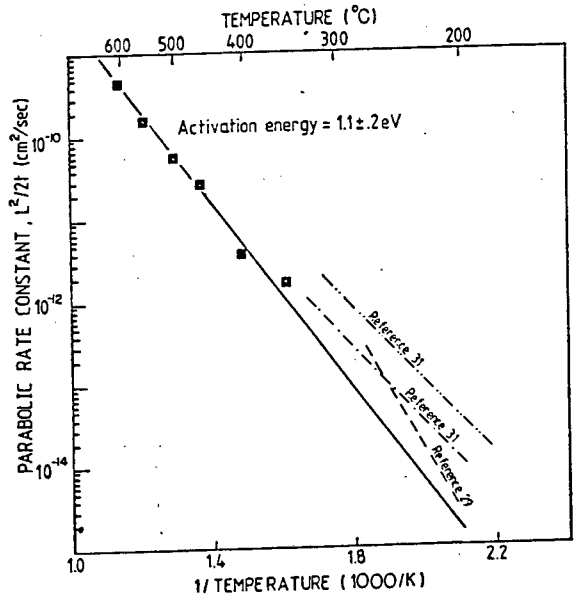

FIG 7-9 The Arrhenius plot of the parabolic growth rate of Pd_2Si in lateral diffusion couples.

is seen to vary from approximately 500 Å in the outside region to 1 μm in the inside region. It should be borne in mind that the grain size of Pd_2Si layers grown from conventional couples have been reported to vary between 200 and 900 Å [31,53]. The grains in the lateral diffusion zone were found to have a

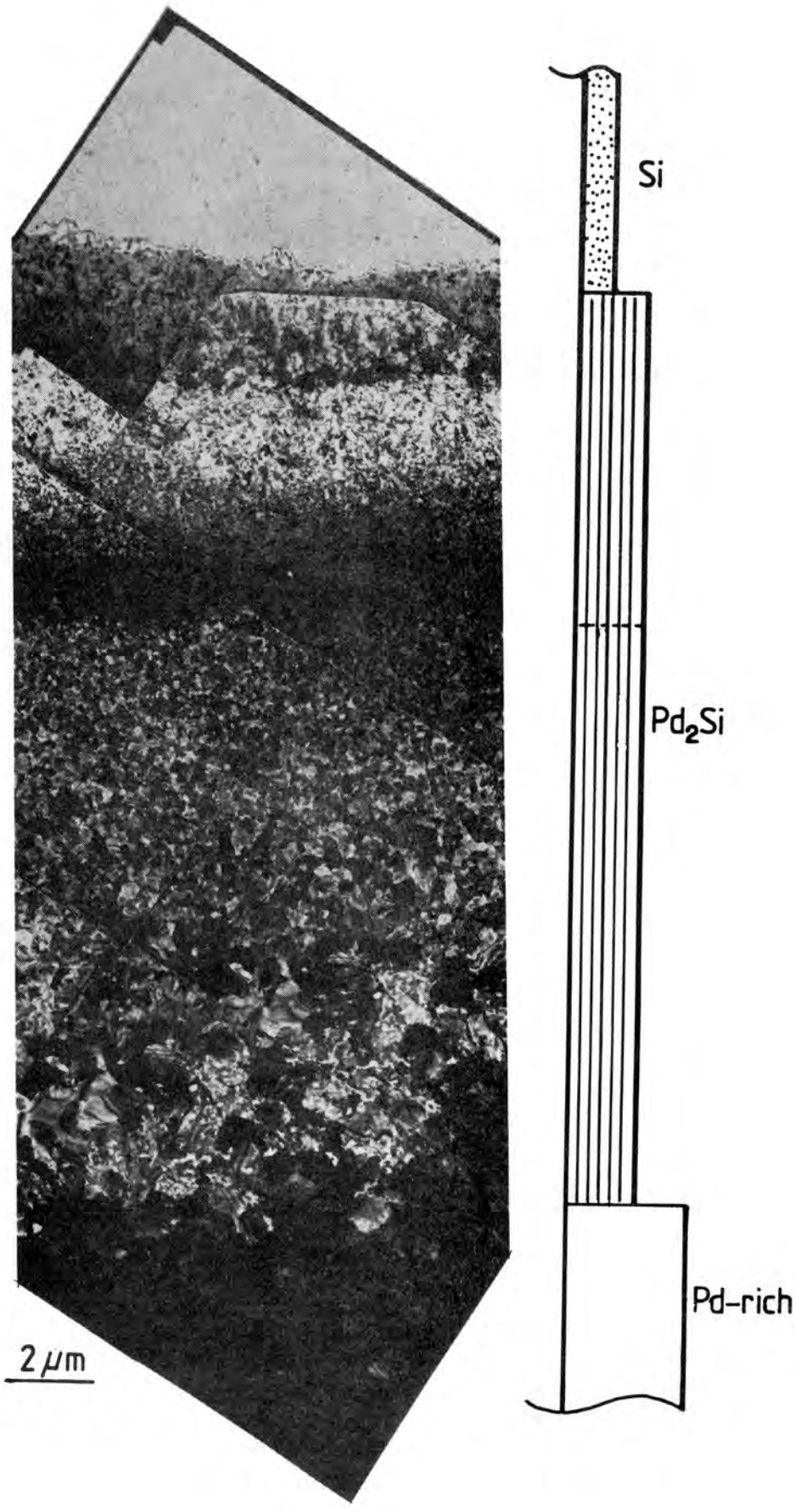

FIG 7-10 Composite transmission electron micrograph of the Pd/Si lateral diffusion zone. The surface topography of the sample is shown schematically on the right.

preferred orientation, namely the hexagonal basal plane being parallel to the specimen surface. This is similar to the case of conventional Pd_2Si layers grown in single crystal or amorphous silicon substrates [28,30].

7.5 DISCUSSION

The difference in thermal behaviour between Pd-rich and Si-rich structures is ascribed to the difference in mobilities of Pd and Si in Pd_2Si. It was schematically shown in Figure 7-4 that when the inward diffusing species has a much higher mobility than the outward diffusing species, the diffusion zone becomes very thin and could eventually lead to crack formation in the film. The cracks observed in the Si-rich samples are therefore believed to indicate that the Si mobility in Pd_2Si is significantly lower than the Pd mobility. This is in agreement with the diffusion membrane results reported in Chapter 6. It is however, in disagreement with the W marker experimental results presented in Chapter 5, which indicate that Si and Pd have comparable fluxes in Pd_2Si during its growth.

The relatively low Si mobility in Pd_2Si, as deduced from the limited lateral diffusional growth and the cracks in the film of Si-rich structures, is ascribed to the particular crystal structure of Pd_2Si. The source region of the Si-rich structures is expected to consist of Pd_2Si + excess Si. (The transformation $Pd_2Si + Si \rightarrow PdSi$ is not expected at temperatures below 750°C [28,29]). It has been reported that Pd_2Si grains, formed by the conventional thin film reaction between Pd and amorphous Si, have a preferred orientation, namely with their

hexagonal plane parallel to the sample (substrate) surface [30]. During lateral diffusion, the atoms (Si and Pd) are required to diffuse through Pd_2Si along the basal plane. It was illustrated in Figure 6-13 that Si atoms do not have Si nearest neighbours in this particular plane. The silicon migration energy will therefore be large, assuming Si vacancy diffusion in this close-packed Pd_2Si lattice. The migration energy of Pd will be relatively low since it is observed that Pd atoms do have Pd nearest neighbours in the plane. Consequently the Pd mobility will be larger than Si mobility in the basal plane.

The lateral diffusional growth of Pd_2Si in Pd-rich specimens is found to be parabolic, similar to Pd_2Si growth in conventional Pd-Si couples, indicating diffusion controlled growth. The activation energy associated with lateral growth is found to be similar to the values reported for conventional growth [31]. This would suggest that the diffusion mechanism in the two cases is the same. It should however be pointed out that the lateral diffusion zone developes predominantly as a result of Pd migration (see (7-7)) whereas both Si and Pd diffusion contribute to the conventional diffusional layer growth of Pd_2Si (see section 5.3.1).

The Pd effective mobility (as determined using (7-7)) compares favourably with the parabolic rate constant for conventional Pd_2Si growth as can be seen when the data in Figure 7-6 are extrapolated to temperatures around 200°C. This good agreement

and the similar activation energies do not necessarily indicate that Pd is the dominant diffusing species during conventional Pd_2Si growth. It was mentioned that the Pd_2Si grains in the Pd-rich specimens were found to have a preferred orientation (basal plane parallel to the specimen surface). During conventional Pd_2Si growth, diffusion occurs perpendicular to the basal plane of Pd_2Si whereas during lateral growth, diffusion occurs in the basal plane. In section 6.4 it was suggested how the Si mobility during conventional Pd_2Si growth (perpendicular to the basal plane) is enhanced by the presence of Pd vacancies. Earlier in this section it was explained why the Si mobility during lateral Pd_2Si growth (along the basal plane) is much lower than the Pd mobility. The diffusion mechanism is therefore different in the two cases although the parabolic rate constants are similar, so that conclusions with regard to the dominant diffusing species in conventional Pd_2Si growth, based on lateral diffusion results, cannot be drawn.

The large grains (1 μm) observed in the Pd_2Si diffusion zone (in the inside region) is ascribed to grain growth subsequent to lateral Pd_2Si formation. In similar lateral diffusion studies using Ni islands on Si layers, the Ni_2Si grains were observed to grow after Ni_2Si formation, using in situ heating in the transmission electron microscope [86]. It is interesting to note that the grain size of conventionally grown Pd_2Si films was not found to exceed 1000 Å, even when formed at temperatures as high as 550°C [53]. The difference

in grain size must be ascribed to the difference in growth mechanisms in the two cases (lateral and conventional). During compound growth (e.g. Pd_2Si from Si and Pd) the volume component is drastically increased (e.g. 1 cc Si transformed to 2,5 cc Pd_2Si). In conventional compound growth the volume increase is along the direction of mass transport i.e. perpendicular to the specimen surface plane. However in lateral diffusional growth the volume increase is perpendicular to the direction of lateral mass transport, (volume increase perpendicular to the specimen surface). The laterally grown Pd_2Si layer is therefore under stress. It is well known that grain growth is a means of relieving stress in polycrystalline films [87]. This explains why laterally formed Pd_2Si grains grow after formation. The fact that the large grains are found in the inside region only, suggests that the film stress is localized.

In Figure 7-11 the effective mobility results as obtained by using the two methods (diffusion membrane in Chapter 6 and lateral diffusion couples), are shown along with parabolic rate constants for conventional Pd_2Si growth (from literature). The good agreement between the Pd effective mobility values (they can be characterized by a single curve) shows that the two techniques are consistant and that both techniques offer reliable means of determining the (effective) mobility of atoms in thin films. The Pd effective mobility values are seen to be of the same order of magnitude as the parabolic rate constant. It is therefore concluded that the parabolic rate constant during conventional Pd_2Si growth does not exceed the con-

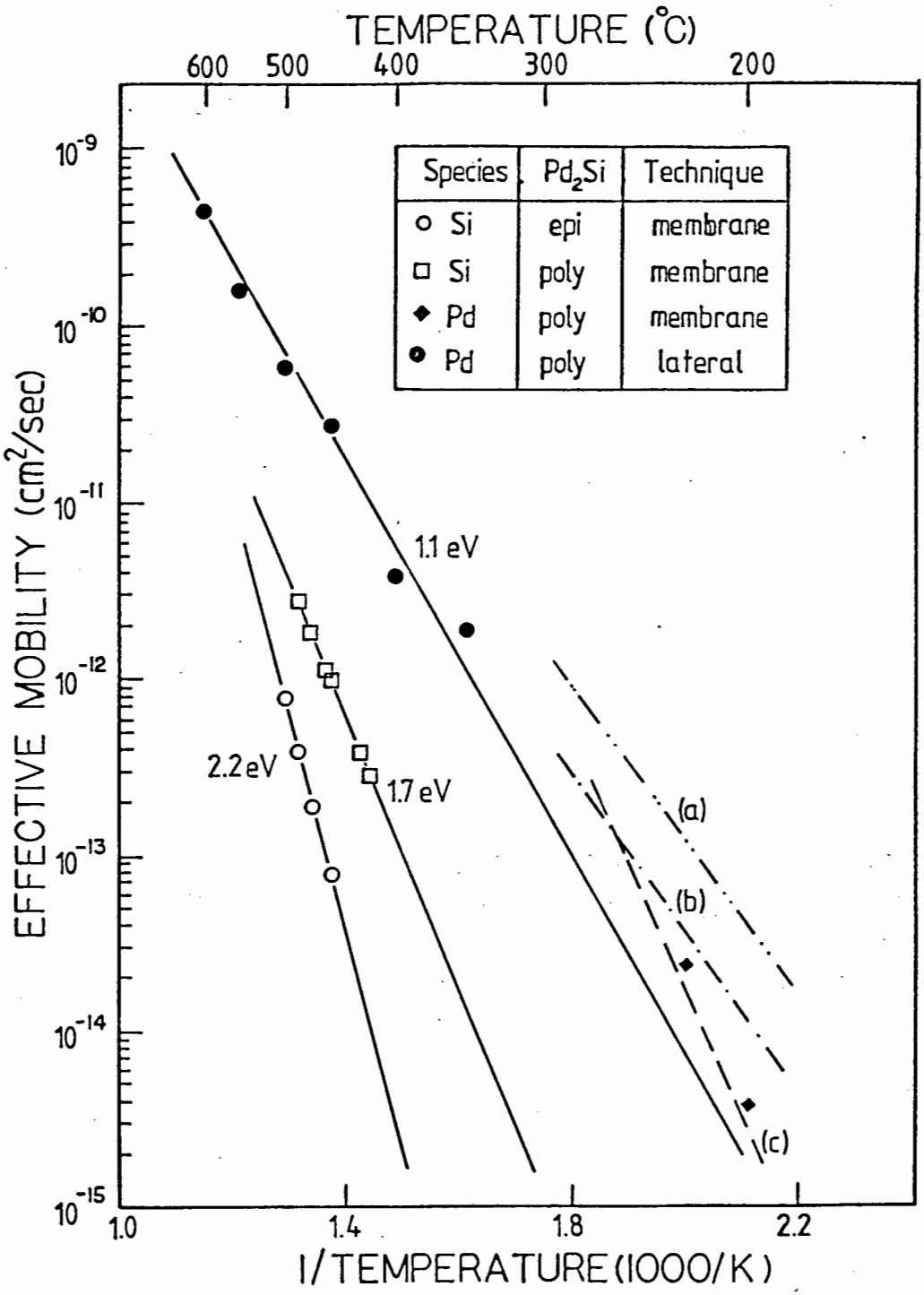

FIG 7-11 Arrhenius plot of the effective mobility of Si and Pd obtained by using different mea-ring techniques. Also shown are published plots of the parabolic rate constant for Pd_2Si grown from conventional Pd/Si couples. a) [31] Si<100> substrate; b) [31] Si<111> substrate; c) [29] Si<100> and Si<111> substrates.

tribution from Pd diffusion by more than an order of magnitude. (Parabolic rate constant is equal to the sum of the respective effective mobilities: $\tilde{B} = \bar{B}_{Si} + \bar{B}_{Pd}$). This is in agreement with the results in section 5.3.1 where it was found that the fluxes of Si and Pd during Pd_2Si growth are comparable. It would appear that the grain size and formation temperature do not affect the diffusion mechanism (single activation energy) during Pd_2Si growth. It is therefore concluded that the atoms are transported predominantly through the Pd_2Si lattice during its growth.

Lateral diffusion has been shown to be an elegant approach for measuring the atomic mobility of components in a compound during its growth, even in cases where both components usually diffuse during compound growth from conventional couples. Care should however be taken when interpreting the mobility results as the microstructure of the compound film could play a significant role in determining the mobility.

CHAPTER 8

SUMMARY AND CONCLUSIONS

Transition metal silicides are used extensively in silicon-based integrated circuits for ohmic and rectifying contacts to silicon while aluminium is commonly used for making interconnections between the various contacts. Such contacts have however been found to degrade upon heat treatment, due to silicide-aluminium and silicon-aluminium interdiffusion. A diffusion barrier layer such as a refractory metal is generally required between the silicide and aluminium layers in order to limit or prevent the degradation of the contacts. The complete metallization therefore contains several layers, each of which can react directly or indirectly with silicon from the substrate during IC processing. Silicide formation in multilayer metal-silicon thin film systems is therefore of prime importance to modern integrated circuit technology, and research in this field is most valuable.

A theoretical treatment of silicide formation in multilayer metal-silicon systems has not been documented. It was thus the purpose of this investigation to develope a model for characterizing the silicide growth kinetics in bilayer metal-silicon thin film systems and to test the validity of the model. Several authors have treated (theoretically) compound formation in binary couples. The approach has been to solve the diffusion equation which is subject to moving boundary conditions.

The essential features of these theories are that they predict compound growth to progress linearly with time in the initial stage, and that the growth eventually slows down and becomes parabolic (layer thickness being proportional to the square root of time). This is in agreement with experimental results. These theories have however been found to be inadequate with regards to quantitative predictions. The diffusing atoms are considered to migrate because of a concentration gradient in the "stoichiometric" compound film. The diffusion coefficient therefore characterizes the migration of the atoms. Concentration variations in stoichiometric compounds are generally thought to be accommodated by vacancies. The vacancy concentration is therefore non-uniform if an atomic concentration gradient is present. If the atoms diffuse via vacancies, the atomic diffusion coefficient, which is proportional to the vacancy concentration, will be non-uniform. Theories based on the assumption of a uniform diffusion coefficient could therefore be erroneous. Furthermore, the concentration gradient in the growing stoichiometric compound proves to be very small and not easily measurable. These factors make the theories for growth kinetics of compounds in binary couples, inadequate for quantitative applications.

A different approach was followed in this work in developing a theory of the growth kinetics. The underlying idea in this theory is that the kinetics of compound growth is determined by the driving force for diffusion through the compound layer which is believed to be the chemical potential gradient.

In order to determine the driving force, it is necessary to establish the process(es) whereby thermodynamic equilibrium is attained at the interfaces.

Since atomic transport in solids is predominantly via defects (vacancies in the case of close-packed crystal structures such as Pd_2Si), vacancy diffusion is assumed to be the dominant transport mechanism. Interfacial atom-vacancy reactions, which could influence the vacancy concentration, are postulated. It is hence proposed that thermodynamic equilibrium at the interfaces is attained through these interfacial reactions whereby equilibrium vacancy concentrations (at the interfaces) are established. Two stages of compound growth can therefore be characterized viz. the initial non-equilibrium stage and the final equilibrium stage.

The total driving force for compound formation is essentially the free energy change of formation ΔG_f^o. This free energy is "spent" in two ways viz. dissipation ΔG_B due to atoms crossing the interfacial boundaries and the dissipation ΔG_D due to atoms diffusing through the compound layer:

$$\Delta G_f^o = \Delta G_D + \Delta G_B$$

In the case of local thermodynamic equilibrium at the interfaces, the energy dissipation at the interfaces is zero so that the driving force for diffusion ΔG_D is a maximum ($\Delta G_D = \Delta G_f^o$) and remains constant. Any deviation from local equilibrium at the interfaces will decrease the free energy dissipation due to diffusion. ($\Delta G_B \neq 0$). It is however shown that during the initial growth stage ΔG_B (Δg^{Si} in (3-17)) decreases linearly

with time so that ΔG_D ($\Delta \mu_{Si}$ in (3-18)) increases linearly with time. Since the driving force increases linearly with time, the planar growth of the compound layer is found to be linear during the initial non-equilibrium stage. When local equilibrium prevails at the interfaces, the driving force for diffusion is constant and the growth of the compound layer is found to be parabolic (square of layer thickness proportional to time).

This theory is in agreement with other documented theories and with experimental results, in that it predicts that planar compound growth in binary couples is initially linear but eventually becomes parabolic. The difference between this theory and others is that the mobility (B) and not the diffusivity (D) of the diffusing atoms in the compound layer is the important parameter which determines the growth rate constant. The parabolic rate constant for compound growth is seen to be equal to the product of the mobility and the driving force for diffusion (free energy change of formation).

In extending this theory to compound growth in bilayer metal-silicon systems, the various concepts (e.g. equilibrium, non-equilibrium, mobility, driving force for diffusion) which were applied to binary couples, are used. Although a variety of interdiffusion mechanisms are possible, attention is given to the specific case where the two metal layers form silicides sequentially, without any metal-metal interdiffusion. The dominant transport mechanism during silicide formation is again assumed to be vacancy diffusion. The interposed metal layer

forms a silicide, independent of the outer metal layer so that the growth kinetics are essentially that of a binary metal-silicon couple. The theory developed for the growth kinetics of the outer silicide layer is based on the fact that the total driving force for the formation reaction (outer silicide) is "spent" through dissipation of free energy in the two silicide layers due to diffusion. The important prediction of the theory is that the growth of the outer silicide layer is linear, not only when equilibirum does not prevail at one of the interfaces, but also in the case of equilibrium, subject to a special condition, this special condition being that the mobility of the diffusant is comparitively low in the interposed silicide layer. The linear kinetics in both cases will however go over into parabolic kinetics when the outer silicide layer has grown sufficiently thick.

It is therefore seen that in binary couples, linear growth of a compound layer is due to an interfacial reaction limiting the growth process. In bilayer metal-silicon systems, linear growth of the outer silicide layer is no longer a sufficient condition for an interfacial reaction to be controlling the growth process. If the interposed layer is relatively "thin", the linear growth is limited by an interfacial reaction. When the interposed layer is relatively "thick", the linear growth of the outer silicide layer is controlled by diffusion through the interposed layer (the thickness of which remains constant during the growth of the outer silicide layer). The criterium for distinguishing between the "thin" and "thick" layers of the interposed silicide is to be known as the critical thickness,

which is found to depend on the mobility of the diffusant and the linear rate constant in the thin regime. In the "thin" regime (interposed layer thickness less than the critical thickness) the linear growth rate constant is found to be independent of the interposed layer thickness. However, in the "thick" regime (greater than the critical thickness) the linear rate constant is found to be inversely proportional to the thickness of the interposed layer thickness.

In order to test the validity of the theory developed for the growth kinetics in bilayer metal-silicon systems, and to apply the theory to atomic mobility measurements, a variety of experiments were performed. Single-layer and multilayer thin films were deposited onto various substrates (Si<100>, Si<111>, SiO_2, Al_2O_3) by means of electron beam evaporation at pressures of about 5×10^{-7} Torr. After annealing the specimens in a vacuum tube furnace (approximately 10^{-7} Torr), different techniques were used to characterize the thin films, interfaces and sample surfaces. The layer thickness, composition and degree of epitaxy were determined by means of backscattering of mega-electron volt alphas's. The phases of the various layers were established by means of glancing angle X-ray diffraction. Specimens used for the study of lateral diffusion were characterized using scanning electron microscopy for surface topography imaging and energy dispersive spectrometry for composition analysis. The surface morphology of exposed interfaces of multi-layer specimens were also studied by means of scanning electron microscopy. Specially prepared thin specimens were analyzed with respect to grain size and compound phase by means

of transmission electron microscopy and transmission electron diffraction repsectively.

A detailed study was made of $CrSi_2$ growth on Pd_2Si layers, grown on Si<100> and Si<111> substrates. The attractive features of the $Si/Pd_2Si/CrSi_2$ system are

(a) that Pd_2Si grown on Si<111> substrates is epitaxial while polycrystalline on Si<100> substrates,

(b) Pd_2Si forms at relatively low temperatures (below 400°C) whereas $CrSi_2$ forms at relatively high temperatures (above 400°C) and

(c) the interdiffusion of Pd and Cr at temperatures below 500°C is relatively slow.

The Si/Pd/Cr multilayer structures used in this study were pre-annealed at 380°C to transform them into $Si/Pd_2Si/Cr$. Subsequently, the structures were annealed at elevated temperatures (400-500°C) for various periods of time.

The planar growth of $CrSi_2$, on both epitaxial and polycrystalline Pd_2Si was found to progress linearly with time. The linear growth is not necessarily an indication that it is reaction controlled. For thin epitaxial Pd_2Si layers (less than approximately 500 Å) the $CrSi_2$ growth rate remained constant at constant temperature which indicates that the growth is reaction limited. When the interposed epitaxial Pd_2Si layer exceeded some critical thickness (around 500 Å at 450°C) the $CrSi_2$, growth rate was found to be inversely proportional to the thick-

ness of the epitaxial Pd_2Si layer. This is characteristic of the $CrSi_2$ growth being limited by diffusion through the interposed Pd_2Si layer. Very similar behaviour was displayed by the Si<100>/Pd_2Si/Cr system. The major difference is that much thicker layers of polycrystalline Pd_2Si layers are required to influence the $CrSi_2$ growth rate. The critical thickness of polycrystalline Pd_2Si was found to be about 6 700 Å whereas that for epitaxial Pd_2Si was approximately 500 Å around 450°C. This large difference in the critical thickness is ascribed to the higher Si mobility in polycrystalline Pd_2Si. The existance of the critical thickness of the interposed Pd_2Si layer and the fact that the growth rate of the silicide is inversely proportional to the thickness of the interposed silicide layer when it exceeds the critical thickness, prove the validity of the model developed for silicide growth in bilayer metal-silicon systems.

The activation energies associated with $CrSi_2$ growth on Pd_2Si are given in Table 8-1 below.

TABLE 8-1. ACTIVATION ENERGY ASSOCIATED WITH $CrSi_2$ GROWTH ON Pd_2Si

INTERPOSED Pd_2Si LAYER		ACTIVATION ENERGY FOR $CrSi_2$ GROWTH (eV)
THICKNESS	MICROSTRUCTURE	
"thin"	polycrystalline	1.6±0.2
"thick"	polycrystalline	1.7±0.2
"thin"	epitaxial	1.6±0.2
"thick"	epitaxial	2.2±0.2

Although the activation energies for $CrSi_2$ growth on "thin" and "thick" polycrystalline Pd_2Si are similar, they are unrelated since they are associated with two distinctly different processes (reaction limited growth and diffusion controlled growth respectively). The similar activation energies are therefore a matter of coincidence. The activation energy of 2.2 eV for $CrSi_2$ growth on "thick" epitaxial Pd_2Si is characteristic of a vacancy diffusion controlled process. When considering $CrSi_2$ growth on "thick" epitaxial and "thick" polycrystalline Pd_2Si (diffusion controlled growth), the significant difference in activation energies is ascribed to the presence of grain boundaries in polycrystalline Pd_2Si. The mobility of Si in polycrystalline Pd_2Si is enhanced due to possible diffusion along grain boundaries. These grain boundaries could also serve as sources for vacancies, thus increasing the vacancy concentration and consequently the atomic mobility in the case of a vacancy diffusion mechanism.

An interesting feature of the $Si/Pd_2Si/CrSi_2$ structures is the relatively non-uniform Si<111>/Pd_2Si interface of specimens with thick interposed epitaxial Pd_2Si layers. The non-uniformity was deduced from the backscattering spectra of the structures (tailing of signals) and SEM images of the exposed (by chemical etching) interface. The Si/Pd_2Si interface of specimens with thin interposed epitaxial Pd_2Si layers and thin and thick polycrystalline Pd_2Si layers was found to be relatively uniform. Interfacial strain and misfit dislocations in the case of thick epitaxial Pd_2Si layers are believed to

result in laterally non-uniform Si-release from the substrate at the Si/Pd_2Si interface, causing the substrate to become pitted.

The atomic ratio of the components of a metal silicide layer is usually found to be uniform (within epxerimental uncertainty) during and after its growth. It was therefore surprising to find that the Si/Pd atomic ratio in the Pd_2Si layer was affected by $CrSi_2$ growth on it, as deduced from the Pd and Si signal plateaus in the backscattering spectra. The Si/Pd atomic ratio in the Pd_2Si layer was found to be greater near the Si/Pd_2Si interface. The different atom/vacancy reactions at the two interfaces (Si/Pd_2Si and $Pd_2Si/CrSi_2$) are thought to establish different vacancy concentrations there, which, when large enough are reflected in different atomic concentrations. It is believed that the observed non-uniform Si/Pd atomic ratio is as a result of a Si (not Pd) concentration gradient which developes in the Pd_2Si layer during $CrSi_2$ growth. This Si concentration gradient is not present before or after complete $CrSi_2$ growth. The presence of the Si concentration gradient in Pd_2Si during $CrSi_2$ growth suggests that the Pd atoms are relatively immobile during $CrSi_2$ growth and that Si is the dominant diffusing species. This is consistent with the results of the tungsten marker experiments.

A thin layer of tungsten in the deposited Pd layers was used as a chemically inert marker to monitor the atomic flux of silicon and palladium in the Pd_2Si layers during its growth and during $CrSi_2$ growth on it. The W marker atoms imbedded

in the initial Pd_2Si sublayer delineate a reference plane across which the flux of Si and Pd is determined. The ratio of silicon to palladium flux during Pd_2Si growth was found to be comparable (2.0 ± 0.6). This result is in agreement with reported results from radio-tracer experiments and oxygen marker experiments which also showed that the silicon and palladium fluxes are comparable. Since temperature and microstructure (epitaxial/polycrystalline) of the Pd_2Si layer were not found to have a significant effect on the flux ratio, the silicon and palladium fluxes are believed to be coupled, owing to the particular crystal structure of Pd_2Si. This explains why Pd_2Si is unique in the sense that it is the only silicide in which both silicon and metal atoms have been found to diffuse during its growth.

During $CrSi_2$ growth on Pd_2Si (epitaxial and polycrystalline) the palladium atoms were found to remain stationary with respect to the W marker atoms imbedded in the Pd_2Si layer. This indicates that Si is the only diffusing species in Pd_2Si during $CrSi_2$ growth on it. This result therefore excludes the possibility of Pd_2Si dissociating near the $Pd_2Si/CrSi_2$ interface, giving up Si for $CrSi_2$ formation and yielding free Pd atoms which diffuse to the Si substrate. The reported results of a radio-active Si tracer study of $CrSi_2$ formation on Pd_2Si, suggest that grain boundary diffusion of Si through polycrystalline Pd_2Si is the dominant transport mechanism. The Pd_2Si in that study was formed by Pd reacting with amorphous Si which generally results in relatively small Pd_2Si grains. The Pd_2Si layers in this study is formed by Pd reacting with

single crystal Si, resulting in large Pd_2Si grains or epitaxial Pd_2Si layers (on Si<111>). Grain boundary diffusion in these cases are expected to be limited. Considering these factors (radioactive Si tracer and W marker results), it is concluded that silicon transport through the Pd_2Si layer during $CrSi_2$ growth in this study, is mostly via Si vacancies. The high activation energy found for diffusion controlled $CrSi_2$ growth on "thick" Pd_2Si layers also supports this Si transport mechanism.

The W marker experiment has shown that the Pd_2Si layer merely serves as a membrane through which Si atoms diffuse for $CrSi_2$ growth. A diffusion membrane technique was developed whereby the mobility of Si in Pd_2Si could be determined, using $Si/Pd_2Si/Cr$ structures. The same technique was used to determine the mobility of Pd in Pd_2Si with the use of $Pd/Pd_2Si/Ge$ structures. Instead of calculating the atomic mobility, the effective mobility (product of mobility and maximum chemical potential difference) was determined since this proves to be a more suitable parameter for comparison with the parabolic rate constant of silicide growth. The measuring technique is simple in that the effective mobility is determined by measuring the thickness of the Pd_2Si membrane and monitoring the growth of the compound on it ($CrSi_2$ growth for Si mobility and Pd_2Ge growth for Pd mobility).

The effective mobility of Si in polycrystalline Pd_2Si was found to be significantly higher than in epitaxial Pd_2Si and, the associated activation energy was higher in epitaxial Pd_2Si

(2,2 eV vs 1.7 eV). The difference in mobility is ascribed to the presence of grain boundaries in polycrystalline Pd_2Si. The grain boundaries offer additional diffusion paths (in addition to lattice diffusion) and serve as sources of point defects (vacancies) so that the atomic mobility is enhanced, assuming that vacancy diffusion is the dominant diffusion mechanism. When extrapolating the Si effective mobility data (at 400-500°C) down to 200°C, it is found to be orders of magnitude lower than the parabolic rate constant of Pd_2Si growth. This indicates that Si diffusion cannot account for the growth of Pd_2Si (Si is not the only diffusing species). The effective mobility of Pd on the otherhand is found to be of the same order of magnitude as the Pd_2Si parabolic growth rate constant which would suggest that Pd could be the only diffusing species during Pd_2Si growth. This would be in disagreement with the results from the W marker experiment and reported radioactive Si tracer experiments which indicate that both Pd and Si diffuse through Pd_2Si during its growth. When considering the crystal structure of Pd_2Si it is obvious that the moblity of Pd should be higher than that of Si since Pd has Pd nearest neighbours whereas Si does not have Si nearest neighbours. It is therefore concluded that the transport mechanism during Pd_2Si growth is different to that during mobility measurements. It is believed that Pd diffusion stimulates Si diffusion during Pd_2Si growth resulting in a high enhanced Si mobility whereas during $CrSi_2$ growth on Pd_2Si, Si is the only diffusing species so that it migrates with its low intrinsic mobility.

The grain boundary diffusion of Ni in Pd_2Si was investigated using $Si/Pd_2Si/Ni$ structures. Nickel was found to diffuse faster than silicon along the Pd_2Si grain boundaries. Considering the chemical similarity of Ni and Pd, it is concluded that Pd should also diffuse faster than Si along the Pd_2Si grain boundaries. The activation energy of Ni grain boundary diffusion in Pd_2Si is found be be 1.2 eV which suggests that the value for Pd grain boundary diffusion in Pd_2Si would also be around 1.2 eV. The diffusion mechanism during Pd_2Si growth is now thought to be as follow: Both Pd and Si diffuse (vacancy diffusion) through the Pd_2Si lattice (epitaxial and polycrystalline Pd_2Si) with comparable fluxes. In addition, Pd diffuses along the grain boundaries of polycrystalline Pd_2Si. This particular diffusion model is supported by reported parabolic rate constant measurements for Pd_2Si growth and cross-sectional TEM studies of the Si/Pd_2Si and Pd_2Si/Pd interfaces. It is very instructive to compare the $Si/Pd_2Si/Ni$ and $Si/Pd_2Si/Cr$ systems. The different thermal behaviour (Ni grain boundary diffusion versus Si lattice diffusion) is ascribed to the chemical similarity between Pd and Ni and the dissimilarity between Pd and Cr, and thus suggests that the use of Ni as a tracer for Pd is justified.

The use of lateral diffusion couples has proved to be an elegant technique for measuring the moblity of the components of a couple even in the case where both components diffuse during compound growth. Two different sample geometries were used in this study.

(a) Device structures were prepared by opening windows (20 μm wide) in the thin SiO_2 layer covering the Si substrate, followed by a thick layer of Pd deposited onto the entire specimen.

(b) Island structures were obtained by depositing a thin layer of Si (or Pd) onto an SiO_2 or Al_2O_3 substrate followed by a thick layer of Pd (or Si) deposited through square openings (400 x 400 m^2)

During the preanealing stage, a laterally well defined metal-rich (or silicon-rich) source region developes. Upon further heat treatment significant lateral diffusion was observed in island structure specimens with Pd-rich source regions only. Limited lateral diffusion was observed in structures with Si-rich source regions. This suggests that the mobility of Si is significantly lower than that of Pd. The lower Si mobility is expected since Si does not have Si nearest neighbours whereas Pd has Pd nearest neighbours. It is perhaps surprising that Si diffusion is not stimulated by Pd diffusing in the opposite direction as was postulated for Pd_2Si growth from conventional Pd/Si couples. The explanation lies in the fact that during conventional Pd_2Si growth, diffusion is along the c-axis of Pd_2Si, whereas during lateral Pd_2Si growth, diffusion is perpendicular to the c-axis. Because of the particular crystal structure of Pd_2Si, the stimulation of Si diffusion by Pd diffusion is effective only along the c-axis.

The lateral extent of the diffusion zone (Pd-rich specimens) was found to progress parabolically with time ($L \propto t^{\frac{1}{2}}$) implying

that the lateral growth process is limited by diffusion through the growing Pd_2Si zone. The parabolic rate constant for lateral Pd_2Si growth and its associated activation energy of 1.1 eV compare favourably with the corresponding parameters reported for conventional Pd_2Si growth (comparison done in Figure 7-11 where lateral diffusion data is extrapolated to temperatures around 200°C). Since the parabolic growth rate in Pd-rich structures reflects the effective mobility of Pd, it is concluded that the effective mobility of Pd is of the same order of magnitude as the parabolic rate constant for conventional Pd_2Si growth. The tungsten marker experimental results have shown that the Pd and Si fluxes during Pd_2Si growth are comparable, so that the effective mobility of Pd should be of the same order of magnitude as the parabolic rate constant since the parabolic growth rate constant is roughly the sum of the Si and Pd effective mobilities. The lateral diffusional growth results and W marker experimental results are therefore in agreement. The large Pd_2Si grains observed in the diffusion zone do not seem to affect the parabolic growth rate since the growth is found to progress parabolically and a single activation energy is measured. If it is borne in mind that the grains probably grew during lateral diffusional growth of the Pd_2Si zone, then it can be concluded that the parabolic growth rate is independent of the grain size. This suggests that the dominant transport mechanism is lattice diffusion (vacancy diffusion in the close-packed structures such as Pd_2Si) and not grain boundary diffusion.

When considering the results of studies regarding Pd_2Si growth from conventional Pd/Si couples, the very similar activation energies reported for epitaxial (1.05 eV) and polycrystalline Pd_2Si (0.95 eV) suggest the same diffusion mechanism for both microstructures. Since it has been shown that (Ni) grain boundary diffusion is insignificant in epitaxial Pd_2Si, it is concluded that the dominant diffusion mechanism during both polycrystalline and epitaxial Pd_2Si growth is lattice diffusion (vacancy diffusion). A similar conclusion was drawn above, regarding the Pd transport mechanism during lateral Pd_2Si growth. The relatively high activation energies determined for Si mobility in polycrystalline and epitaxial Pd_2Si (1.7 and 2.2 eV respectively) also suggest that Si is transported through Pd_2Si via vacancy diffusion. It should however be borne in mind that both Si and Pd diffuse through Pd_2Si during conventional Pd_2Si growth (W marker results) whereas only Pd or Si diffuse through Pd_2Si during its lateral growth or during $CrSi_2$ growth on Pd_2Si (W marker results). The atomic transport in all three cases however appear to proceed via the Pd_2Si lattice alhtough the diffusion mechanisms are different. This can be ascribed to the particular crystal structure of Pd_2Si (hexagonal close-packed). The peculiar diffusional behaviour of Pd_2Si makes it unique but interesting, and one should be cautious when comparing experimental results obtained under different diffusional environments. The atomic mobility of Si and Pd in Pd_2Si is therefore very sensitive to the driving forces (diffusional environment) for diffusion.

The theory of the silicide growth kinetics developed for single- and bi-layer metal silicon systems should prove most valuable for interpreting experimental results. It should thus contribute to the understanding of the silicide formation process. It has been shown that the atomic mobility is easily measurable. This parameter should be given some consideration when evaluating the reliability of electronic devices (interdiffusion could lead to contact degradation of silicon/silicide contacts).

APPENDIX A

SYMBOLS

B - mobility

B_M - mobility of metal atoms

B_{Si} - mobility of silicon atoms

B_1 - mobility of silicon in Ml_ySi

B_2 - mobility of silicon in $M2_xSi$

$\bar{B}_1$ - effective mobility of silicon in Ml_ySi

$\tilde{B}_{M_ySi}$ - parabolic rate constant of M_ySi growth

C - concentration of diffusant

∇C - concentration of diffusant

d_i - length of inside region of lateral diffusion zone

d_o - length of outside region of lateral diffusion zone

Δd_i - increase in d_i during time interval $\Delta\tau$

D - diffusion coefficient

D_{gb} - grain boundary diffusion coefficient

D_V - diffusion coefficient for vacancies in the compound layer

E - energy

E_o - energy of incident projectiles

ΔE_W - energy shift of W signal in the backscattering spectrum

Δg^M - partial molar free energy change associated with the reaction at the M_ySi/M interface

Δg^{Si} - partial molar free energy change associated with the reaction at the Si/M_ySi interface

$\Delta g^{M,e}$ - standard partial molar free energy change associated with the reaction at the M_ySi/M interface

ΔG - total driving force for the reaction

ΔG_B - free energy dissipation due to atoms crossing the interface

ΔG_D - free energy dissipation due to atoms diffusing through the compound

ΔG_f - free energy of formation of vacancies

ΔG_m - free energy of migration of the atoms

ΔG_f^o - standard free energy change for compound formation

$\Delta G_f^{o(M2_xSi)}$ - standard free energy change for $M2_xSi$ formation

h_M - deposited metal layer thickness

h_{Si} - deposited silicon layer thickness

H_A - height of the signal in the backscattering spectrum, due to scattering from A atoms

ΔH_f^o - standard heat of compound formation

J - flux of diffusant

J_{Si} - flux of silicon atoms

k_M - rate constant of reaction at the M_ySi/M interface

k_{Si} - rate constant of reaction at the Si/M_ySi interface

k_1 - reaction rate constant at Si/Ml_ySi interface

K - kinematic factor

K_1 - effective reaction rate associated with the interfacial reaction rate k_1

L - thickness of layer

m - mass of projectile

M - mass of target atom

M - free metal atom

M^x - metal atom in a lattice site in the M_ySi layer

$[M^x]$ - metal atom concentration in the M_ySi layer

$[M^x]^e$ - equilibrium concentration of metal atoms in the M_ySi layer

n - stoichiometric atomic fraction of diffusant in the compound

n_A - atomic concentration of A atoms in a layer

q_M - atomic fraction of M in the solid solution

q_m^s - stoichiometric atomic fraction of M in the compound M_ySi

Q - amount of diffusant accumulated on the surface

R - universal gas constant

R_{M_ySi} - linear rate constant for M_ySi growth

R_o - maximum growth rate of $M2_xSi$ on the interposed Ml_xSi layer

R_2 - growth rate of $M2_xSi$ on Ml_ySi when Ml_ySi layer exceeds the critical thickness

Si^x - silicon atom on lattice site in M_ySi

Si^{xl} - silicon atom on lattice site in Ml_ySi

$[Si^x]$ - concentration of Si atoms in M_ySi

t - time

t - penetration depth of projectile

T - temperature

$\langle v \rangle$ - mean drift velocity

V_{Si} - silicon vacancy in M_ySi layer

$[V_{Si}]$ - silicon vacancy concentration in M_ySi layer

$[V_{Si}]_M$ - silicon vacancy concentration in M_ySi layer at the M_ySi/M interface

$[V_{Si}]_M^e$ - equilibrium concentration of silicon vacancies in the M_ySi layer at the M_ySi/M interface

$\left[V_{Si}\right]_M^o$ - initial value of $\left[V_{Si}\right]_M$ at the M_ySi/M interface

$\left[V_{Si}{}^{Ml_ySi}\right]_M^e$ - equilibrium concentration of silicon vacancies in the Ml_ySi layer at the $Ml_ySi/M2_xSi$ interface

x - atomic ratio of metal (M2) to silicon in $M2_xSi$

y - atomic ratio of metal to silicon in M_ySi

Y - thickness of the interposed layer

Y_{Pd} - thickness of Pd_2Si sublayer formed by Pd atoms diffusing through the Pd_2Si layer

Y_{Si} - thickness of Pd_2Si sublayer formed by Pd atoms diffusing

Y_o - thickness of the deposited Pd layer

Y_o - critical thickness of the interposed layer

Y_1 - thickness of Ml_ySi layer

Y_2 - thickness of $M2_ySi$ layer

z - atomic number of projectile

Z - atomic number of target

α_o - concentration of diffusant at the entrance to the grain boundaries

γ - density of the grain boundaries

γ_{Pd} - activity coefficient

Γ - probability that the atom migrates to a neighbouring plane

ε_{Pd} - stopping cross-section factor for Pd in Pd

$\varepsilon_{Pd}^{Pd_2Si}$ - stopping cross-section factor for Pd in Pd_2Si

$\nabla\mu$ - chemical potential gradient

μ_M - chemical potential of M

μ_{Si} - chemical potential of Si

$\Delta\mu_{Si}$ - chemical potential difference of Si across the compound layer

$\Delta\mu^{e}_{Si}$ - equilibrium chemical potential difference across the compound layer

ν - natural vibration frequency of the atoms

λ - spacing between neighbouring atomic planes

θ - scattering angle

θ_1 - angle between incident ion beam and sample surface normal

θ_2 - angle between backscattered ion beam and sample surface normal

σ - scattering cross-section

Ω - solid angle

Ω - probability that the lattice site on the neighbouring plane is vacant

$\Delta\tau$ - time interval

APPENDIX B

THE RATIO : $\left[V_{Si}\right]^{e}_{Si} / \left[V_{Si}\right]^{e}_{M}$

Consider silicon vacancies V_{Si} in the Si sublattice of a compound. The vacancy concentration $\left[V_{Si}\right]$ is usually very low so that the silicon sublattice, is considered to be a dilute solution of vacancies (the solvent being the silicon atoms on the lattice sites). In the dilute regime, the chemical potential of the vancancies $\mu_{V_{Si}}$ is given by (see [21]):

$$\mu_{V_{Si}} = \mu^{o}_{V_{Si}} + RT\ell n \left[V_{Si}\right] \qquad \text{(B-1)}$$

where $\mu^{o}_{V_{Si}}$ is a constant and R and T have their usual meanings. Vacancies are virtual particles (absent atoms) so that the associated chemical potential is also virtual [21]. Since the concentration of Si lattice sites remains constant, the concentration of Si atoms $\left[Si^{x}\right]$ plus the concentration of Si vacancies V_{Si} also remains constant.

$$\left[Si^{x}\right] + \left[V_{Si}\right] = \text{constant.}$$

An increase in Si vacancies results in a decrease in occupied Si lattice sites:

$$d\left[V_{Si}\right] = -d\left[Si^{x}\right] \qquad \text{(B-2)}$$

The change in Gibbs free energy (of a unit volume of the lattice) is given by (see [21]):

$$dG = \mu_{Si^x}\, d\left[Si^x\right] + \mu_{V_{Si}}\, d\left[V_{Si}\right] \qquad \text{(B-3)}$$

where μ_{Si^x} and $\mu_{V_{Si}}$ are the chemical potentials of Si and V_{Si} in the compound respectively. When thermodynamic equilibrium prevails, the free energy is a minimum so that dG = 0. Equation (B-3) now becomes:

$$0 = \mu_{Si^x}\, d\left[Si^x\right] + \mu_{V_{Si}}\, d\left[V_{Si}\right]$$

Upon substituting (B-2) in the above equation:

$$\mu_{Si^x} = -\mu_{V_{Si}} \qquad \text{(B-4)}$$

A usefull expression for the chemical potential of Si in the Si sublattice is now obtained by substituting (B-1) into (B-4)

$$\mu_{Si^x} = -\mu^{o}_{V_{Si}} - RT\ell n\left[V_{Si}\right] \qquad \text{(B-5)}$$

Consider a partially reacted Si-M binary couple in which the compound M_ySi has formed (y is a constant). The equilibrium chemical potential of Si in the compound μ_{Si^x} near the two interfaces is then given by:

Si/M_ySi interface:

$$\mu_{Si}\Big|^{e}_{Si} = -\mu^{o}_{V_{Si}} - RT\ell n\left[V_{Si}\right]^{e}_{Si}$$

M_ySi/M interface:

$$\mu_{Si}\Big|_M^e = -\mu^o_{V_{Si}} - RT\ell n \left[V_{Si}\right]_M^e$$

The equilibrium chemical potential difference of Si across the M_ySi layer is therefore:

$$\Delta\mu^e_{Si} = \mu_{Si}\Big|_M^e - \mu_{Si}\Big|_{Si}^e$$

$$= RT\ell n \left[V_{Si}\right]_{Si}^e - RT\ell n \left[V_{Si}\right]_M^e$$

or

$$\Delta\mu^e_{Si} = RT\ell n \frac{\left[V_{Si}\right]_M^e}{\left[V_{Si}\right]_{Si}^e}$$

APPENDIX C

MOBILITY

During planar diffusion in the absence of external forces being exerted on the individual atoms, the flux J of diffusing species (say Si atoms) is characterized by Fick's first law of diffusion;

$$J = -D \frac{d}{dx} [Si] \qquad (C-1)$$

where D is the diffusion coefficient,

[Si] is the concentration of the Si atoms and

x is the direction of diffusion.

The diffusion process described by the above equation takes place as result of the concentration gradient of the diffusing atoms.

Consider vacancy diffusion to be the dominant mechanism whereby the atoms migrate during diffusion. The atoms exchange positions with neighbouring vacancies and the frequency of jumps is isotropic. When there are driving forces which make the individual atomic jump probability higher in one direction than in another, there is an overall migration of atoms in one direction which is characterized by an average drift velocity. Examples of driving forces are chemical potential gradients and electrical, magnetic or mechanical stress fields applied across the diffusion matrix. A diffusion coefficient gradient, although not considered to be a true driving force, also gives rise to the atoms drifting in a particular direction. Atomic migration during

compound growth in bilayer or multilayer thin film structures usually proceeds as a result of the presence of a chemical potential gradient across the growing layer. In this work, where compound layer growth is being addressed, the chemical potential gradient is considered to be the dominant driving force for diffusion while the atomic concentration is assumed to be uniform.

The atom flux between two neighbouring planes in a crystal lattice is determined by the mobility of the diffusing atoms. In order to obtain a physical interpretation of the mobility and to find a suitable expression for it, the energetics of the migration process needs to be considered. The following factors influence the mobility and therefore also the atomic flux between neighbouring planes:

(a) The natural vibration frequency ν of the atoms since these vibrations are the sources of atomic motion in the lattice.
(b) The probability Γ that the atom from a particular plane will reach the neighbouring plane.
(c) The probability Ω that the lattice site on the neighbouring plane is vacant.

The free energy of an atom in a lattice in the absence of a driving force is usually a minimum when such an atom occupies a regular lattice position, whereas the free energy is a maximum when the atom is midway between the neighbouring sites. The height of the maximum with respect to the minimum is denoted by ΔG_m. An energy barrier ΔG_m therefore hinders the atom from migrating to a neighbouring lattice site. The probability Γ that the vibrating atom will overcome the energy barrier ΔG_m

is given by [19]:

$$\Gamma = \exp\left(-\Delta G_m/RT\right) \qquad \text{(C-2)}$$

where R and T have their usual meanings.

The probability Ω that the neighbouring lattice site is vacant is determined by the free energy of formation of vacancies ΔG_f, assuming a vacancy diffusion mechanism. By applying statistical mechanical principles [19], an expression for Ω can be found:

$$\Omega = \exp\left(-\Delta G_f/RT\right) \qquad \text{(C-3)}$$

In the presence of a driving force for diffusion (e.g. chemical potential gradient), the probability factors in (C-2) and (C-3) are influenced, depending on the nature of the driving force. In Appendix B it was shown that the chemical potential difference across the growing layer determines the vacancy concentration in the layer. This implies that the driving force for diffusion influences the probability that the neighbouring lattice site will be vacant.

Consider two neighbouring planes (+) and (-) between which the atoms migrate in both directions. Let Ω_+ and Ω_- be the probabilities that the lattice sites on the respective planes are vacant. In the absence of a driving force, these probabilities would have been equal ($=\Omega$). The chemical potential gradient causes Ω_+ and Ω_- to be different. Using statistical mechanics principles, it can be shown that [88]:

$$\Omega_+ = \Omega_o \exp\left(-\frac{\partial \mu}{\partial x}\,\lambda / 2RT\right)$$

and $$\Omega_- = \Omega_o \exp(+\frac{\partial \mu}{\partial x} \lambda/_{2RT})$$

where Ω_o is a constant,

μ is the chemical potential of the diffusant,

λ is the spacing between neighbouring planes,

x is the direction of motion (perpendicular to the lattice planes,

and R and T have their usual meanings.

Since the atom jump probability is now different in the two directions, there will be an overall migration (drift) of the atoms in one particular direction (say from (-) to (+)) and the flux will be determined by the difference in probabilities Ω_+ and Ω_-. Therefore:

$$\Omega_+ - \Omega_- = \Omega_o[\exp(-\frac{\partial \mu}{\partial x}\lambda/_{2RT}) - \exp(+\frac{\partial \mu}{\partial x}\lambda/_{2RT})]$$

Since the exponents in the above expression are very small, a first order Taylor's expansion is justified so that it becomes:

$$\Omega_+ - \Omega_- = -\Omega_o \frac{\partial \mu}{\partial x} \frac{\lambda}{RT} \qquad \text{(C-4)}$$

A vibrating atom (natural frequency ν), in migrating successfully to the neighbouring plane, is displaced a distance λ, the spacing between neighbouring planes. The frequency with which these jumps occur is not ν but $\nu\Gamma(\Omega_+ - \Omega_-)$. The mean drift velocity of the atoms (displacement x jump frequency) is therefore given by:

$$\langle v \rangle = \lambda \nu \Gamma (\Omega_+ - \Omega_-)$$

$$= \lambda^2 \nu \Gamma \Omega_o \frac{\partial \mu}{\partial x}/_{RT} \qquad \text{(C-5)}$$

The flux of atoms (say Si) migrating as a result of the drift

is given by [19]:

$$J = [Si^x]\langle v\rangle$$

Upon substituting (C-5) into the above expression;

$$J = [Si^x]\lambda^2 \nu\Gamma\Omega_o \partial\mu/RT$$

which can be written as

$$J = [Si^x]\, B\, \frac{\partial\mu}{\partial x} \qquad \text{(C-6)}$$

where

$$B = \frac{\lambda^2 \nu\Gamma\Omega_o}{RT} \qquad \text{(C-7)}$$

In equation (C-7) B is known as the atomic mobility. In the absence of a driving force for diffusion, an analogous expression is found for the diffusivity D [19];

$$D = \lambda^2 \nu\Gamma\Omega \qquad \text{(C-8)}$$

which would suggest that BRT = D. It should however be pointed out that the probabilities Ω_o and Ω differ.

In the absence of a driving force, an equilibrium concentration of vacancies is present and the probability is given by;

$$\Omega = \exp(-\Delta G_f/RT) \qquad \text{(C-2)}$$

where ΔG_f is the free energy of formation of the vacancies. It was however shown in Appendix B that the chemical potential gradient determines the vacancy concentration so that (C-2) is no longer applicable and consequently Ω_o is a constant, independent of temperature. The expression for the mobility, equation (C-7) therefore becomes:

$$B = \frac{\lambda^2 \nu\Omega_o}{RT} \exp(-\Delta G_m/RT) \qquad \text{(C-9)}$$

The analogous expression for the diffusivity D is [19]:

$$D = \lambda^2 \nu \exp[-(\Delta G_f + \Delta G_m)/RT] \qquad (C\text{-}10)$$

The activation energy of the mobility B is therefore ΔG_m, the free energy of migration whereas the activation energy of the diffusivity D is larger and equal to the sum of the free energies of formation and migration, $\Delta G_f + \Delta G_m$. This difference in activation energies of the diffusivity (driving force absent) and the mobility (driving force present) is analogous to the activation energy difference between intrinsic and extrinsic ionic diffusion [19]. In the intrinsic regime (low impurity concentration) the ionic diffusivity is given by (C-10). In the extrinsic regime (high impurity concentration) the vacancy probability is no longer given by (C-3) so that the activation energy of the diffusivity is ΔG_m only, similar to that of the mobility in (C-9).

REFERENCES

1. R.A. Colclaser, *Microelectronics: Processing and Device Design*, (John Wiley and Sons, New York 1980)

2. C.M. Osburn, M.Y. Tsai, S. Roberts, C.J. Lucchese and C.Y. Ting, Proc. First Int. Symp. on VLSI Science and Technology, Electrochemical Soc. Inc. 213 (1982)

3. K.N. Tu and J.W. Mayer in *Thin Films - Interdiffusion and Reactions*, Edited: J.M. Poate, K.N. Tu and J.W. Mayer, John Wiley and Sons, New York 1978

4. R.M. Walser and R.W Bené, Appl. Phys. Lett. 28, 624 (1976)

5. U. Gösele and K.N. Tu, J. Appl. Phys., 53, 3252 (1982)

6. S.P. Murarka, *Silicides for VLSI Applications* (Academic Press, New York, 1983)

7. M.A. Nicolet and S.S. Lau,VLSI: Microstructure Science, edited by N. Einspruch (Academic Press New York, 1983) Vol. 6 Chapter 6

8. H. Geiger and E. Marsden, Phil. Mag. 25 , 606 (1913)

9. W.K. Chu, J.W. Mayer and M.A. Nicolet, Backscattering Spectrometry, (Academic Press, New York, 1978)

10. S.T. Picraux, in *New Uses of Ion Accelerators*, edited by J.F. Ziegler (Plenum Press, New York, 1975)

11. S.S. Lau, W.K. Chu, J.W. Mayer and K.N. Tu, Thin Solid Films, 23, 205 (1974)

12. B.D. Cullity, *Elements of X-ray diffractions*, (Addison Wesley, Reading 1978)

13. G.V. Kidson, J. Nucl. Mat. 3, 21 (1961)

14. S.R. Shatynski, J.P. Hirth and R.A. Rapp, Acta Met., 24, 1071 (1976)

15. C. Wagner, Acta, Met., 17, 99 (1969)

16. H. Schmalzried, *Solid State Reactions*, (Verlag Chemie, Weinheim, 1981)

17. F.A. Kröger, *The Chemistry of Imperfect Crystals*, (North Holland, Amsterdam, 1973)

18. K. Denbigh, *The Principles of Chemical Equilibrium*, (Cambridge University Press, London 1966)

19. P.G. Shewmon, *Diffusion in Solids*, (McGraw Hill, New York, 1963)

20. B.E. Deal and A.S. Grove, J. Appl. Phys., 36 3770 (1965)

21. R.A. Swalin, *Thermodynamics of Solids*, (John Wiley and Sons, New York, 1972)

22. G.M. Mladoenow and B. Emnoth, Appl. Phys. Lett., 33 754 (1978)

23. J.O. Olowolafe, M-A Nicolet and J.W. Mayer, J. Appl. Phys., 47, 5182 (1976)

24. A. Martinez, D. Esteve, A. Guivarch, P. Aucray, P. Henoc and G. Pelosis, Solid State Electronics, 23, 55 (1980)

25. E.G. Golgan, B-Y Tsaur and J.W. Mayer, Appl. Phys. Lett., 37 938 (1980)

26. A.P. Botha and R. Pretorius, Thin Solid Films, 93, 127 (1982)

27. W.G. Moffat, *Handbook of Binary Phase Diagrams*, (General Electric Company, New York, 1978)

28. W.D. Buckley and S.C. Moss, Solid State Electronics, 15, 133 (1972)

29. G. Hutchins and A. Shepela, Thin Solid Films, 18, 343 (1973)

30. R.W. Bower, D. Sigurd and R.E. Scott, Solid State Electronics, 16, 1461 (1973)

31. N. Cheung, S.S. Lau, M-A Nicolet, J.W. Mayer and T.T. Sheng, in J.E.E. Baglin and J.M. Poate (eds.), Proc. Symp. on Thin Film Interfaces and Interaction, Vol. 80-2, Electrochemical Society, Princeton, N.J., 1980 p 494

32. N. Cheung M-A Nicolet, M. Wittmer, C.A. Evans and T.T. Sheng, Thin Solid Films, 79, 51 (1981)

33. R. Pretorius, C.L. Ramiller and M-A Nicolet, Nucl. Inst. Meth. 49, 629 (1978)

34. J.E.E. Baglin, F.M. d'Heurle, W.N. Hammer and S. Peterson, Nucl. Inst. Meth. 169, 4191 (1980)

35. H. Foll and P.S. Ho, J. Appl. Phys., 52 5510 (1981)

36. D.M. Scott, S.S. Lau, P.L. Pfeffer, R.A. Lux, J. Mikkelson, L. Wielunski and M-A Nicolet, Thin Solid FIlms, 104, 227 (1983)

37. U. Köster, P.S. Ho and M. Rom, Thin Solid Films, 67, 35 (1980)

38. J.O. Olowolafe, M-A Nicolet and J.W. Mayer, Solid State Electron., 20, 413 (1977)

39. S. Solomonson, K.E. Holm and T.G. Finstad, Physica Scripta, 24, 401 (1981)

40. M-A Nicolet and M. Bartur, J. Vac. Sci. Technol., 19, 786 (1981)

41. J.K. Howard, R.F. Lever, P.J. SMith and P.S. Ho, J. Vac. Sci. Technol., 13, 18 (1976)

42. T.G. Finstad and M-A Nicolet, Thin Solid Films 68, 393 (1980)

43. J.W. Mayer, S.S. Lau and K.N. Tu, J. Appl. Phys., 50, 5855 (1979)

44. M.O. Naude, R. Pretorius and D.J. Marais, Thin Solid Films, 89, 339 (1982)

45. E.Raub and W. Mahler, Z. Metallkunde, 45, 648 (1954)

46. C.P. Flynn, *Point Defects and Diffusion* (Oxford University Press, 1972)

47. R. Pretorius, A.P. Botha and J.C. Lombaard, Thin Solid Films, 79, 61 (1981)

48. H. Chen, G.E. White, S.R. Stock and P.S. Ho, M.R.S. Symp. Proc. 10, 165 (1982)

49. F.C. Frank and J.H. Van der Merwe, Proc. Roy. Soc. A198, 216 (1949)

50. F.C. Tomkins in *Treatise in Solid State Chemistry*, Vol. 4 Ed. N.B. Hannay (Plenum Press, New York, 1976)

51. K.N. Tu, Appl. Phys. Lett. 27, 221 (1975)

52. R. Pretorius, J. O. Olowolafe and J.W. Mayer, Phil. Mag. A, 37, 327 (1978)

53. S.S. Lau and D. Sigurd, J. Electrochem. Soc. 121, 1538 (1974)

54. E.O. Kirkendal, Trans. AIME, 147, 104 (1942)

55. W-K Chu, S.S. Lau, J.W. Mayer, H. Muller and K.N. Tu, Thin Solid Films, 25, 393 (1975)

56. G.J. van Gurp, W.F. van der Weg and D. Sigurd, J. Appl. Phys., 49, 4011 (1978)

57. K.N. Tu, J. Appl. Phys., 48, 3379 (1977)

58. M. Bartur and M-A Nicolet, J. Appl. Phys., 54, 5404 (1983)

59. C.A. Crider, J.M. Poate, J.E. Rowe and T.T. Sheng, J. Appl. Phys., 52, 2860 (1981)

60. J.O. Olowolafe, M-A Nicolet and J.W. Mayer, Thin Solid Films, 38, 143 (1976)

61. S.S. Lau, J.W. Mayer and K.N. Tu, J. Appl. Phys., 49, 4005 (1978)

62. L.S. Hung, J. Gyulai, J.W. Mayer, S.S. Lau and M-A Nicolet, J. Appl. Phys., 54, 5076 (1983)

63. L.S. Darken, Trans. AIME, 175, 184 (1948)

64. U. Gösele, K.N. Tu and R.D. Thompson, J. Appl. Phys., 53, 8759 (1982)

65. J.K. Hirvonen, W.H. Weisenberger, J.E. Westmoreland and R.A. Meussner, Appl. Phys. Lett., 21, 37 (1972)

66. M. Wuttig and H.K. Birnbaum, Phys. Rev., 147, 495 (1966)

67. G.C. Nelson and P.H. Holloway, ASTM Special Publ. 596, Philidelphia (1976) p. 68

68. J.C.M. Hwang, J.D. Pan and R.W. Balluffi, J. Appl. Phys., 50, 1349 (1979)

69. P.H. Holloway, D.E. Amos and G.C. Nelson, J. Appl. Phys., 47, 3769 (1976)

70. J.C.M. Hwang and R.W. Balluffi, J. Appl. Phys., 50 1339 (197)

71. B-Y Tsaur, D.J. Silversmith, R.W. Mountain and C.H. Anderson Jr., Mat. Res. Soc. Symp., 10, 341 (1981)

72. T.G. Finstad, Thin Solid Films, 51, 411 (1978)

73. C.A. Crider and J.M. Poate, Appl. Phys. Lett., 36, 417 (1980)

74. K.T. Ho, M-A Nicolet and L Wielunski, Thin Solid Films, 104, 243 (1983)

75. L.S. Hung, L.R. Zheng and J.W. Mayer, J. Appl. Phys., 54, 792 (1983)

76. A.P. Botha, *Solid State diffusion in Metal Silicides*, Ph.D thesis, University of Stellenbosch (1982)

77. A. Nyland, Acta. Chem. Scand., 20 , 2381 (1966)

78. S. Okada, K. Oura, T Hanawa and K. Satoh, Surface Science, 97, 88 (1980)

79. J.E.E. Baglin, F.M. d'Heurl and C.S. Peterson, J. Appl. Phy., 52, 2841 (1981)

80. M. Hansen, *Constitution of Binary Alloys*, 2nd edition (McGraw-Hill New York, 1958)

81 L.R. Zheng, L.S. Hung, J.W. Mayer, G. Majni and G. Ottaviani, Appl. Phys. Lett., 41, 646 (1982)

82. L.R. Zheng, L.S. Hung and J.W. Mayer, J. Vac. Sci. Technol. A1, 758 (1983)

83. L.R. Zheng, L.S. Hung and J.W. Mayer, Thin Solid Films, 104, 207 (1983)

84. L.R. Zheng, E.C. Zingu and J.W. Mayer, MRS Symp. Proc., 25, 75 (1984)

85. C. Canali, L. Silvestri and G. Celotti, J. Appl. Phys., 50, 5768 (1979)

86. S.H. Chen, R.L. Zheng, J.C. Barbour, E.C. Zingu, L.S. Hung, C.B. Carter and J.W. Mayer, Mat. Lett., 2, 469 (1984)

87. J.E.E. Baglin and J.M. Poate in *Thin Films Interdiffusion and Reactions*, Edited J.M. Poate, K.N. Tu and J.W. Mayer (John Wiley and Sons New York, 1978)

88. J.R. Manning, Phys. Rev., 124, 470 (1961)